공학박사 학위논문

Understanding the behavior of copper ions in Cu-SSZ-13 under selective catalytic reduction of nitrogen oxides with ammonia

선택적 촉매 환원 반응에서 Cu-SSZ-13의 Cu 이온 거동에 대한 이해

2021 년 2 월

서울대학교 대학원
화학생물공학부
이 황 호

Understanding the behavior of copper ions in Cu-SSZ-13 under selective catalytic reduction of nitrogen oxides with ammnoia

지도교수 김 도 희

이 논문을 공학박사 학위논문으로 제출함

2021 년 **1** 월

서울대학교 대학원

화학생물공학부

이 황 호

이황호의 박사 학위논문을 인준함

2021 년 **1** 월

위 원 장 이 원 보 (인)

부 위 원 장 김 도 희 (인)

위 원 강 종 헌 (인)

위 원 김 지 만 (인)

위 원 박 영 권 (인)

Abstract

Understanding the behavior of copper ions in Cu-SSZ-13 under selective catalytic reduction of nitrogen oxides with ammonia

Hwangho Lee
School of Chemical and Biological Engineering
The Graduate School
Seoul National University

Abatement technologies for nitrogen oxides (NOx) have received a significant attention in industry due to the detrimental effects of the NOx on human health and the environment. Among them, selective catalytic reduction of NOx with NH_3 (NH_3-SCR) is the most effective technology to remove harmful NOx by reducing it to harmless N_2. Cu ion-exchanged SSZ-13 (Cu-SSZ-13), which has a chabazite structure, has been successfully commercialized as an NH_3-SCR catalyst for its excellent performance and

hydrothermal stability. However, there is growing need for the Cu-SSZ-13 catalyst with superior NOx removal ability since regulation of NOx emissions is getting more stringent. In order to develop the Cu-SSZ-13 catalyst with better performance, more understanding about the behavior of Cu^{2+} ion, which is an active site of the NH_3-SCR reaction, is required.

There are two types of Cu ions in Cu-SSZ-13, 1Al-Cu and 2Al-Cu, and these are determined by the positions where the Cu ions are located. 1Al-Cu is a Cu^{2+} ion coordinating to a single Al site that exists in the form of Z-(Cu^{2+}-OH^-). 2Al-Cu is a Cu^{2+} ion that coordinates to two adjacent Al sites as 2Z-Cu^{2+}. These species have different properties and one of them is their different mobility. Here, we tried to observe the mobility of these species and reveal its relationship with the SCR reactivity. To observe the mobility of Cu ion in the cage, Cu-SSZ-13 was physically mixed with H-SSZ-13 using two different method. One was grinding them with mortar, and the other was mixing them after making large granules separately. The former made the Cu-SSZ-13 and H-SSZ-13 contact closely each other (PM-C), and in latter case, they were mixed but present separately with little contact (PM-L). Compared to the PM-L where Cu ion could not migrate to H-SSZ-13, conformation change of Cu species was observed from 2Al-Cu to 1Al-Cu in the PM-C. Based on such shift in Cu species, it can be inferred that Cu ions in the Cu-SSZ- 13 migrated toward the H-SSZ-13 in the PM-C. This phenomenon did not occur by thermal treatment without the presence of H_2O implying that solvation by H_2O is crucial to the migration of Cu ion. This study demonstrated that Cu ion can migrate

macroscopic distance from a particle to another particle under hydrothermal condition.

The mobility of Cu ion is known to be an important property in SCR reaction since the formation of reaction intermediate is governed by the Cu ion diffusion. As the 1Al-Cu and 2Al-Cu species have different mobility, it can be inferred that reactivity is also different depending on the Cu ion species, however, their discrepancy has not been revealed in selective catalytic reduction (SCR). Herein, we investigated the different SCR reactivity of two Cu ion species in the Cu-SSZ-13 controlling ratio of Cu species by hydrothermal treatment. The results for reactivity and DRIFT analysis unambiguously demonstrated that the 1Al-Cu species is more active in the SCR than the 2Al-Cu species and this difference occurs when the reaction is governed by a specific rate-limiting-step. Based on the kinetic study, we found out that the ion mobility is a significant factor that gives rise to the different reactivity of two Cu ion species, indicating that high mobility of the 1Al-Cu species determines its superior reactivity.

In order to improve the reactivity of Cu-SSZ-13, we designed the catalysts to have more reactive species (1Al-Cu) rather than less active species (2Al-Cu). Co^{2+} ion was introduced to block the 2Al sites of SSZ-13 and induce the Cu ion to be selectively located at 1Al sites. H_2-TPR results showed that when Co^{2+} was introduced, the 1Al-Cu/2Al-Cu ratio was dramatically increased as we expected. The effect of Co^{2+} ion was differently facilitated in SCR reactivity depending on the reaction temperature. The cobalt introduced

Cu-SSZ-13 catalysts demonstrated a higher SCR reactivity than conventional Cu-SSZ-13 catalyst at medium and high temperature (250-450 ℃). Kinetic study allowed us to reveal that the high mobility of 1Al-Cu species enhances the formation of active reaction intermediates. At low temperature, such different mobility was faded, which indicates that such increasing effect in Cu ion mobility did not appear at low temperature. This study suggests a new strategy for tuning the ion mobility to develop the Cu-SSZ-13 catalyst with higher performance.

Keywords: Nitrogen oxide; Selective catalytic reduction of NOx with NH_3; Cu-SSZ-13; Copper ion; ion mobility; Reaction kinetics;

Student Number: 2015-21081

Contents

List of Tables

List of Figures

Chapter 1. Introduction

1.1. Emission of nitrogen oxides and its effect

Nitrogen oxides (NOx) refer to the compounds including NO, NO_2 and N_2O which are known to cause a serious air pollution. They are produced by the reaction of nitrogen (N_2) and oxygen (O_2) in the air. Since the reaction requires high pressure and temperature, most of the NOx has emitted from the anthropogenic sources such as vehicles, power plants and incinerators [1]. Once NO and NO_2 emitted, they react to the various molecule in atmosphere (Figure 1-1). When dissolved to water in the air, acidic rain occurs, acidifying the soil and corroding the human facilities. They can also cause the photochemical smog which had incurred a number of casualties at London in 1952 [2]. Recently, the particulate matter (PM) becomes a huge issues due to its fatal effect on the human respiratory system. Especially, the $PM_{2.5}$ that is fine fraction with a size up to 2.5 μm can get deep into the lungs and finally reduce the lung function [3]. The formation of PM was suggested to be originated from the reaction of NOx and SOx with volatile organic compound (VOC) and NH_3 in the atmosphere producing the fine salt. Therefore, NO and NO_2 emissions from the plants and vehicles is considered a major contributor to the formation of the particulate matter. In the case of the N_2O, it is a greenhouse gas that has about 300 times global warming potential than carbon dioxide.

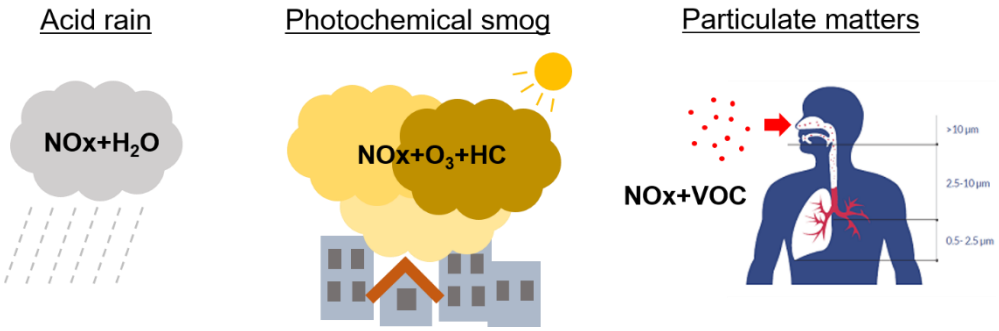

Figure 1-1. Various air pollutions derived from emitted NOx.

1.2. NOx abatement with selective catalytic reduction (SCR)

Due to their detrimental effects on environment and human health, many countries have restricted the emission of NOx from vehicles and plant since 1992. As a result, the NOx abatement technology was introduced in after treatment system of the plant and vehicle, and one of the most effective technology is a selective catalytic reduction with NH_3 (NH_3-SCR). NH_3-SCR is a technology that utilized the NH_3 as a reducing agent to convert the harmful NOx to inert N_2 (Figure 1-2). The NH_3 is injected as a form of urea that decompose to gaseous NH_3 at around 150 ℃. The injected amount NH_3 is controlled with a ratio of NO/NH_3=1 under standard SCR condition by following stoichiometry.

Standard SCR: $4NO + 4NH_3 + O_2 \rightarrow 4N_2 + 6H_2O$

Slow SCR: $2NO_2 + 4NH_3 + O_2 \rightarrow 2N_2 + 6H_20$

Fast SCR: $NO + NO_2 + 2NH_3 \rightarrow 2N_2 + 3H_2O$

When the feed contains only NO_2, the NH_3 reacted via slow SCR pathway that is much slower process than the standard SCR. The reaction rate of SCR is the fastest when the NO/NO_2 ratio=1, which is called the fast SCR.

Vanadia tungsta catalyst supported on titania was first commercialized as a SCR catalyst owing to its good redox properties and high tolerance to SO_2 which is contained in fuels. However, it was found to have a limitation in long-term usage, especially in automobiles, because the commercial TiO_2 collapsed above temperature

550 °C, so the catalyst was seriously degraded. To solve the thermal stability issues, the researchers exploited the cation-exchanged zeolites as the NOx abatement catalysts, which were known to have superior thermal stability. Since Iwamoto et al. first reported NO decomposition ability of Cu^{2+} ion exchanged ZSM-5 zeolite catalyst, many research groups have investigated the NH_3-SCR reaction over various types of zeolites with many different kinds of metal cations [4-8]. In spite of their excellent thermal stability, there was a huge hindrance to commercialize the zeolite catalysts in the NOx removal industry, which was dealumination issue by hydrothermal aging condition. The dealumination is Si-O-Al bond breakage by the hydrolysis of framework by H_2O under hydrothermal condition, which results in the collapse of zeolite structure and the serious catalytic deactivation [9, 10].

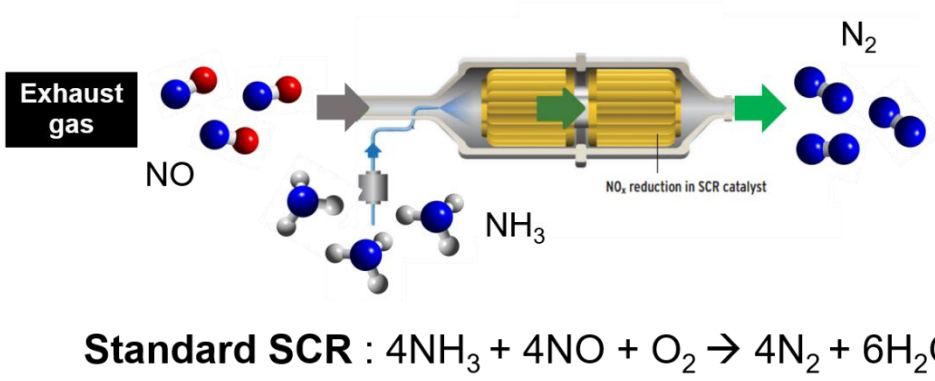

Figure 1-2. The schematic of standard NH_3-SCR reaction in after treatment system.

1.3. Cu-SSZ-13 catalyst for the NH_3-SCR

Cu-SSZ-13, which is Cu ion exchanged zeolite with a chabazite structure has been suggested in 2010 for its superior NOx abatement activity and hydrothermal stability [11]. It consists of six and eight membered aluminosilicate rings with a pore size of 4-5 Å (Figure 1-3). Chabazite structure with small pores gave rise to their superior hydrothermal stability because the steric effect of their small pore hindered the formation of $Al(OH)_3$ and $CuAlO_x$ like species that were deactivation-causing materials [12]. Owing to its great performance, it is successfully commercialized especially in after treatment system of vehicle, where the catalyst is exposed to high temperature gases.

Ionic Cu^{2+} is an active site of Cu-SSZ-13, which adsorbs NH_3 and reduces NO to N_2. The nature of the Cu^{2+} cation has been investigated extensively to understand the interesting behaviors of Cu-SSZ-13 during the NH_3-SCR reaction and its mechanism [13-19]. Under SCR condition, Cu^{2+} coordinates to multiple NH_3 as $Cu^{2+}(NH_3)x$ species. NH_3 adsorbed on Cu ion reacts with NO and convert NO to N_2. In this process, $Cu^{2+}(NH_3)x$ is reduced to $Cu^{+}(NH_3)x$ and re-oxidation process is needed to regenerate the active Cu^{2+}. Oxidation of $Cu^{+}(NH_3)x$ is activated by the formation of dimeric Cu intermediates ($[Cu^{I}(NH_3)_2]^{+}-O_2-[Cu^{I}(NH_3)_2]^{+}$) [20-22]. Formation of this species is plausible since the Cu ions have a mobility in the SSZ-13 cage. It is proposed that the electrostatic interaction between Cu^{2+} ions and Al sites of SSZ-13 weakens by the solvation effect of NH_3, which enables the migration of Cu

ion and formation of dimeric Cu species. Such oxidation process is known as a rate determining step of SCR reaction over the Cu-SSZ-13.

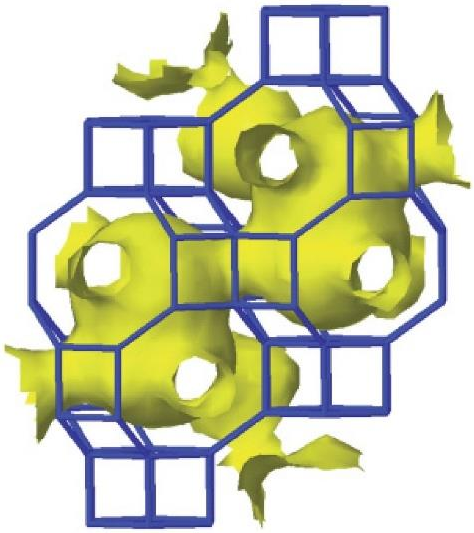

Figure 1-3. The structure of chabazite zeolite.

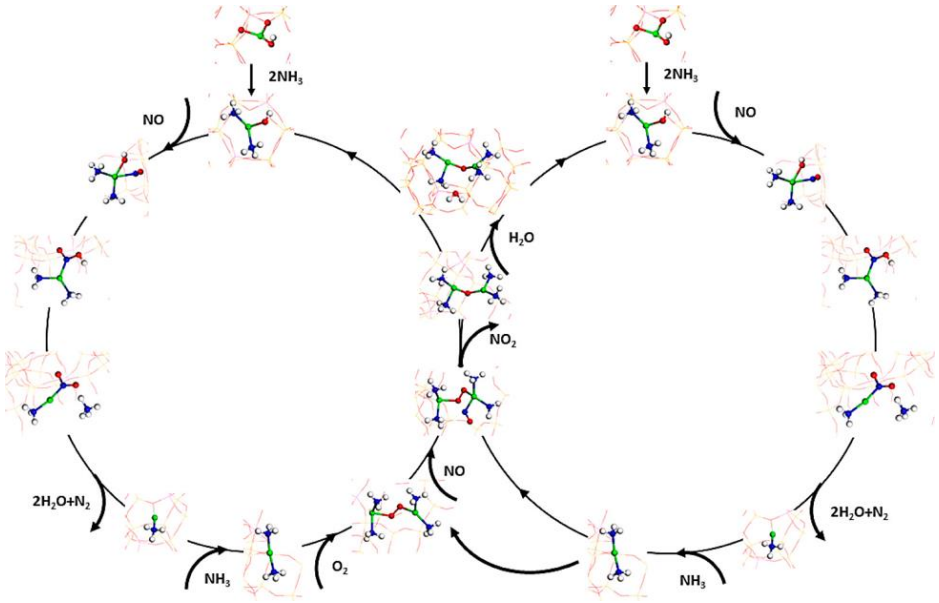

Figure 1-4. Mechanism of NH_3-SCR reaction over the Cu-SSZ-13 catalyst.

1.4. Objectives

Despite excellent performances of Cu-SSZ-13 catalyst, there have been many efforts to improve the catalysts due to the strengthened regulation on NOx emission and implementation of real-driving emission [23-26]. Especially to achieve the super ultra low energy and emission vehicle (SULEEV), it is essential to improve the NOx removal efficiency at the low temperature. In this thesis, we try to understand the behavior of Cu ion under NH_3-SCR reaction, and apply it to development of the rational Cu-SSZ-13 catalyst with high performance. In Chapter 1, the mobility of Cu ion was experimentally observed. Mixture catalysts of Cu-SSZ-13 and H-SSZ-13 were prepared using different physical mixing methods to control the contact between them. When the Cu-SSZ-13 and H-SSZ-13 particles closely contact with each other, there was change in the species of Cu ion after the hydrothermal treatment. It was attributed to the migration of Cu ion from Cu-SSZ-13 to H-SSZ-13. Such change in species was not observed under thermal treatment without H_2O. It demonstrated that the Cu ion could migrate from a particle to another particle, and the presence of H_2O affects the mobility of Cu ions. In Chapter 3, the relationship between the mobility of Cu ion and the SCR reactivity was investigated. To prepare the catalyst with different mobility, the Cu species were controlled using hydrothermal treatment. Two Cu ion species, 1Al-Cu and 2Al-Cu, have different mobility due to their different coordination environments in SSZ-13 cage. Results for reactivity and characterization clearly demonstrated that the 1Al-Cu species are more active than the 2Al-Cu species. Kinetic study revealed that the discrepant reactivity is determined

by different mobility of Cu species, indicating that the high mobility of 1Al-Cu species leads to its superior SCR activity. In Chapter 4, we utilized the high mobility of 1Al-Cu species to improve the activity of Cu-SSZ-13. Co^{2+} ions were introduced into SSZ-13 to block the 2Al site of SSZ-13, inducing the Cu ion to be selectively located at 1Al sites. As a result, designed CuCo-SSZ-13 catalysts with higher ratio of 1Al-Cu species demonstrated higher SCR reactivity at 250-450 ℃ than conventional Cu-SSZ-13 catalysts. Based on the kinetic study, we found that high mobility of 1Al-Cu species enhanced the activity of catalyst, which showed the potential to develop the rational catalysts by tuning the mobility of ion in zeolite.

Chapter 2. Investigation of Cu ion mobility in the physical mixed Cu-SSZ-13

2.1. Introduction

Ionic Cu in Cu-SSZ-13 is known as the active site of the NH_3-SCR reaction [13, 17, 27]. One of the interesting properties of Cu ion is its mobility in the cage. According to a previous study, copper ions can move and change their position within a zeolite cage as temperature increase [28]. They also have mobility when molecules, such as water and NH_3, are adsorbed [13, 21, 29]. Deka *et al*. reported that the conformation of Cu ion changes from a center of six membered ring to a distorted tetrahedron site after the NH_3 adsorption[13]. Zema *et al*. proposed the positional changes of copper ion in a zeolite cage as a result of the hydration and dehydration process. The mobility of Cu ion in Cu-SSZ-13 is important because it is closely linked to the catalytic property [30]. According to previous reports from Paolucci *et al*.[21] and Gao *et al*.,[29] the formation of $[(NH_3)_2Cu^{II}]$-O_2-$[Cu^{II}(NH_3)_2]$ dimer that stems from migration of two copper ions is the rate-limiting step of low temperature NH_3-SCR reaction. They proposed that the low temperature NH_3-SCR activity in low copper loading samples is proportional to the copper loading in a square position due to dimer formation.

Despite these previous researches, the behavior of copper ions at high temperatures is still unidentified. The migration of the copper ions at high temperatures is important because it is related to the catalytic mechanism at high temperatures and deactivation process that stems from hydrothermal aging. Hydrothermal stability is regarded as one of the most critical issues for the zeolite catalyst in the NH_3-SCR. This is because it is a huge barrier for the catalyst to be utilized in a diesel engine of automobiles. There have been controversies over which of them is the main cause of the deactivation for the zeolite catalyst. Two paths have been proposed for the hydrothermal deactivation. One path is dealumination, which means the desertion of aluminium from the zeolite framework. The second path is the formation of copper oxide [10, 31]. It was previously suggested that the Cu-SSZ-13 catalyst would be deactivated by dealumination, which induced the formation of copper oxide and its agglomeration [23, 32]. On the contrary, Kim *et al*. insisted that the deactivation of Cu-SSZ-13 was attributed to the growth of copper oxide, which is formed by hydrothermal aging [33]. They suggested that Cu-SSZ-13 catalysts were more deactivated as the copper loading increased, which means that there were more chances of copper agglomeration. This result strongly supports the argument that the formation of copper oxide is the main cause of zeolite deactivation by hydrothermal aging, and not the dealumination that is widely accepted in recent researches [33-35]. The formation of copper oxide under the hydrothermal aging is expected to be relevant to the movement of

copper ions because the copper oxide clusters are formed by the agglomeration of the copper. However, the detailed process of their formation during the hydrothermal aging process is still not known. This needs to be investigated extensively to understand the hydrothermal deactivation mechanism.

In this study, we identified the long distance inter-particle migration of copper ions by comparing differently prepared and physical-mixed SSZ-13 catalysts treated by hydrothermal aging. We then characterized them by using various characterization methods. The different physical mixing methods gave rise to discrepancy of copper ions species in catalyst samples. They also resulted in the variation of the NH_3-SCR reaction in the catalysts. The inter-particle movement of copper ions is expected to provide insight in understanding the process of hydrothermal aging and the corresponding catalytic reaction at high temperatures.

2.2. Experimental

2.2.1. Catalysts preparation

The Cu-SSZ-13 catalysts were prepared by applying the conventional two-step ion exchange method. The zeolite that was used for ion exchange was the commercial H-SSZ-13 (provided by Heesung catalysts corp., Si/Al = 11.8 measured by 500 MHz solid nuclear paramagnetic resonance (Figure 2-1). First, the H-SSZ-13 was ion-exchanged with 1 M ammonium nitrate (NH_4NO_3, Sigma Aldrich, >98%) solution at 65 ℃ for 24 hours. Second, the ammonium exchanged SSZ-13 (NH_4-SSZ-13) was filtered with water washing. The filtered NH_4-SSZ-13 was dried overnight at the temperatures measuring 105 ℃. The prepared NH_4-SSZ-13 was ion-exchanged with 0.05 M copper nitrate ($Cu(NO_3)_2 \cdot 3H_2O$, Sigma Aldrich, >99%) solution at 65 ℃ for 24 hours to produce a Cu-SSZ-13 sample. A low copper loading SSZ-13 sample was prepared by ion-exchanging the NH_4-SSZ-13 with 0.0025 M $Cu(NO_3)_2 \cdot 3H_2O$ solution while stirring for 1 hour at 65 ℃. It also went through same filtration and drying steps. The dried catalysts were calcined at 550 ℃ for 4 hours. The copper loadings of the samples that were measured by an inductive coupled plasma-atomic emission spectroscopy (ICP-AES), were 1.72 and 0.75 wt. %, respectively (Table 2-1). The physical mixing of SSZ-13 was carried out by using two different methods. In the first method, the prepared high loading Cu-SSZ-13 and bare H-SSZ-13 were mixed at 1:1 weight ratio. The mixture was

ground in a mortar to promote a better mix and to ensure there was direct contact between the particles. We then sieved the ground mixture with a mesh that ranged from 35-50 and treated it under hydrothermal conditions (at 550 ℃ for 4 hours, 20% O_2 and 10% H_2O balanced with N_2). This catalyst is a physically mixed SSZ-13 with close contact and notated as PM-C-SSZ. Secondly, the Cu-SSZ-13 and H-SSZ-13 were sieved separately (35-50 mesh) and the mixture of the sieved granules, was treated under same hydrothermal condition. The catalyst, notated as PM-L-SSZ, is a physically mixed SSZ-13 where Cu-SSZ-13 and H-SSZ-13 particles were mixed with loose contact. The PM-C-SSZ and PM-L-SSZ have the same copper loading because they were same mixture of the Cu-SSZ-13 and H-SSZ-13. The low loading Cu-SSZ-13 (0.75 wt. % of Cu) after the hydrothermal treatment was compared with the physically mixed catalyst as a reference catalyst, and designated as $Cu_{0.75}$-SSZ.

2.2.2. Characterization

A H_2-temperature programmed reduction (H_2-TPR) analysis was carried out on a BEL-CAT II (BEL Japan Inc.). The catalyst samples were pretreated at 500 ℃ for 1 hour under O_2/He condition and cooled down to about 60 ℃. The samples were then heated up to 900 ℃ with the ramping rate of 10 ℃/min under 5% H_2/Ar flow. Hydrogen consumption of the catalysts were monitored by a thermal conductivity detector (TCD). The DRIFT experiments were performed in a diffuse reflectance cell (Praying Mantis, Harrick) installed in a Fourier transform infrared (FT-IR) spectroscopy (IS-50, Thermo Fischer Scientific) with an MCT detector. Before the experiments, the catalyst samples were pretreated in an air condition (80% N_2 and 20% O_2) at 400 ℃. After the pretreatment, the samples were exposed to 500 ppm of NH_3 at 200 ℃. The spectra were collected at 200 ℃ after NH_3 adsorption at a resolution of 4 cm^{-1} with 128 scans

NH_3-temperature programmed desorption experiments were performed by the use of a BEL-CAT I (BEL Japan Inc.). The samples were saturated with gaseous 1% NH_3 for 2 hours at the temperature of 160 ℃ after pretreatment at 400 ℃, for 1 hour under the O_2/N_2 condition. The saturated samples were purged with 10% H_2O and N_2 at 200 ℃ for 12 hours. The purged samples were heated to 800 ℃ with He flow, and the desorbed NH_3 was detected with the help of a TCD. Electron paramagnetic resonance (EPR) spectra were collected by EMX micro-9.5/2.7 (Bruker) at 150 K. Two kinds of

samples were prepared by using different pretreatment steps before the EPR measurement. One of the samples was the hydrated sample that was exposed to ambient condition. The second sample was the dehydrated sample that was pretreated at 200 ℃ in an argon glove box. Inductive coupled plasma-atomic emission spectroscopy (ICP-AES) analysis was performed with the use of the OPTIMA 4300DV, Perkin-Elmer (USA).

2.2.3. Reaction test

Standard NH_3-SCR reactions were performed in a fixed bed quartz tubular reactor with 0.05 g of catalysts. The total flow rate was 200 mL/min with the gas hourly space velocity (GHSV) of 240,000 mL g^{-1} h^{-1}. The NH_3-SCR reactivity is demonstrated by the NO_x conversion, and the N_2O concentration indicates the amount of by-product. NO_x concentration during the SCR reaction was measured by use of the NO_x chemiluminescence analyzer (42i High level, Thermo Scientific) under 500 ppm NO, 500 ppm NH_3, 8% O_2 and 5% H_2O balanced with N_2. The N_2O concentration was monitored by a FT-IR spectroscopy (Nicolet 6700, Thermo Fischer Scientific) with a 2 m gas cell that was heated at 120 ℃. The spectra were collected by the use of an MCT detector with 16 scans at a resolution of 1 cm^{-1}. The reactions were performed from temperatures starting from 150 ℃ to 500 ℃ with steps of 50 ℃. The NO_x conversion values of each temperature were then calculated from the collected data at a steady state by use of the following equation (Eq. (1)).

$$NO_x \text{ conversion } (\%) = \frac{[NO_x]_{in} - [NO_x]_{out}}{[NO_x]_{in}} \times 100 \qquad (1)$$

.

2.3. Results and Discussion

2.3.1. Different distribution of Cu ions in the physically mixed catalysts

It is generally known that two types of Cu ions, isolated Cu^{2+} on 2Al site (2Al Cu^{2+}) and $[Cu\text{-}OH]^{+}$ on 1Al site of SSZ-13 (1Al $[Cu\text{-}OH]^{+}$) exist in the Cu-SSZ-13 [36]. The copper species in the Cu-SSZ-13 can be distinguished and measured by using various characterization methods due to their different intrinsic properties [16, 37, 38]. The distribution of copper species was compared to display the difference in the physically mixed catalysts. The PM-C-SSZ and PM-L-SSZ showed different H_2 reduction peaks in the H_2-TPR profiles (Figure 2-2). The PM-C-SSZ had a smaller low temperature peak of 280 ℃ and a larger high temperature peak of 420 ℃ than the PM-L-SSZ. Since the H_2 consumption at high and low temperatures indicates the reduction of Cu^{2+} in 2Al Cu^{2+} and 1Al $[Cu\text{-}OH]^{+}$, respectively, the two physically mixed samples may have different distributions of copper species [16, 36-38]. The amount of copper ion species is quantified by deconvoluting hydrogen consumption profiles from the H_2-TPR of the catalysts (Figure 2-3, Table 2-2). The ratio of the 2Al Cu^{2+} increased in order of PM-L-SSZ, PM-C-SSZ, $Cu_{0.75}$-SSZ (0.275, 0.529, 0.619). That of 1Al $[Cu\text{-}OH]^{+}$ decreased (0.725, 0.471, 0.381). These variations were also displayed in the zeolite T-O-T vibration in the DRIFT spectra. After the NH_3 adsorption, the negative perturbation peaks at 945 cm^{-1} and 900 cm^{-1} appeared, which corresponded with 2Al Cu^{2+} and

1Al [Cu-OH]$^{+}$, respectively (Figure 2-4) [36, 39]. The PM-C-SSZ had the highest peak of 2Al Cu^{2+} and lowest at 900 cm^{-1} of 1Al [Cu-OH]$^{+}$. These were opposite for the PM-L-SSZ, which is good agreement with the H_2-TPR data.

The difference in the 2Al Cu^{2+} and 1Al [Cu-OH]$^{+}$ ratio was confirmed quantitatively by using the NH_3 wet TPD. When copper ions were exchanged with the H^{+}, which is a Brønsted acid site of SSZ-13, one 2Al Cu^{2+} was exchanged with two H^{+}, and one 1Al [Cu-OH]$^{+}$ was exchanged with one H^{+} due to charge balance. If all the copper ions are present in the form of 2Al Cu^{2+}, exchange stoichiometry of H^{+} to Cu would be 2:1. If they existed as the form of 1Al [Cu-OH]$^{+}$, the stoichiometry would be 1:1 [40]. Such coverage differences allow us to determine the relationship between amount of Brønsted acid sites and Cu ions in the Cu-SSZ-13 (Eq. (2)) [40]. The H^{+} indicates amount of Brønsted acid sites in the catalysts sample, and the H^{+}_{parent} is amount of Brønsted acid sites in the bare H-SSZ-13.

$$H^{+} = H^{+}_{parent} - 2 \times Cu_{2Al} - 1 \times Cu\text{-}OH_{1Al} \quad (2)$$

$$Cu_{total} = Cu_{2Al} + Cu\text{-}OH_{1Al} \quad (3)$$

In these relationships, we ignored the presence of CuO_x because the hydrothermal aging condition was too mild to form CuO_x. Moreover, there was no CuO_x reduction peak in the H_2-TPR profiles, which appeared as a sharp peak at 300 ℃ [33, 34]. If the amount of Brønsted acid sites is quantitatively measured (H^{+}_{parent}, H^{+}), the amount of 2Al Cu^{2+} and 1Al [Cu-OH]$^{+}$ can be

calculated from equations 2 and 3. This is because Cu_{total} is already known from the ICP-AES result. In order to titrate the Brønsted acid sites (H^+, H^+_{parent}), the NH_3-TPD experiment was performed after wet purging with H_2O. The weakly adsorbed NH_3 on Lewis acid sites of a zeolite was selectively desorbed through the purging process with H_2O [40, 41]. Only a single Brønsted acid peak at 450 ℃ was shown, which indicated that NH_3 on Lewis acid sites was fully desorbed. This means that the amount of the Brønsted acid sites was successfully titrated (Figure 2-5). The ratios of the remaining Brønsted acid sites of the physically mixed catalysts (H^+) to the total Brønsted acid sites in bare H-SSZ-13 (H^+_{parent}) were calculated by integrating the NH_3 desorption profiles (Table 2-3, Figure 2-6). From the NH_3 TPD in the wet conditions, the ratios of 2Al Cu^{2+} in PM-L-SSZ, PM-C-SSZ and $Cu_{0.75}$-SSZ were calculated and found to be 0.240, 0.532 and 0.578, respectively. The PM-C-SSZ has much higher 2Al Cu^{2+} ratio than the PM-L-SSZ. It is also close to that of $Cu_{0.75}$-SSZ, which corresponds well to the H_2-TPR results

Further quantification was performed through the EPR, which has been widely used to measure the amount of Cu^{2+} ion of zeolite in various researches [34, 37, 42, 43]. The amount of Cu^{2+} ion can be measured from the area of an integrated EPR spectra. Figures 2-7(a) and 2-7(b) represent the EPR spectra of hydrated and dehydrated samples, respectively. All the EPR spectra were collected at a cryogenic temperature (150 K) to freeze the mobility of copper ions. The two copper species can be identified by using their different

responses on EPR. Under hydrated conditions, the two kinds of hydrated copper species, $[Cu(H_2O)_6]^{2+}$ and $[(Cu\text{-}OH)(H_2O)_5]^{+}$, were both EPR active and detectable. After full dehydration, the Cu^{2+} on 2Al site was still detectable by the EPR, while $[Cu\text{-}OH]^{+}$ on 1Al site became EPR silent by a pseudo Jahn-Teller effect [44]. According to Figure 2-7(a), the EPR spectra of the hydrated samples have very similar shapes and intensity. On the other hand, the spectra of dehydrated samples had low intensity compared to the spectra of the hydrated samples. Moreover, each curves was also largely different both in shape and intensity, as shown in Figure 2-7(b). The different EPR spectra in the dehydrated samples mean different amount of 2Al Cu^{2+} because only 2Al Cu^{2+} was EPR active in the dehydrated form. By comparing the difference in the EPR spectra between the hydrated and dehydrated samples, the ratio of the two species of Cu ion, 2Al Cu^{2+} to 1Al $[Cu\text{-}OH]^{+}$, could be measured. The presence of CuO_x was ignored in the experiments due to the same reason as the one in the NH_3 wet TPD experiment. The ratios of the 2Al Cu^{2+} in PM-L-SSZ, PM-C-SSZ and $Cu_{0.75}$-SSZ that were obtained from the EPR experiments were 0.246, 0.596 and 0.568, respectively (Table 2-4). Figure 2-8 represents the quantified ratios of 2Al Cu^{2+} and 1Al $[Cu\text{-}OH]^{+}$ of the samples obtained from the H_2-TPR, NH_3 wet TPD and EPR experiments. It is worth noting that the three different methods provide similar ratios of copper ions in the physically mixed Cu-SSZ-13 and $Cu_{0.75}$-SSZ catalysts

Table 2-1. Amount of Cu and Al in Cu-SSZ-13 and low loading Cu-SSZ-13 from ICP-AES results.

Sample	Al (wt. %)	Cu (wt. %))	Cu/Al (mol ratio)
Cu-SSZ-13	2.52	1.75	0.296
$Cu_{0.75}$-SSZ	2.48	0.76	0.130

Table 2-2. Amount of two types of Cu ions in physically mixed SSZ-13 and reference from H_2-TPR.

Sample	Cu^{2+} amount from H_2 consumption (mmol/cat g)			
	1Al $[Cu\text{-}OH]^+$_1	1Al $[Cu\text{-}OH]^+$_2	2Al Cu^{2+}	Total
PM-L-SSZ	0.072	0.028	0.038	0.138
PM-C-SSZ	0.038	0.028	0.074	0.140
$Cu_{0.75}$-SSZ	0.028	0.020	0.078	0.126

Table 2-3. Quantification results and ratio of Cu species calculated from EPR analysis.

Sample	EPR spin concentration under hydrated	EPR spin concentration under dehydrated	Ratio of 2Al Cu	Ratio of 1Al Cu
PM-L-SSZ	1.05×10^{10}	2.56×10^{9}	0.246	0.754
PM-C-SSZ	1.25×10^{10}	7.47×10^{9}	0.596	0.404
$Cu_{0.75}$-SSZ	1.04×10^{10}	5.90×10^{9}	0.568	0.432

Table 2-4. Amount and occupied ratio of H^+ sites measured by NH_3 wet TPD

Sample	**Si/Al**[a]	**Al_f/Al**[a]	**Cu/Al_f**[b]	**H^+ (mmol/g)**[c]	**H^+/H^+_{parent}**[d]
H-SSZ-13	11.8	0.846	-	0.907[d]	1.000
PM-L-SSZ	11.8	0.846	0.175	0.710	0.783
PM-H-SSZ	11.8	0.846	0.175	0.664	0.732
$Cu_{0.75}$-SSZ	11.8	0.846	0.154	0.687	0.757

[a] Determined by ^{27}Si and ^{29}Al-solid NMR (Figure 2-1).

[b] Determined by ICP-AES.

[c] Determined by NH_3-TPD with wet purging.

[d] Determined by NH3-TPD of H-SSZ-13 with wet purging (H^+ parent).

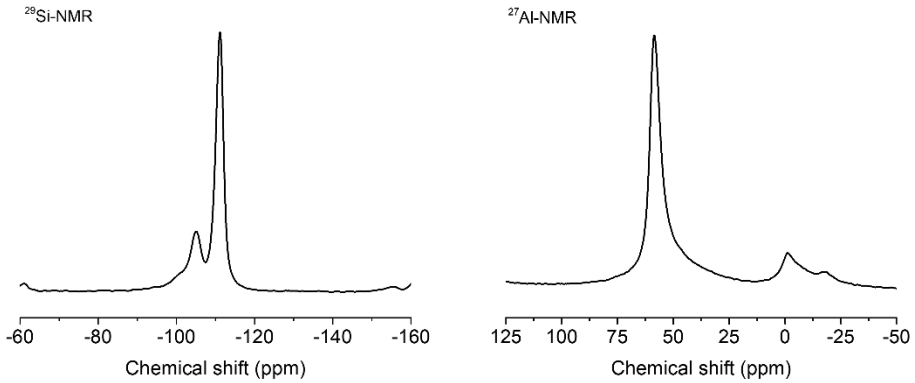

Figure 2-1. ^{27}Si and ^{29}Al solid NMR spectra of H-SSZ-13 with Si/Al=11.8.

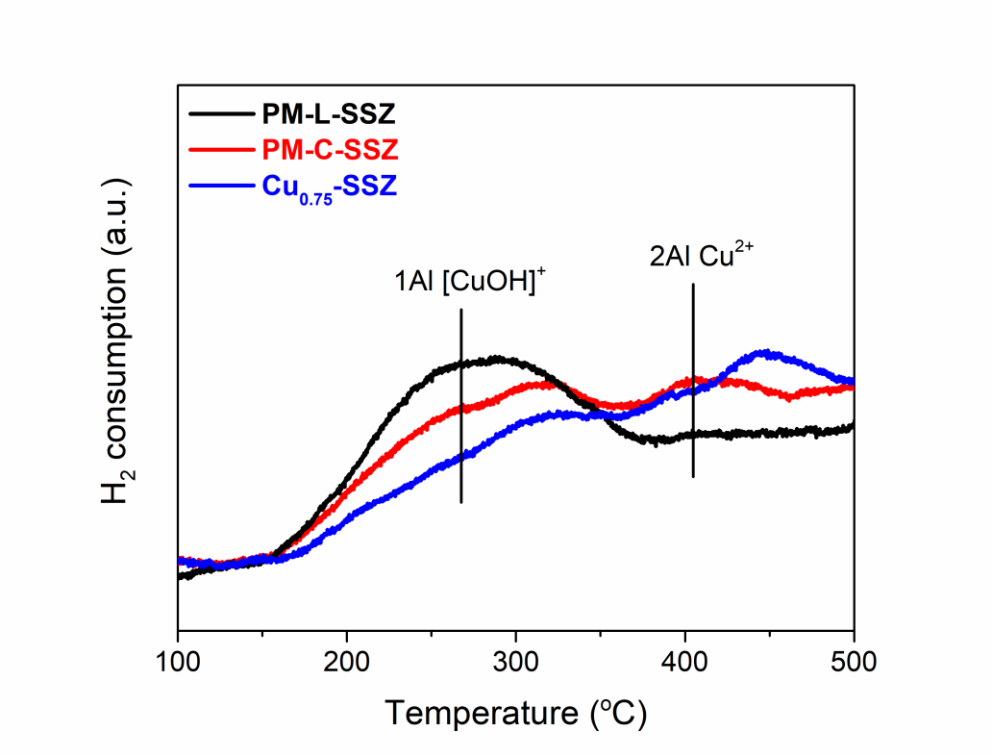

Figure 2-2. H_2-TPR profiles of PM-L, PM-C and $Cu_{0.75}$-SSZ catalysts. Peaks at 270 and 400 ℃ are assigned to reduction of the 1Al-Cu and 2Al-Cu species respectively.

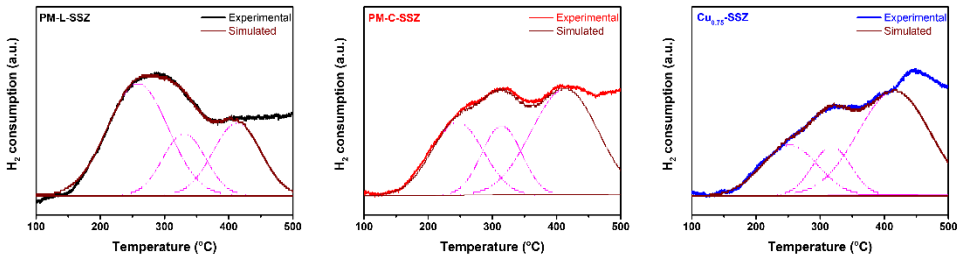

Figure 2-3. Deconvolution results of H_2-TPR profile in Figure 2-2.

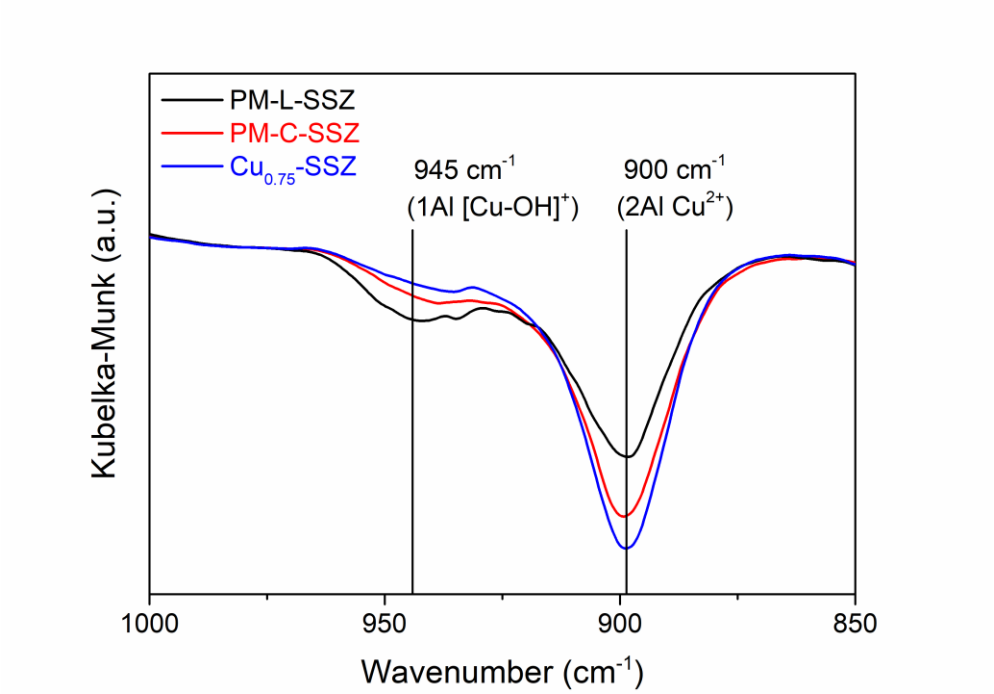

Figure 2-4. DRIFT spectra of T-O-T vibration peaks in PM-L, PM-C and $Cu_{0.75}$-SSZ catalysts after NH_3 adsorption for 60 min. The spectra of each samples before NH3 adsorption was used as background spectra.

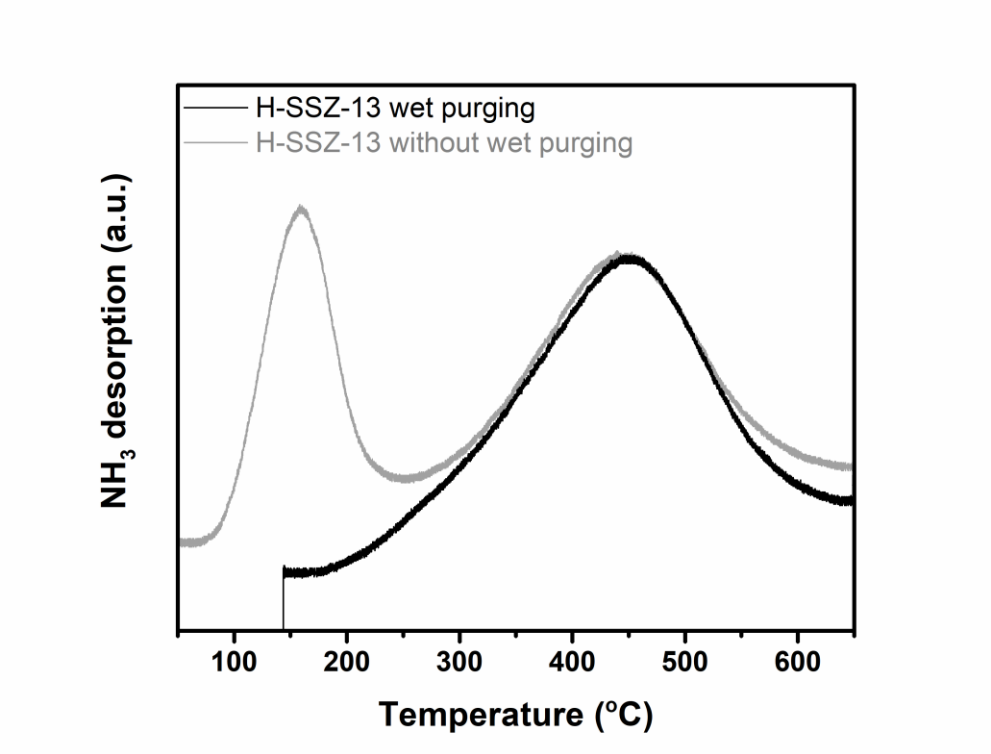

Figure 2-5. Comparison of NH_3 desorption profiles of H-SSZ-13 between with and without H_2O purging. Peaks at low and high temperature are assigned to desorption of NH_3 at Lewis and Brønsted acid sites, respectively.

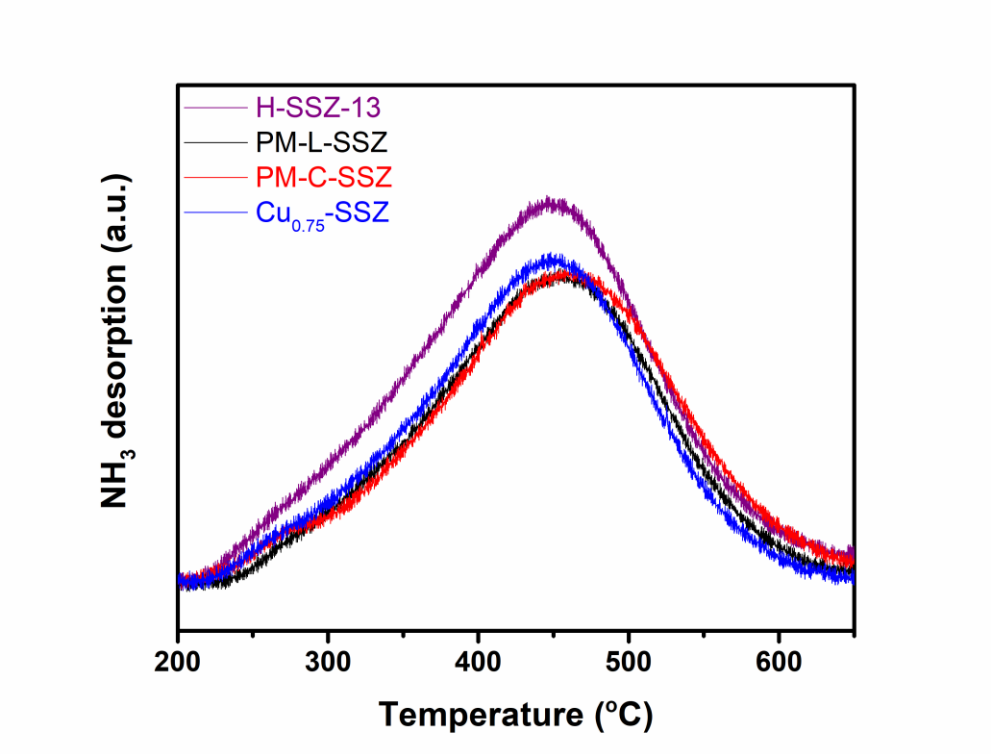

Figure 2-6. NH_3 desorption profiles over PM-L, PM-C, $Cu_{0.75}$ and H-SSZ-13 catalysts after H_2O purging.

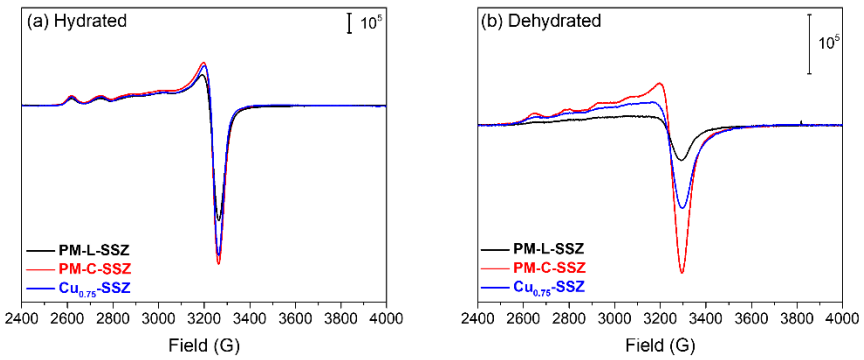

Figure 2-7. EPR spectra of PM-L, PM-C and $Cu_{0.75}$-SSZ catalysts collected at 150 K under (a) hydrated and (b) dehydrated condition.

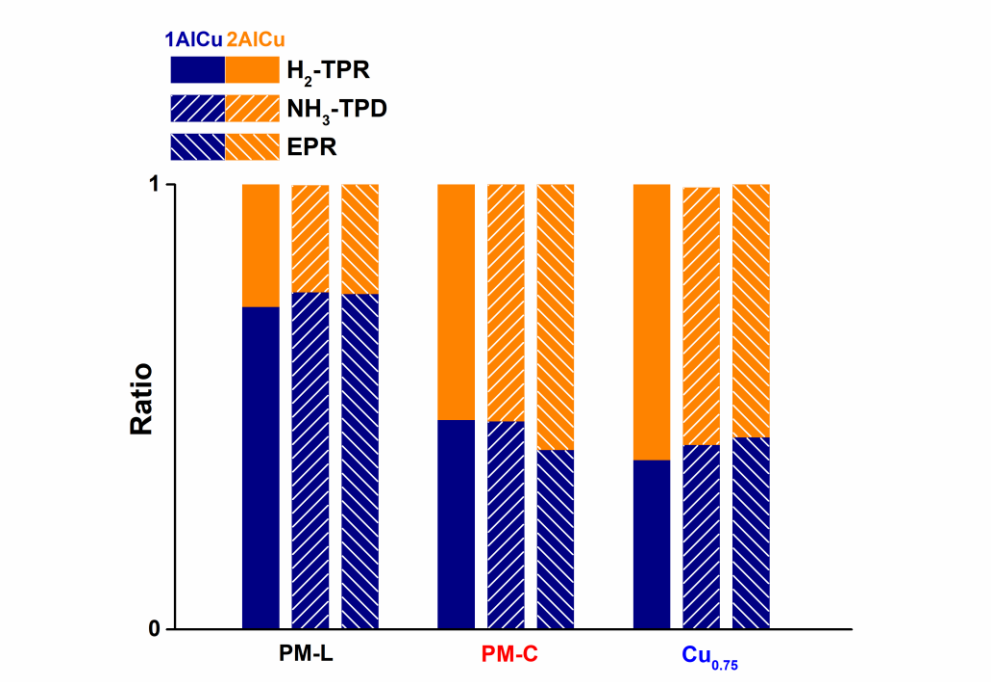

Figure 2-8. Ratio of the 2Al-Cu and 1Al-Cu of PM-L, PM-C and $Cu_{0.75}$-SSZ catalysts from quantification results by H_2-TPR, NH_3-TPD and EPR.

2.3.2. Variation of NH_3-SCR reactivity in the physically mixed catalysts

Different distributions of copper ions in the physically mixed catalysts must result in the variation of the catalytic properties. To examine the catalytic differences of the catalysts, a NH_3-SCR reaction was carried out. The NO_x conversion and N_2O concentration profiles from the NH_3-SCR reaction are as shown in Figure 2-9. The NH_3-SCR activity and N_2O formation at low temperatures increased in the order of $Cu_{0.75}$-SSZ, PM-C-SSZ and PM-L-SSZ. It was notable that the PM-C-SSZ and PM-L-SSZ had different NO_x conversion and N_2O concentration profiles, even though they had the same loading of copper. In addition, the profiles of the PM-C-SSZ showed similar trends to those of the $Cu_{0.75}$-SSZ. Contrary to the PM-L-SSZ, both the PM-C-SSZ and $Cu_{0.75}$-SSZ catalysts displayed concave curves at low temperatures and a small decrease in the NO_x conversion at 350 ℃. Despite large increases at 250 ℃ in the N_2O concentration of PM-L-SSZ, no drastic changes in the N_2O formation were shown in that of the PM-C-SSZ and $Cu_{0.75}$-SSZ within the temperature range. It was inferred that the PM-C-SSZ and $Cu_{0.75}$-SSZ have similar catalytic properties, probably attributed to the similar distribution of copper ions as observed by various characterizations.

2.3.3. Inter-particle migration by hydrothermal treatment

All the characterization results clearly indicate that the PM-C-SSZ has a higher ratio of 2Al Cu^{2+} than the PM-L-SSZ, even though the copper loading of the catalyst was the same. Compared to the original Cu-SSZ-13, which was used in the physical mixing, the PM-L-SSZ showed almost similar copper species in the H_2-TPR (For precise comparison, the Cu-SSZ-13 was also treated under same hydrothermal aging condition, and the H_2 consumption profile of the Cu-SSZ-13 was multiplied by 1/2 to adjust the copper loading) (Figure 2-10). It means that the amount of 2Al Cu^{2+} in the PM-C-SSZ increased, whereas there was few changes in the distribution of copper ions in the PM-L-SSZ treated by hydrothermal aging, after the physical mixing. The increased amount of 2Al Cu^{2+} was the same as with the decrease in the 1Al $[Cu\text{-}OH]^{+}$ (Table 2-2). These results indicate that some of the 1Al $[Cu\text{-}OH]^{+}$ changed their conformation to the 2Al Cu^{2+} in the PM-C-SSZ following the hydrothermal treatment. It can be claimed that such a difference originates from changing the method of physical mixing because all other factors are same.

In order to explain the phenomenon, we suggested that the conformation change of the copper ions originated from the copper ion migration from the Cu-SSZ-13 particles to H-SSZ-13 particles in the PM-C-SSZ, as shown in Scheme 1. It is generally known that Cu ion becomes mobile under hydrothermal conditions, which was also mentioned in the Introduction Section [28, 30]. Copper ions were confined in the Cu-SSZ-13 particles of the

PM-L-SSZ and could not move to the H-SSZ-13 particles because the particles in the PM-L-SSZ were remotely located, so that, there was no change in the conformation of Cu ion compared to the original Cu-SSZ-13. On the other hand, as the Cu-SSZ-13 and H-SSZ-13 particles in the PM-C-SSZ come into direct contact, some of the copper ions might be able to migrate the interface of the Cu-SSZ-13 and H-SSZ-13 (Figure 2-11). When some of the $[Cu\text{-}OH]^+$ on 1Al sites, with higher mobility, move to H-SSZ-13 particles, they preferentially occupy the empty 2Al sites of H-SSZ-13 because the 2Al site is a thermodynamically more stable site than the 1Al site [16, 36, 45]. In this process, the migrated copper ions change their conformation from the 1Al $[Cu\text{-}OH]^+$ to the 2Al Cu^{2+}. The process illustrates the reason as to why the 2Al Cu^{2+} ratio in the PM-C-SSZ increases after inter-particle ion migration.

If exactly a half of copper ions in the Cu-SSZ-13 (Cu loading: 1.7 wt. %) move to the H-SSZ-13, the PM-C-SSZ theoretically becomes a mixture of Cu-SSZ-13, which has 0.85 wt. % copper. In this case, the PM-C-SSZ probably had almost the same distribution of Cu ions as the $Cu_{0.75}$-SSZ, whose copper loading was nearly a half of the Cu-SSZ-13 (Figure 2-11). As more copper ions migrate to the H-SSZ-13, the PM-C-SSZ became closer to the $Cu_{0.75}$-SSZ, which is similar to the ideal migration case and farther from the PM-L-SSZ, where no migration of the copper ion occurs. It was confirmed that the PM-C-SSZ had a commensurate ratio of 2Al Cu^{2+} and 1Al $[Cu\text{-}OH]^+$ with the $Cu_{0.75}$-SSZ, which was a different value with the PM-L-SSZ in all the

quantification results (Figure 2-8). Hence, it can be stated that the considerable amount of copper ions in the PM-C-SSZ migrates from the Cu-SSZ-13 to the H-SSZ-13 particles through the hydrothermal treatment. The similarity between the PM-C-SSZ and $Cu_{0.75}$-SSZ also ensured that there was copper ion migration in the PM-C-SSZ.

The same result is also displayed in the NH_3-SCR reactivity tests. The PM-C-SSZ shows lower NH_3-SCR reactivity than the PM-L-SSZ (Figure 2-9 (a)). This probably resulted from the variation in the distribution of copper ions arising from the ion migration. The PM-L-SSZ has a higher volumetric density of copper than the PM-C-SSZ because copper ions in the PM-L-SSZ were confined to the Cu-SSZ-13 particles. This means that they existed only in the Cu-SSZ-13 occupying only a half of the total SSZ-13 volume. On the other hand, as a result of ion migration, copper ions in the PM-C-SSZ were present in both the Cu-SSZ-13 and H-SSZ-13 particles. Moreover, its average Cu-Cu distance became longer than that of the PM-L-SSZ (Figure 2-11). The change in density gave rise to the difference of the NO_x conversion in the physically mixed SSZ-13. This is because the low temperature NH_3-SCR activity of Cu-SSZ-13 depends on the volumetric density of Cu ions [29]. At low temperatures, the oxidation of Cu^+ to Cu^{2+}, which is a rate-limiting step of the NH_3- SCR reaction cycle occurred via the formation of the oxygen-bridged copper dimer ($[(NH_3)_2Cu^{II}]$-O_2-$[Cu^{II}(NH_3)_2]$). Such a dimer is produced by the reaction of two copper species solvated by NH_3. Since shorter Cu-Cu distance leads to

faster reactions, the volumetric density of copper ions has a positive correlation with the low temperature NH_3-SCR reactivity. This theory illustrates that the PM-L-SSZ that has a high density of copper ions shows higher NO_x conversion than the PM-C-SSZ, which has low density of copper ions (Fig. 5(a)). The similarity between the PM-C-SSZ and $Cu_{0.75}$-SSZ was also confirmed by the analogous trends of the NO_x conversion and N_2O concentration profiles, which means that copper density in the PM-C-SSZ becomes closer to $Cu_{0.75}$-SSZ, resulting from the ion migration (Figure 2-9, 2-11). It was expected that the reactivity tests of the PM-C-SSZ and $Cu_{0.75}$-SSZ were not exactly the same, because the copper ions were not ideally migrated.

The suggested migration model clearly explains the variation of the 2Al Cu^{2+} ratio and NH_3-SCR reactivity in the catalysts. We call this 'inter-particle ion migration'. Most of the previous researches regarding ion migration in zeolite report on the ion movement inside a cage or inter-cage of a particle [13, 21, 28, 29]. It is a very short distance migration that is about a few angstroms. However, the inter-particle migration is a much longer movement than those of former studies, which is longer than the order of a few hundred nanometer. It is noteworthy that not only typical intra-particle movement in a cage, but also longer distance of copper ions which is referred in this study as inter-particle migration is possible in Cu-SSZ-13. Two factors were suggested as driving forces of the inter-particle ion migration. One of this was the simple concentration gradient and the other was a preference to a more

energetically stable site. The conformation change of copper ions, especially, occurs by the preference to stable site. One of the other important factors for the inter-particle migration is the presence of water. Physically mixed catalyst with close contact that was treated under a thermal aging condition at 550 ℃, without H_2O (PM-C-SSZ_TA), had a lower 2Al Cu^{2+} peak in the H_2-TPR than the PM-C-SSZ. It also had almost a similar peak height with the PM-L-SSZ (Figure 2-12). This indicates that the little amount of copper ions migrate to other H-SSZ-13 particles, since the mobility of copper ions was not strong enough to move across the particle-particle interface without water. The hydration effect on the ion mobility was also previously suggested by Psofogiannakis et al. [46]. This result shows that the presence of water plays a significant role for the copper ions to move more actively in the longer distance.

2.3.4. Migration of Cu ions and hydrothermal stability

Hydrothermal stability is one of the most important issues for applying the zeolite catalyst to the NH_3-SCR. This is because it is closely related to the catalytic deactivation [47, 48]. There were two suggested deactivation pathways; one was the dealumination and the other was the formation of copper oxide [10, 33, 49-51]. In recent studies, the formation of copper oxide was proposed as the main cause of deactivation for zeolite catalysts after hydrothermal aging [33, 34]. Song *et al*. reported that the $[Cu\text{-}OH]^+$ was converted to the copper oxide cluster as the hydrothermal aging temperature increased [34]. Since the 1Al $[Cu\text{-}OH]^+$ had a lower hydrothermal stability than the 2Al Cu^{2+}, it was designated as the main cause of deactivation [48, 52]. We speculated that the formation of copper oxide cluster from $[Cu\text{-}OH]^+$ was closely related to the mobility of copper, because several copper ions should encounter each other, resulting in the formation of a copper oxide cluster. In a low copper loading zeolite, whose Cu-Cu distance is far, a long distance migration of copper ions is an essential process to form a copper oxide cluster. This process explains the poor hydrothermal stability of the 1Al $[Cu\text{-}OH]^+$ because it has a weaker bond with the zeolite framework and higher mobility than the 2Al Cu^{2+}. We propose that the higher mobility of copper ion leads to a longer migration, which means a higher probability to encounter and aggregate, as a result, more deactivation. Deka *et al*. also agreed that a high mobility of copper ion can lead to the formation of copper oxide clusters [53].

In conclusion, the migration of copper ions resulted in the formation of copper oxide during the hydrothermal aging, which deactivates the Cu-SSZ-13 catalysts. This implies that the mobility of copper ions would determine the hydrothermal stability of copper-zeolite. The research for ion migration would provide insights to understand the deactivation mechanism of Cu-SSZ-13 zeolite catalysts.

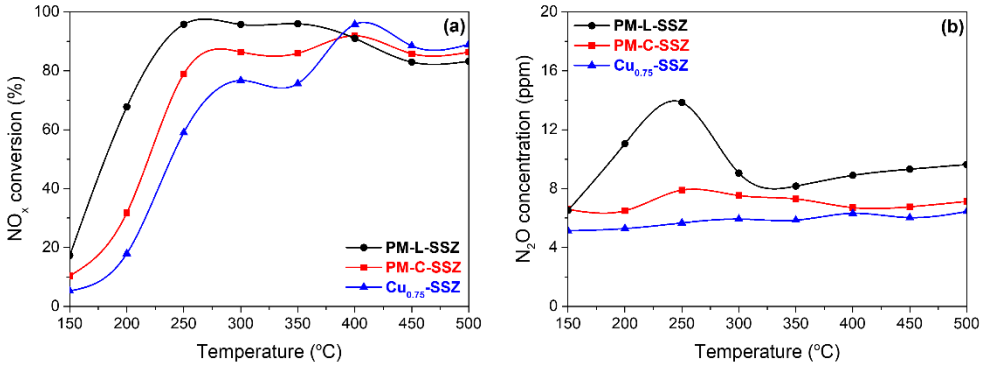

Figure 2-9. SCR reactivity over PM-L, PM-C and $Cu_{0.75}$-SSZ catalysts: (a) NO_x conversion, (b) N_2O concentration. Reaction condition: 500 ppm NO, 500 ppm NH_3, 8% O_2, and 5% H_2O balanced with N_2 at a GHSV of 240,000 mL g^{-1} h^{-1}.

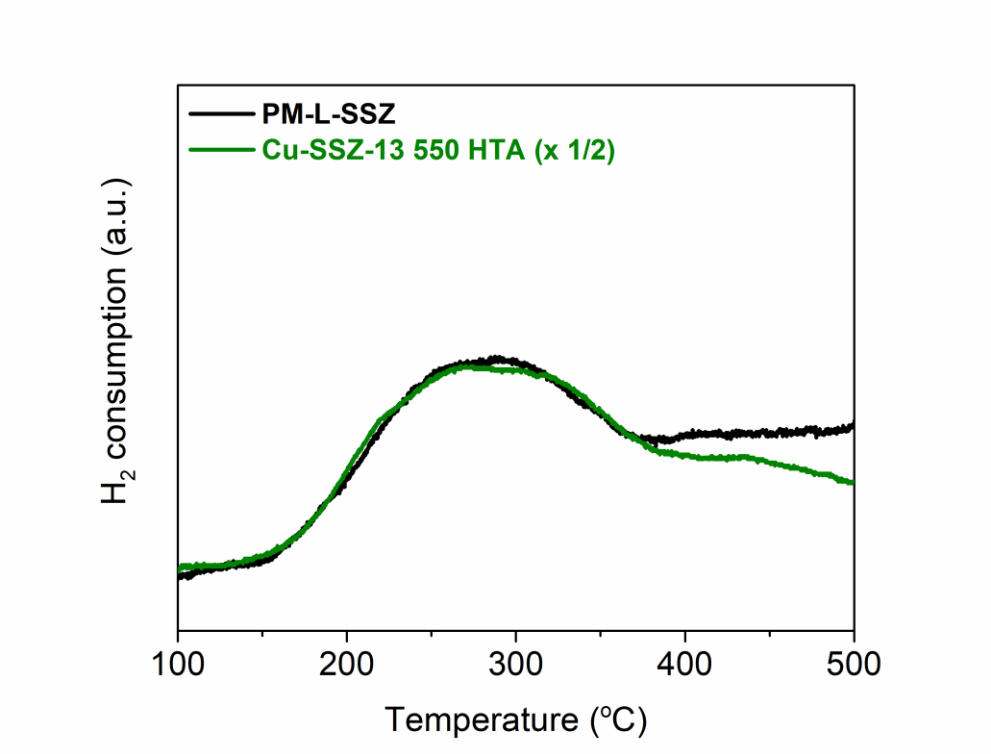

Figure 2-10. H_2-TPR profiles over the PM-L-SSZ and Cu-SSZ-13 HTA 550. Hydrogen consumption profiles of Cu-SSZ-13 are multiplied by 1/2 for comparison by same amount of Cu ion

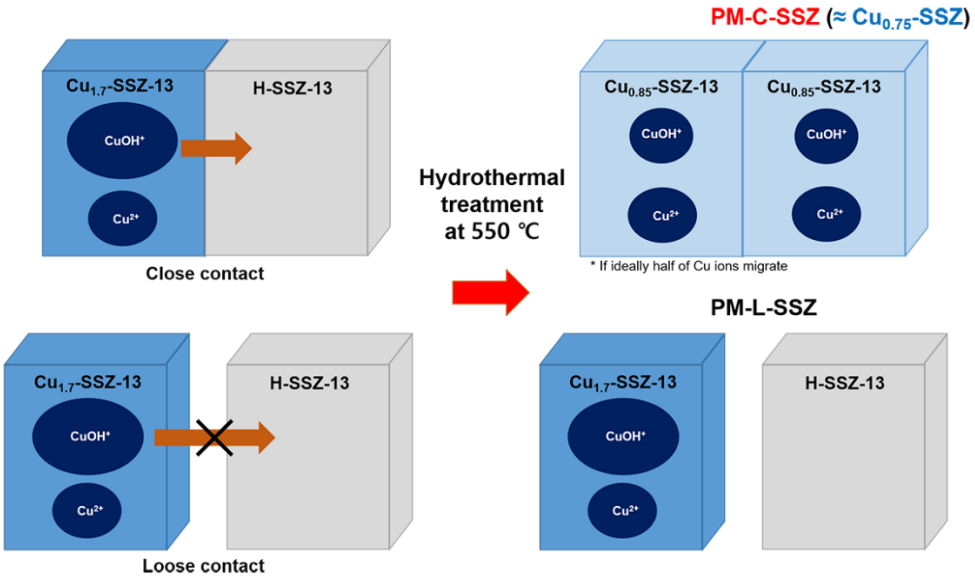

Figure 2-11. Schematic of inter-particle migration of copper ion over physically mixed SSZ-13 catalysts and comparison with $Cu_{0.75}$-SSZ.

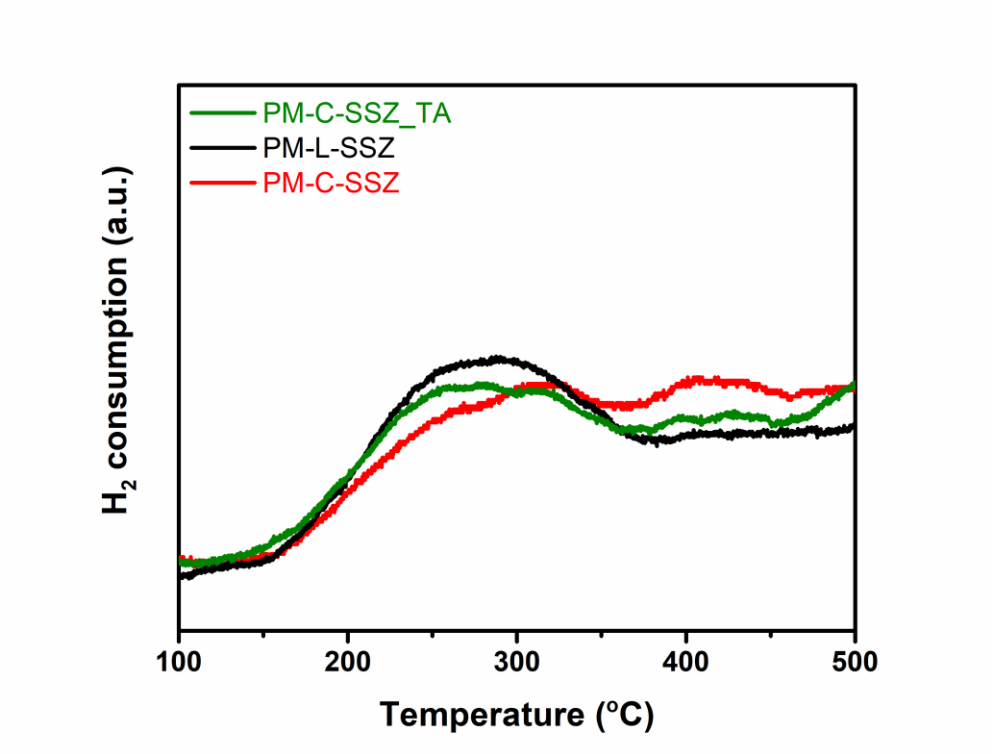

Figure 2-12. H_2-TPR profiles over physically mixed SSZ-13 catalysts treated under hydrothermal condition (black, red line) and only thermal condition without H_2O (green line).

.

Chapter 3. Relationship between mobility of Cu ions and NH_3-SCR reactivity of Cu-SSZ-13

3.1. Introduction

1Al-Cu and 2Al-Cu are the two types of Cu ions in Cu-SSZ-13, and these are determined by the positions where the Cu ions are located [36, 54]. 1Al-Cu is a Cu^{2+} ion coordinating to a single Al site that exists in the form of Z-(Cu^{2+}-OH^-) [38]. 2Al-Cu is a Cu^{2+} ion that coordinates to two adjacent Al sites as 2Z-Cu^{2+}. Many researchers have reported that these species have different reactivities in various reactions, such as NO, CO and NH_3 oxidation [55-59]. On the other hand, in the case of NH_3-SCR, such site-specific reactivity has not been clearly established. Paolucci et al. proposed that the two Cu ion species have an equivalent activity over the NH_3-SCR reaction regardless of their sites by comparing two model catalysts, which predominantly contained the 1Al-Cu or 2Al-Cu species [16, 60]. They insisted that NH_3 solvation liberated Cu ions from the framework and masked the difference between two Cu species. However, these model catalysts were compared under the limited condition with a fixed Cu content and reaction temperature, which should have considered other parameters such as the reaction kinetics.

Recent researches have suggested different SCR reactivities of the Cu ion species [30, 61]. Godiksen et al. used *in-situ* EPR analyses to report different reactivities for two kinds of 2Al-Cu sites in a 6-membered ring. However, they were not able to compare the reactivity of 1Al-Cu and 2Al-Cu due to a limitation of the EPR spectroscopy [61]. Gao et al. emphasized the significance of the 1Al-Cu species in the SCR reaction since the 1Al-Cu species have a higher mobility due to a weaker electrostatic interaction with the zeolite framework [20]. The authors asserted the existence of a unique homogeneous-catalyst-like mechanism of the Cu-SSZ-13 governed by NH_3-solvated mobile Cu ion species at temperatures under 250 °C, which implied the importance of Cu ion mobility in NH_3-SCR [62]. However, there has still been controversy regarding the higher SCR reactivity of the 1Al-Cu species related to their high mobility, since it has not been clearly verified [62].

In this study, we attempt to resolve this controversy by experimentally demonstrating the different NH_3-SCR reactivity between 1Al-Cu and 2Al-Cu. We tried to elucidate the origin of the discrepancy in the SCR reactivity of the Cu ion species and revealed that the different mobility of 1Al-Cu and 2Al-Cu determined their different reactivity, which was theoretically suggested by Gao et al. in the previous report [20].

3.2. Experimental

3.2.1. Catalyst synthesis

SSZ-13 ($Si/Al_2 = 9$) was synthesized by hydrothermal synthesis using our previous methodology [63, 64]. 0.8 g of NaOH (Sigma Aldrich) and 25 g of Na_2SiO_3 (Sigma Aldrich) were dissolved in D.I water 52 mL. After vigorous stirring for 30 min under ambient condition, 2.5 g of CBV 500 (Zeolyst) and TMAdaOH (SACHEM) 10.5g were added and stirred for 30 min under ambient condition. Prepared mixture was transferred 200 mL Teflon-lined stainless steel autoclaves and placed in a forced convection oven at 140 °C for 5 days. The obtained solution was washed with D.I water, dried at 105 °C and calcined at 550 °C for 8 hours with ramping rate 1 °C /min. Ammonium ion exchange was process repeated two times using 1 M ammonium nitrate solution (Sigma Aldrich) at 65 °C to get an NH_4^+ form SSZ-13. Cu ion was also exchanged by using a conventional ion exchange method. NH_4^+-SSZ-13 was added in 0.0046 M copper nitrate trihydrate precursor (Sigma Aldrich), and stirred at 65 °C for 24 hours for Cu ion exchange. The mixture was filtered and dried in a forced convection oven at 105 °C. Dried catalyst was calcined at 550 °C for 4 hours denoted as Cu-SSZ-13. The Cu-SSZ-13 2.7wt, 6wt HT-x catalysts were synthesized using same method with different concentration precursor solution (0.0075, 0.087 M respectively), and their Cu loading was

verified by using an ICP-AES (data were not shown).

3.2.2. Catalyst characterization

Electron paramagnetic resonance (EPR) experiments were conducted on an EMXmicro-9.5/2.7 spectrometer (Brucker). Hydrated samples were prepared overnight hydration under saturated vapor pressure at an ambient condition. Samples were dehydrated overnight under flowing dry air at 200 °C, and sealed in an Ar glove box to obtain dehydrated samples. Powder samples (~10 mg) were loaded in 5 mm OD quartz tube (Wilmad). Microwave power was 0.73 mW, and the frequency was 9.41 GHz. The field was swept by 3000 G in 31 s, and modulated at 100 kHz with 1 G amplitude. Time constant was 1.28 ms. All spectra were obtained at -123 °C to freeze mobile Cu ions. Amount of Cu^{2+} ion was calculated from double integration of the spectra. The area of spectra was quantified from one-point calibration using Cu-EDTA standard solution (0.025 M, Sigma Aldrich). All measurements were conducted three times per each samples. Amount of Cu ion species was quantified by averaging the values, and errors of the data were below 3.5 %.

Micropore volumes of Cu-SSZ-13 HT-x were measured from Ar adsorption isotherm by using a Micromeritics 3Flex Surface and Catalyst Characterization. Typically, 0.02-0.03g of samples were loaded on the cell, and isotherms were obtained at -186 °C after degassing at 120 °C overnight. X-ray diffraction (XRD) patterns were obtained on a Smartlab (Rigaku)

operated at 40 kV and 30 mA.

Solid-state ^{29}Si-NMR spectra were obtained at 130.32 MHz on a Brucker Avance III HD (Brucker) under ambient condition (23 °C). All data were measured under magic angle spinning (MAS) at a spinning rate of 10 kHz. The pulse length was 2 μs, and the delay time was 0.1 s.

ICP-AES results were obtained by OPTIMA 8300 (Perkin-Elmer) to measure the amount of copper and aluminum in Cu-SSZ-13. DRIFT spectra were obtained in a diffuse reflectance cell (Praying Mantis, Harrick) using a Fourier transform infrared (FT-IR) spectroscopy (Nicolet 6700, Thermo Fisher Scientific). In the DRIFT experiments, the samples were pretreated at 400 °C under air condition for 1 hour. After pretreatment, NH_3 was adsorbed at 200 °C under 500 ppm NH_3 and 10% O_2 with N_2 balanced. Then, it was purged with N_2+O_2 for 30 min, and pre-adsorbed NH_3 was reacted with 500 ppm NO and 10% O_2.

3.2.3. NH_3-SCR reaction tests

Reactivity data of NH_3-SCR were measured in a down-flow 1/4'' ID tubular quartz reactor. All samples were pelletized and sieve to 300-500 μm particles to prevent pressure drop. Reactions were performed under 500 ppm NO (5000 ppm in N_2, Deokyang Co., Ltd.), 500 ppm NH_3 (5000 ppm in N_2, Deokyang Co., Ltd.), 10% O_2 (99.995%, Daesung industrial gases Co., Ltd.), 5% H_2O (deionized, introduced from PURELAB Chorus, ELGA in the wet SCR) and balance N_2 (99.999%, Daesung industrial gases Co., Ltd.). The gas hourly space velocity (GHSV) was 240,000 mL/h·g_{cat}. NOx concentration was recorded using NOx chemiluminescence analyzer (42i High level, Thermo Scientific). NOx conversion was calculated using the following equation. In the case of dry SCR reaction, the catalysts were pretreated at 200 °C under air condition for a dehydration before the reaction.

$$NOx\ \ conversion\ \ (\%) = \frac{[NOx]_{in} - [NOx]_{out}}{[NOx]_{in}} \times 100$$

NOx consumption rate in the NH_3-SCR reaction is calculated using

$$r = \frac{F}{W}(-ln(1 - X))$$

where F is the molar NOx feed rate (mol/s), W the catalyst weight (g) and X the NOx conversion [42]. NH_3-SCR reactivity of the catalyst is represented by

turnover frequency (TOF) defined as the NOx consumption rate per mol of active Cu ion. The apparent activation energy of the catalyst is obtained from Arrhenius equation by plotting 1000/T (K^{-1}) vs ln(TOF).

3.3. Results and Discussion

3.3.1. Controlling the Cu ion species

The synthesized Cu-SSZ-13 catalyst was treated under a hydrothermal condition (under 20% O_2, 10% H_2O balanced with N_2 at 550 °C) for 0.5, 1, 2 and 8 hours to control the ratio of 1Al-Cu to 2Al-Cu (denoted as Cu-SSZ-13 HT-x, x indicating treatment duration time) [34, 39]. Electron spin resonance (EPR) was performed for the hydrated and dehydrated Cu-SSZ-13 HT-x to measure the amount of total Cu ions and the ratio of 1Al-Cu to 2Al-Cu in the catalysts. In the hydrated Cu-SSZ-13, all isolated Cu^{2+} ions were detected in the EPR measurement, and their amount was quantified using a Cu-EDTA standard solution (0.025 M, Sigma Aldrich) (Figure 3-1, 3-2). The measured amount of Cu^{2+} ions was 2.09 wt.% on average, which was almost the same value as that obtained from an ICP-AES (2.08 wt.%) (Table 3-1, Figure 3-3a), illustrating that all Cu species existed as an ionic Cu^{2+} without forming CuOx and Cu^{+} ion. All catalysts were confirmed to have almost identical crystallinity, surface area and Si/Al ratio based on XRD, BET and ^{29}Si-NMR results, respectively (Figure 3-4a, 3-5, 3-6a, Table 3-2), ruling out the deterioration in the structure of SSZ-13 after the hydrothermal treatment.

In the case of dehydrated Cu-SSZ-13, only 2Al-Cu were detected via

EPR analysis because the dehydrated 1Al-Cu was EPR-silent due to a pseudo-Jahn-Teller effect (Figure 3-3b) [34, 65]. Using the different EPR-responses of 1Al-Cu and 2Al-Cu, each amount of 1Al-Cu and 2Al-Cu could be calculated by comparing the EPR spectra of the hydrated and dehydrated catalysts (Figure 3-7a, Table 3-1). As the duration of the hydrothermal treatment increased from 0.5h to 8h, the ratio of 1Al-Cu decreased from 0.177 to 0.104. Such conformation change from 1Al-Cu to 2Al-Cu is supposed to be a result of the following two reasons. First, the hydrothermal treatment provided sufficient thermal energy enabling conversion from 1Al-Cu to a more thermodynamically stable 2Al-Cu [34, 39]. Second, the paired 2Al sites increased due to the redistribution of Al in Cu-SSZ-13 after hydrothermal treatment, as evidenced by the increase in the 2Al-Si in the ^{29}Si-NMR data (Figure 3-6b).

The change in the ratio of 1Al-Cu and 2Al-Cu was also confirmed by a DRIFT analysis. NH_3 pre-adsorbed Cu-SSZ-13 HT-x catalysts showed negative perturbation peaks at 940 and 897 cm^{-1} assigned to the 1Al-Cu and 2Al-Cu species, respectively (Figure 3-7b) [36, 66]. The perturbation peak of 2Al-Cu in the DRIFT spectra increased in the order of HT-0.5h, 1h, 2h and 8h, which showed a linear relationship with the results from the EPR analysis (Figure 3-7c). It implies that our EPR quantification of 1Al-Cu and 2Al-Cu is

reliable. These results indicate that the ratio of 1Al-Cu was successfully tuned in our Cu-SSZ-13 HT-x catalysts without deteriorating the zeolite structure.

3.3.2. Species dependent SCR reactivity of Cu-SSZ-13

The NH_3-SCR reactivity of the Cu-SSZ-13 HT-x catalysts was measured using a fixed-bed reactor at a temperature from 130 to 300 °C to identify the species-dependent reactivity. Under a dry standard SCR reaction, the catalysts had a different reactivity (Figure 3-8a). The reactivity increased in the order of the Cu-SSZ-13 HT-8, 2, 1 and 0.5h samples, which demonstrated the same trend to increase in the 1Al-Cu ratio, indicating that the 1Al-Cu is more active in the SCR than the 2Al-Cu species. Interestingly, after the addition of H_2O (under a wet SCR condition), all catalysts showed the same NOx conversion regardless of having different 1Al-Cu/2Al-Cu ratios, which was consistent with the precedent result proposing equivalent reactivity of the Cu ion species (Figure 3-8b) [16]. The addition of H_2O in the reactants is known to alter only the reaction rates, rather than the overall mechanism of the SCR reaction [66-68]. Therefore, understanding different reaction kinetics between dry and wet reactions will be the main key to reveal the origin of the different SCR reactivity of both Cu ion species. An apparent activation energy (E_a) of the dry and wet SCR reaction was obtained based on the Arrhenius equation as ~45 kJ/mol and ~70 kJ/mol, respectively (Figure 3-8c, d, Table 3-1). Previous studies have already revealed which rate-limiting factors governed the reactions depending on each of the activation energy values. The

obtained activation energy values of ~45 kJ/mol from our dry SCR data demonstrate that the reactions were limited by a mass-transfer of two Cu ion species to form dimeric Cu ion intermediates, $[Cu^{I}(NH_3)_2]^{+}-O_2-[Cu^{I}(NH_3)_2]^{+}$ [20-22]. The mobility of the Cu ions is significant in this chemistry because the migration of the Cu ion species is essential to meet each other to form dimeric Cu species [69]. The rates of dry SCR reaction at 200 °C actually have a linear correlation to the square of the Cu/Al ratio, which is clear evidence to substantiate that the rate-limiting step of the reaction is the participation of two Cu ion species (Figure 3-9, 3-10) [20]. The apparent E_a values ~70 kJ/mol of the Cu-SSZ-13 in the wet SCR indicate that the reactions were no longer limited by the Cu ion transport and were instead governed by the re-oxidation process of Cu^{+} and the formation of NO_2 [20]. The presence of H_2O is believed to have sufficiently increased the diffusion rate of the Cu ion species so that the ion mobility had little effect on the reaction rate of wet SCR [64, 70, 71].

Table 3-1. Structural properties of the Cu-SSZ-13 HT-x catalysts.

Samples	Si/Al[a]	BET surface area[b] (m^2/g)	Relative crystallinity[c]
Cu-SSZ-13 HT-0.5h	5.25	560	1
Cu-SSZ-13 HT-1h	5.33	660	0.92
Cu-SSZ-13 HT-2h	4.84	613	1.1
Cu-SSZ-13 HT-8h	4.91	547	0.93

[a] Calculated from ^{29}Si-NMR.

[b] Measured by Ar-adsorption BET.

[c] Normalized values based on the crystallinity of the Cu-SSZ-13 HT-0.5h catalyst. Crystallinity was calculated from sum of the intensity at 9.6 °, 20.8 °, 30.8 ° in the XRD patterns.

Table 3-2. Composition characteristics and apparent activation energy of Cu-SSZ-13 HT-x catalysts

Samples	Cu loading[a] (wt.%)	Amount of Cu^{2+}[b] (wt.%)	1Al-Cu /Cu_{total}[c]	Activation energy (kJ/mol)	
				Dry	Wet
Cu-SSZ-13 HT-0.5h	2.08	2.12	0.177	45.2	73.8
Cu-SSZ-13 HT-1h		1.94	0.152	46.2	69.5
Cu-SSZ-13 HT-2h		2.17	0.125	47.7	65.6
Cu-SSZ-13 HT-8h		2.12	0.104	49.6	67.3

[a] Measured by an ICP-AES.

[b] Calculated from the EPR spectra of the hydrated samples.

[c] Calculated from the difference between EPR spectra of the hydrated and dehydrated samples.

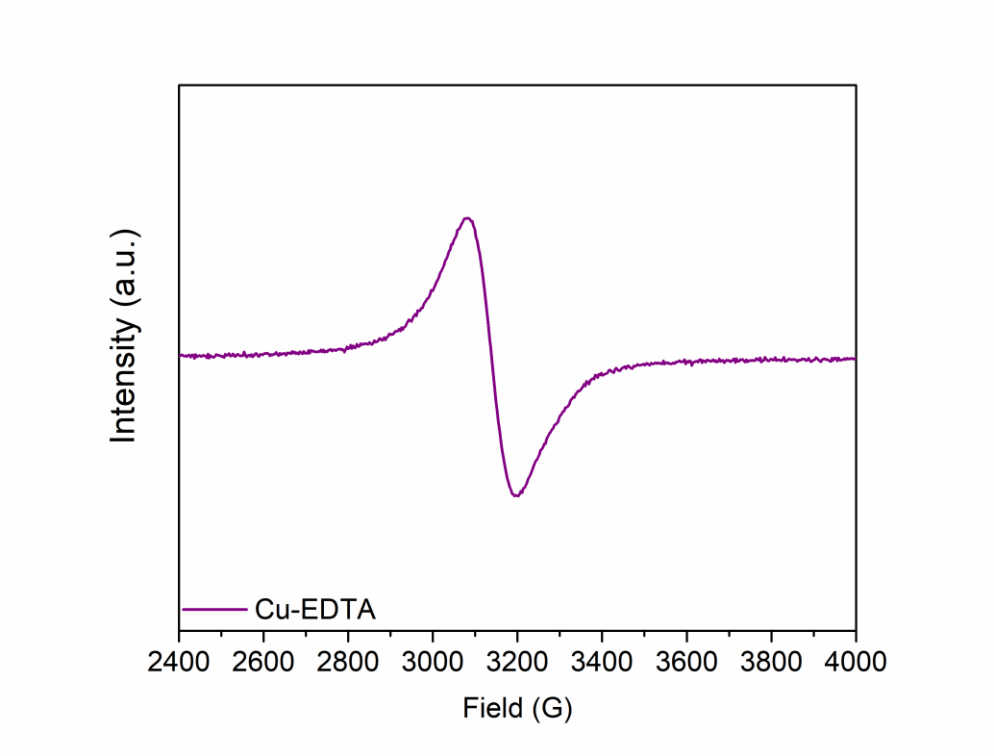

Figure 3-1. EPR spectrum of the Cu-EDTA standard solution (0.025 M).

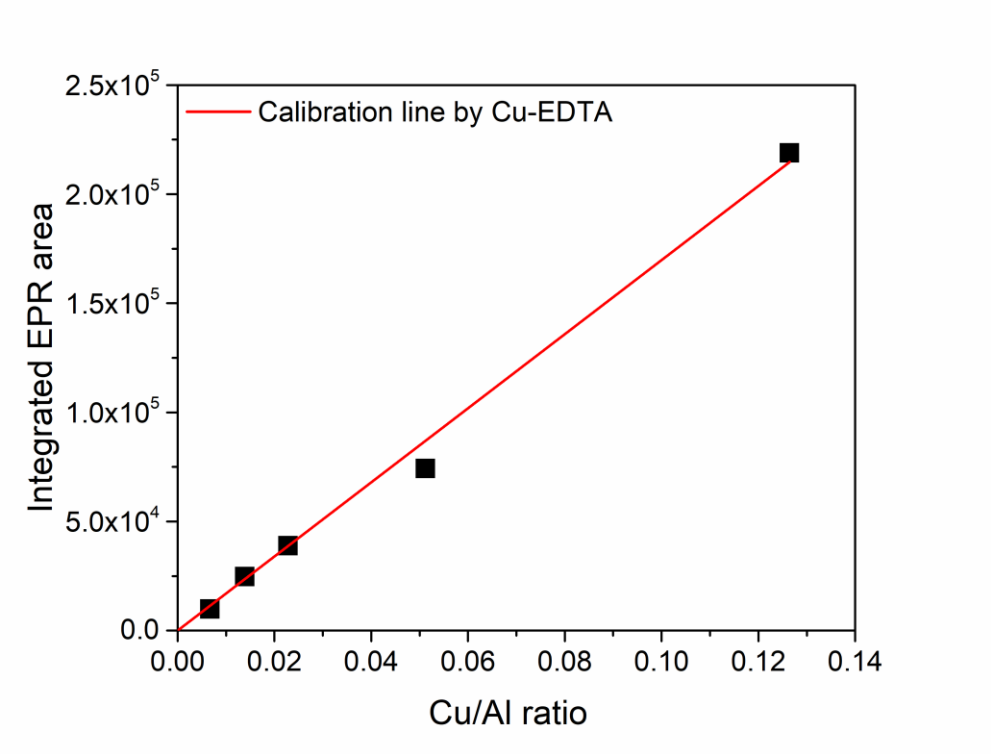

Figure 3-2. Integrated EPR area vs Cu/Al ratio and calibration line (red line) obtained from EPR spectrum of Cu-EDTA.

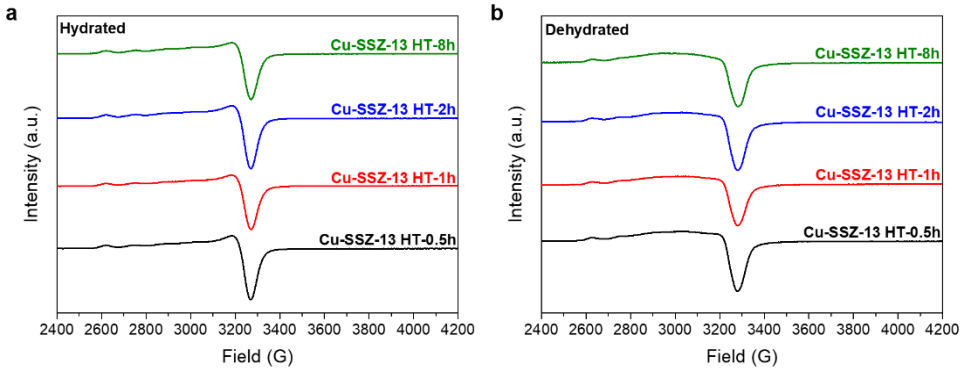

Figure 3-3. EPR spectra of (a) the hydrated and (b) dehydrated Cu-SSZ-13 HT-x catalysts.

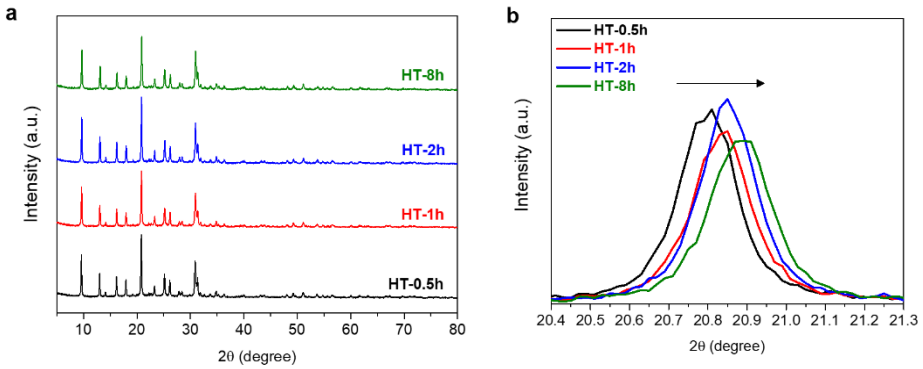

Figure 3-4. (a) XRD patterns of the Cu-SSZ-13 HT-x catalysts. All patterns were assigned to chabazite structures. (b) XRD peak at 20.4~21.3 °. The peak was shifted to higher angle as hydrothermal treatment duration increased. It indicates a cage shrinkage resulting from the increase of 2Al-Cu species, which have stronger interaction to framework than the 1Al-Cu species.

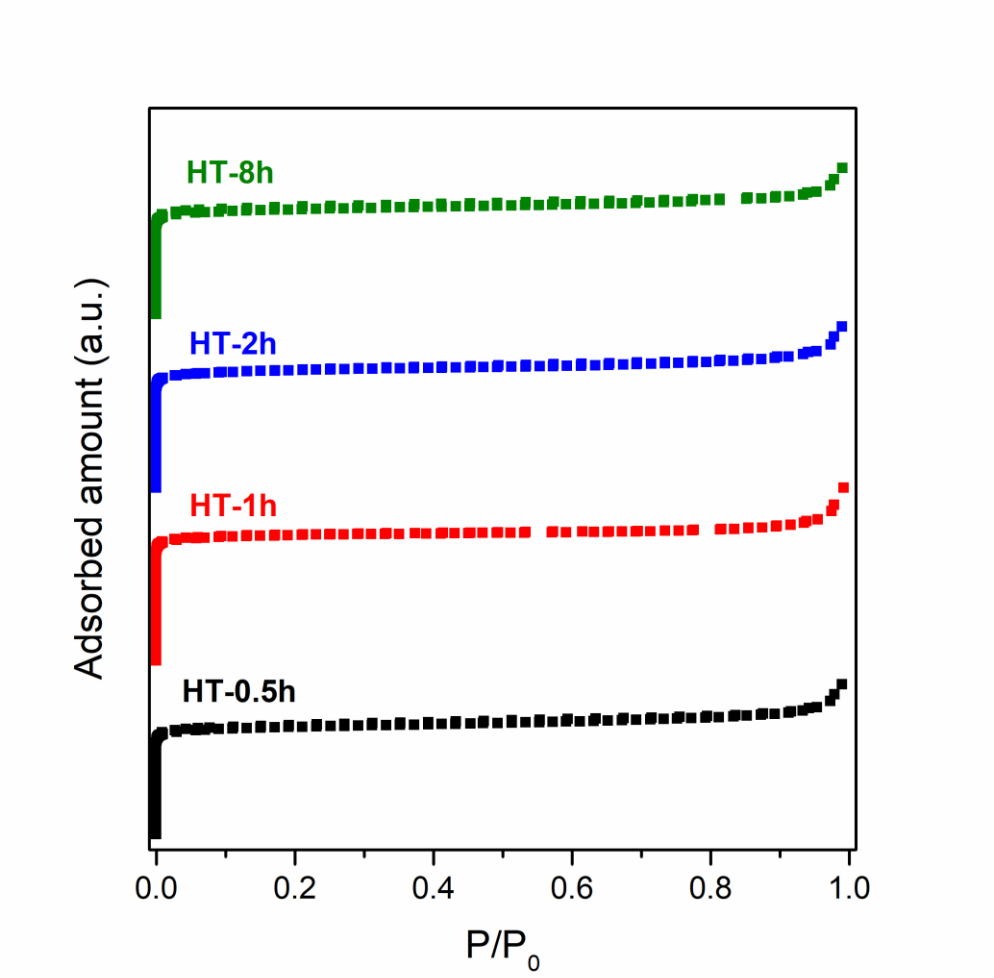

Figure 3-5. Isotherm of the Cu-SSZ-13 HT-x catalysts obtained from the Ar-adsorption experiments.

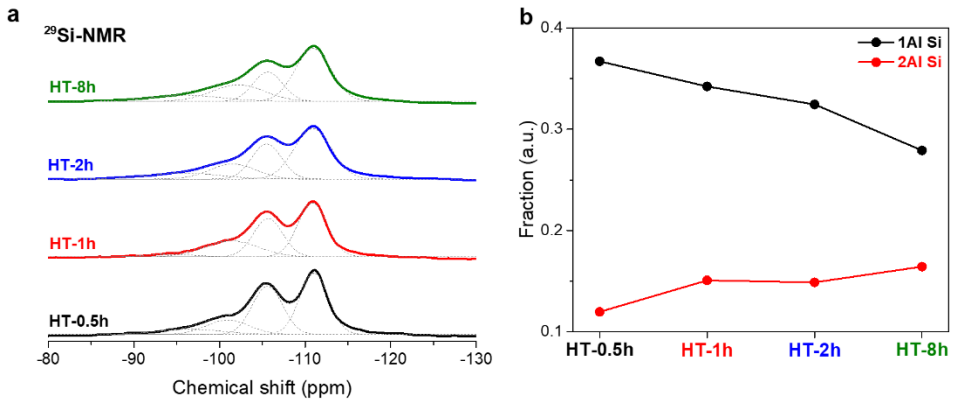

Figure 3-6. (a) ^{29}Si-NMR of the Cu-SSZ-13 HT-x catalysts. The spectra were deconvoluted to four peaks at 111, 107, 101, 97 ppm which indicate Si(4)Al(0), Si(3)Al(1), Si(2)Al(2), Si(1)Al(3), respectively. (b) As hydrothermal treatment time got longer, the Si(3)Al(1) peak decreased, and the Si(2)Al(2) peak increased. It indicates that Al on the framework was redistributed by the hydrothermal treatment.

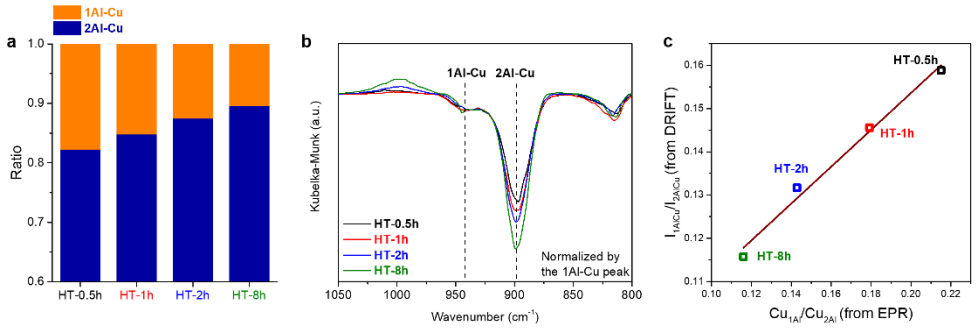

Figure 3-7. (a) Ratio of 1Al-Cu and 2Al-Cu over the Cu-SSZ-13 HT-x quantified using the EPR spectra. (b) The perturbation peaks of Cu-SSZ-13 HT-x catalysts in DRIFT spectra after NH_3 adsorption for 60 min. (c) Correlation between 1Al-Cu/2Al-Cu values measured by using EPR and DRIFT spectra.

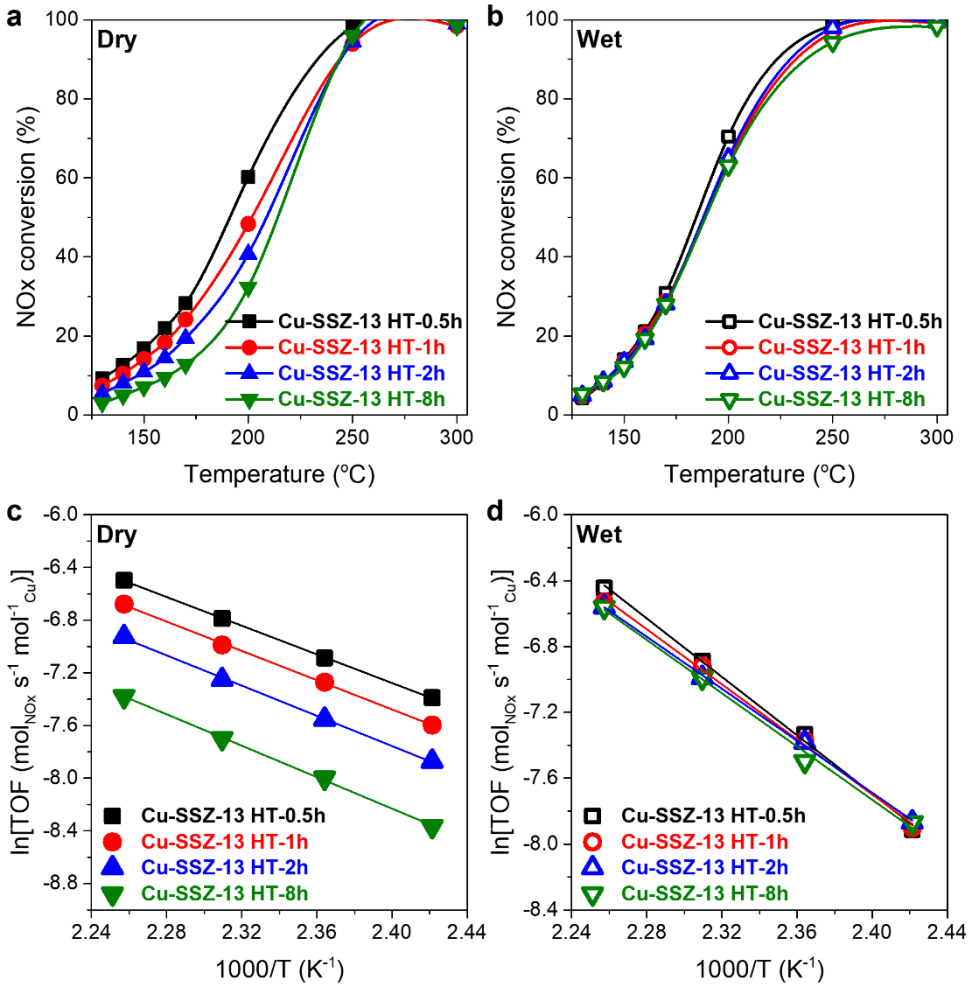

Figure 3-8. (a, b) NOx conversion data and (c, d) Arrhenius plots of the Cu-SSZ-13 HT-x catalysts under dry (solid symbol) and wet (open symbol) SCR conditions, respectively. NH_3-SCR reactions were performed under 500 ppm NO, 500 ppm NH_3, 10% O_2, 5% H_2O (when used) and N_2 balanced with gas hourly space velocity (GHSV) 240,000 mL/h·g_{cat}.

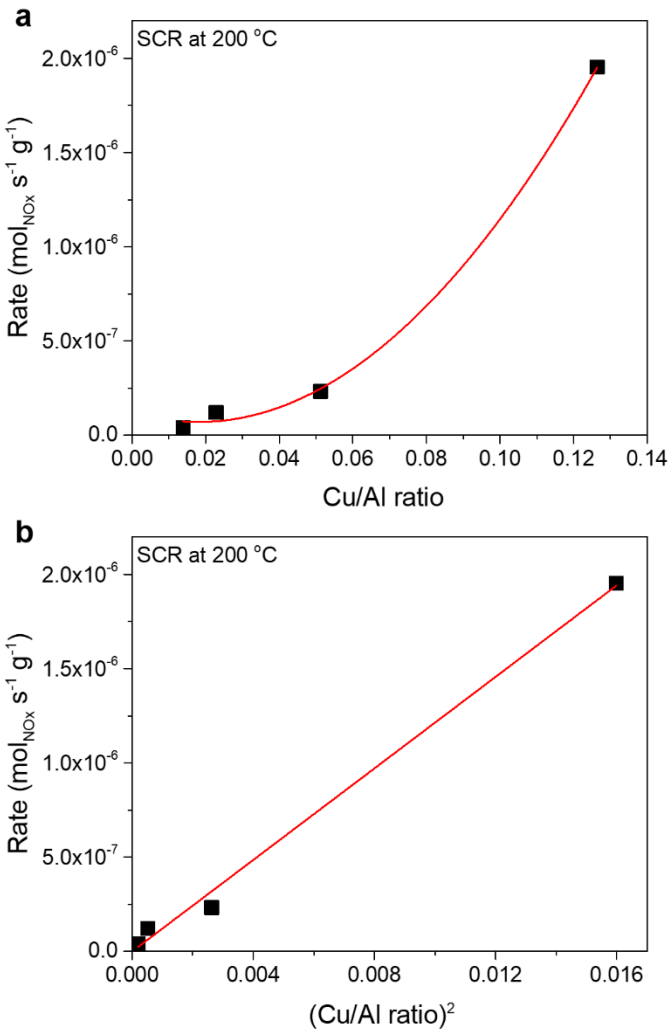

Figure 3-9. (a) SCR rates under dry condition vs Cu/Al ratios obtained at 200 °C. (b) SCR rate vs (Cu/Al ratio)^2 replotted using data in the upper panel, which demonstrates linear correlation.

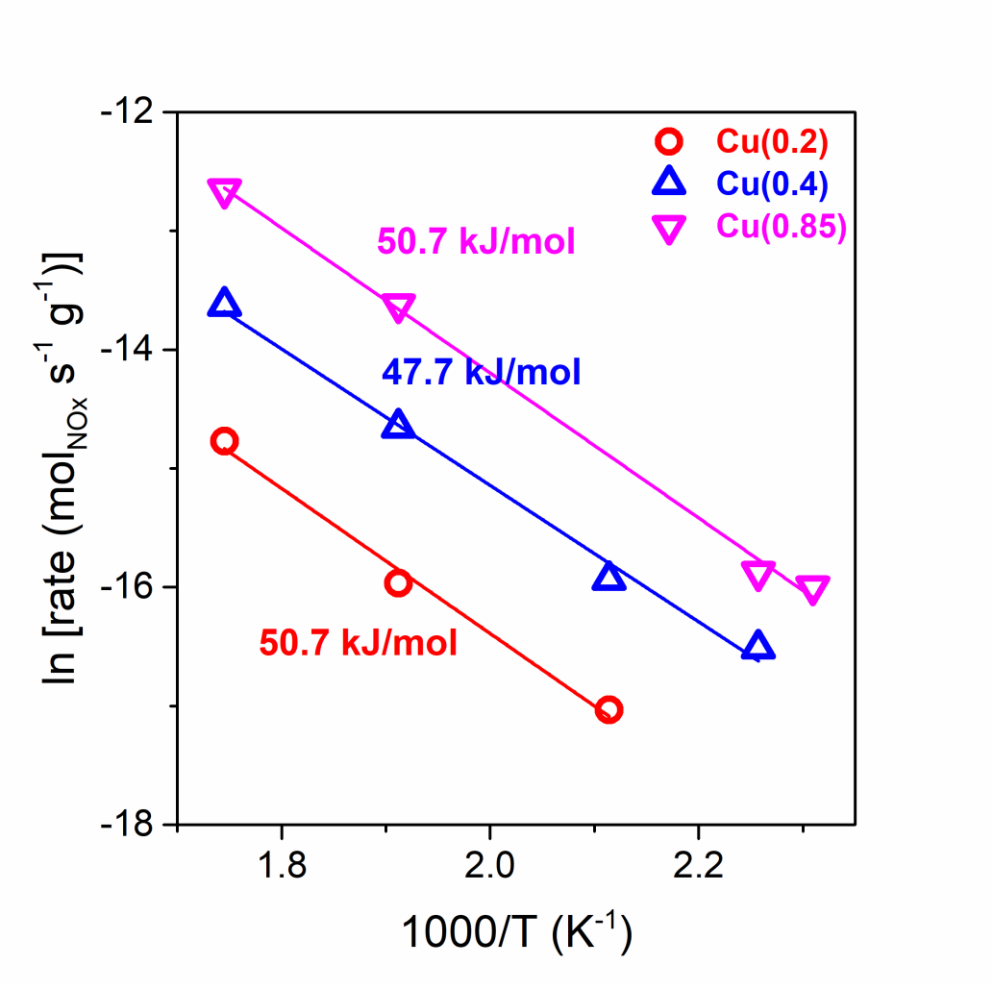

Figure 3-10. Arrhenius plot of Cu-SSZ-13 samples with different Cu loadings (0.2, 0.4, 0.85 wt.% [Cu/Al= 0.014, 0,023, 0.051], respectively). All samples have almost same activation energy values ~45 kJ/mol.

3.3.3. Reaction determining kinetic factor in Cu-SSZ-13

The kinetic studies make us postulate that the discrepant reactivity of the 1Al-Cu and 2Al-Cu in the Cu-SSZ-13 HT-x exists only under ion-transfer limiting condition. To confirm this, the same experiments were conducted with different loadings of Cu-SSZ-13 HT-x catalysts (2.7 wt.%, 6 wt.%, Cu/Al ratio = 0.165, 0.344, respectively. At each Cu loading, the HT-0.5h catalysts have a higher 1Al-Cu/2Al-Cu ratio than the HT-8h) (Figure 3-11, 3-12, 3-13). Figure 3-14 illustrates the relationship between the turnover frequencies and the Cu ion species depending on the kinetic regimes of the SCR reaction. First, the HT-x catalysts that have different 1Al-Cu/2Al-Cu ratios have analogous activation energy values within each reaction and Cu loading, indicating that the reactions were under the same kinetic regime regardless of the 1Al-Cu/2Al-Cu ratios. Comparing the kinetics in the wet and dry reactions, all wet SCR reactions showed the same apparent activation energy of ~70 kJ/mol, implying that the re-oxidation step is rate-limiting (Figure 3-14a). In the case of the dry reactions, the apparent activation energy altered from ~ 45 kJ/mol to ~70 kJ/mol with an increase in the Cu loadings, which demonstrates the shift of the rate-determining step from the ion-transfer to the re-oxidation process. Such a shift in the rate-determining step was consistent with previous research by Gao et al. that claimed that diffusion of the Cu ion species no

longer determines the overall reaction rates because the formation of dimeric Cu species becomes more facile at high Cu loadings [20].

In Figure 3-14b, the TOFs of the HT-0.5h and HT-8h catalysts that had different 1Al-Cu/2Al-Cu ratios were almost identical ($TOF_{HT\text{-}0.5h}/TOF_{HT\text{-}8h} \sim 1$) when they were under a re-oxidation limiting regime (green area, E_a~70 kJ/mol), and different ($TOF_{HT\text{-}0.5h}/TOF_{HT\text{-}8h} >> 1$) when they were under an ion-transfer limiting regime (yellow area, E_a~45 kJ/mol). It is worth noting that the TOF under a dry SCR of HT-0.5h was much higher than that of HT-8h at a low Cu loading. However, as the rate-limiting step shifted from the ion-transfer to the re-oxidation process at a high Cu loading, their TOFs became almost identical (Figure 3-14). These results strongly indicate that we can observe the different reactivity of the 1Al-Cu and 2Al-Cu species only under an ion-transfer limiting condition. In the case of a previous study which reported the same reactivity of 1Al-Cu and 2Al-Cu, the reactivity was not measured under an ion-transfer limiting condition, as evidenced by the proposed apparent E_a values of 60 and 74 kJ/mol [16]. Such reaction condition was supposed to make the different mobility of the Cu species insignificant.

The *in-situ* DRIFT analyses allowed us to directly compare the SCR reactivity of the two Cu species by simulating a dry SCR reaction (Figure 3-15). When the adsorbed ammonia on each Cu ion species reacts with $NO+O_2$,

the negative peaks at 940 and 897 cm^{-1} decrease due to a restoration of the interaction between the Cu ions and the framework, and their decreased rates represent the reaction rates of each species. During the reaction of pre-adsorbed ammonia with $NO+O_2$ at 200 °C in the Cu-SSZ-13 HT-0.5h, the peak of 1Al-Cu decreased faster than that of 2Al-Cu, which evidently demonstrated a higher SCR reactivity of NH_3 species on the 1Al-Cu than that on the 2Al-Cu (Figure 3-15a) [66]. In contrast, the two Cu species showed almost the same reaction rate over the Cu-SSZ-13 6wt HT-0.5h catalyst (Figure 3-15b). The DRIFT results were consistent with our reaction data in that a higher reactivity of the 1Al-Cu species was presented only under the dry SCR reaction of the Cu-SSZ-13 HT-x catalysts.

We suppose that the higher reactivity of the 1Al-Cu is related to the formation of dimeric Cu intermediates ($[Cu^{I}(NH_3)_2]^{+}-O_2-[Cu^{I}(NH_3)_2]^{+}$). As these intermediates are formed via the diffusion of Cu ions, the 1Al-Cu species can form the dimeric Cu intermediates more facilely than the 2Al-Cu due to their higher mobility under the ion-transfer limiting condition. This is consistent with DFT calculation results reported by Chen et al. that the intermediates on the 2Al sites have low stability [72]. This enhancement in the intermediates formation increases the rate of rate determining step in the SCR resulting in higher NH_3-SCR reactivity (Figure 3-16) [20, 21]. In the case of

re-oxidation limiting condition, the formation of the intermediates is sufficiently facile due to increased Cu mobility by the presence of H_2O or the close Cu-Cu distance at high loading Cu. Therefore, the different mobility of two Cu species becomes meaningless, and they demonstrate the same reactivity.

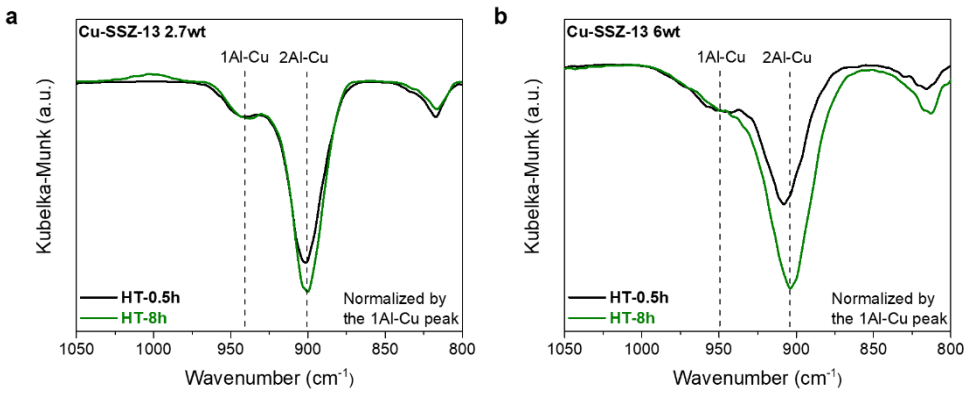

Figure 3-11. The perturbation peaks of (a) Cu-SSZ-13 2.7wt HT-x catalysts and (b) Cu-SSZ-13 6wt HT-x catalysts in DRIFT spectra after the NH_3 adsorption 60 min.

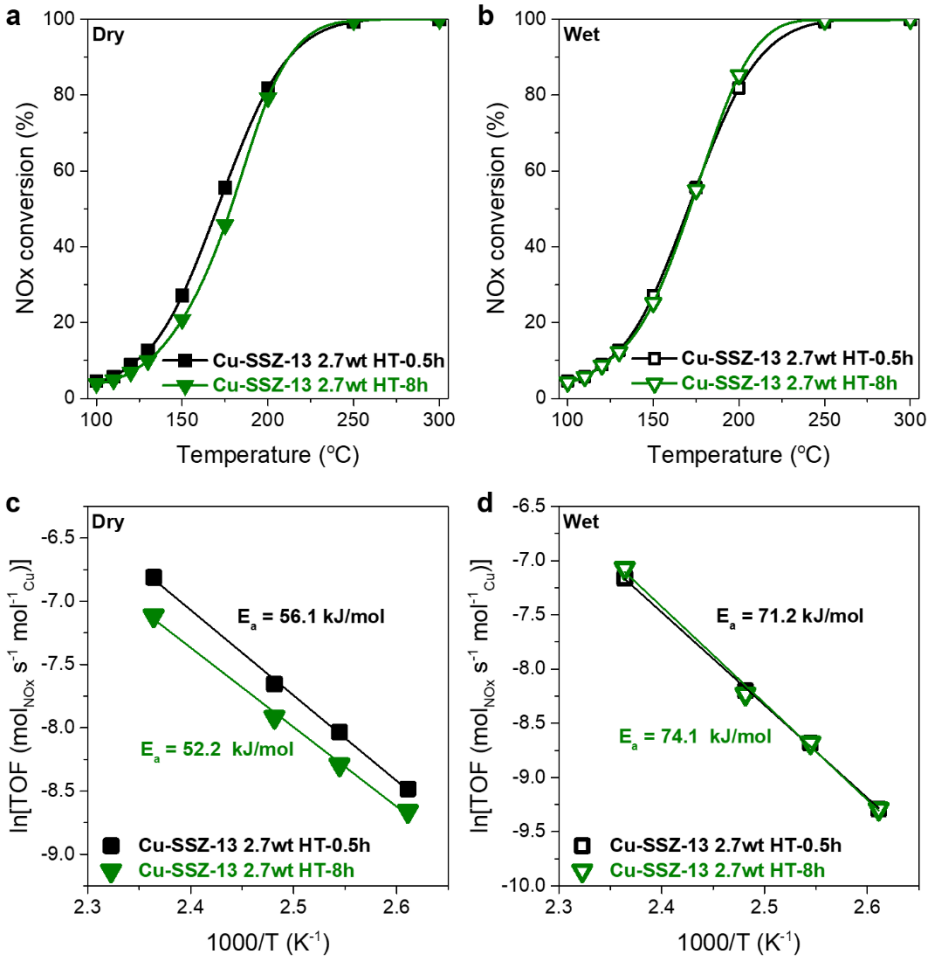

Figure 3-12. (a, b) NOx conversion data and (c, d) Arrhenius plots of the Cu-SSZ-13 2.7wt HT-x catalysts under dry (solid symbol) and wet SCR condition (open symbol), respectively.

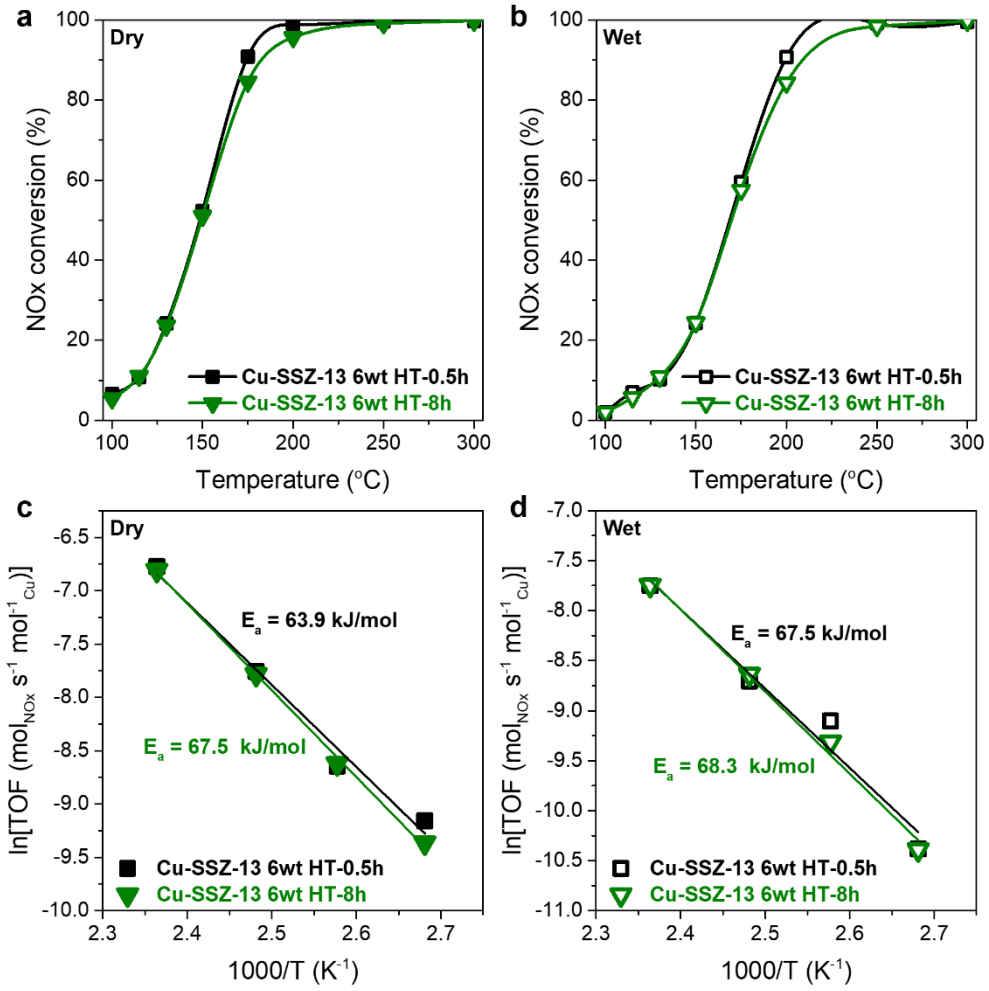

Figure 3-13. (a, b) NOx conversion data and (c, d) Arrhenius plots of the Cu-SSZ-13 6wt HT-x catalysts under dry (solid symbol) and wet SCR condition (open symbol), respectively.

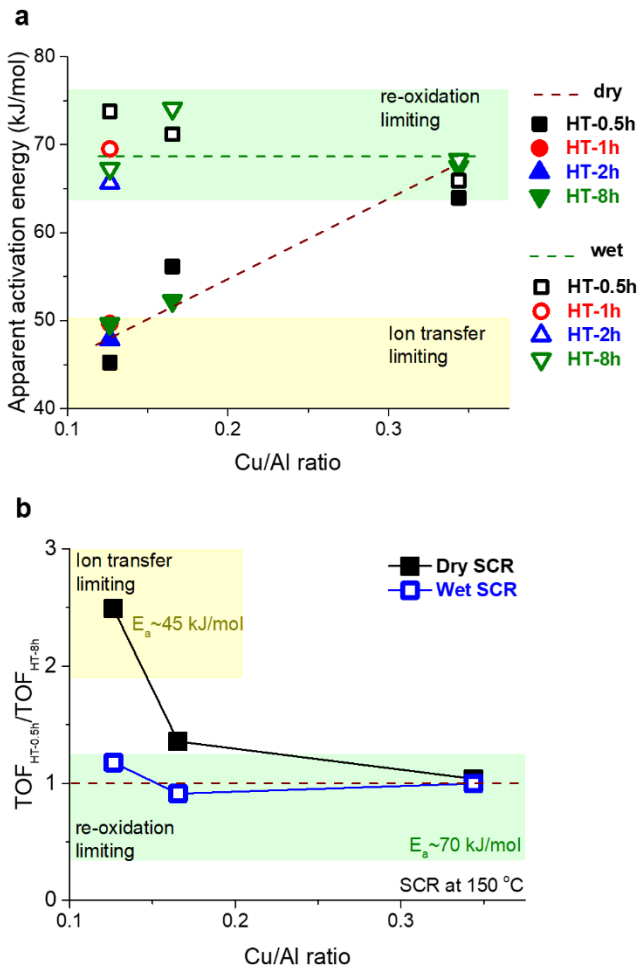

Figure 3-14. (a) Apparent activation energy values of the dry and wet SCR reactions of Cu-SSZ-13 catalysts depending on the Cu loadings. (b) The ratio of TOFs of the HT-0.5h to HT-8h catalysts over dry and wet SCR reactions at 150 ºC depending on the Cu loadings. The kinetic regimes of the reactions were marked by green (re-oxidation limiting regime, E_a values ~ 70 kJ/mol) or yellow (ion transfer limiting regime, E_a values ~45 kJ/mol).

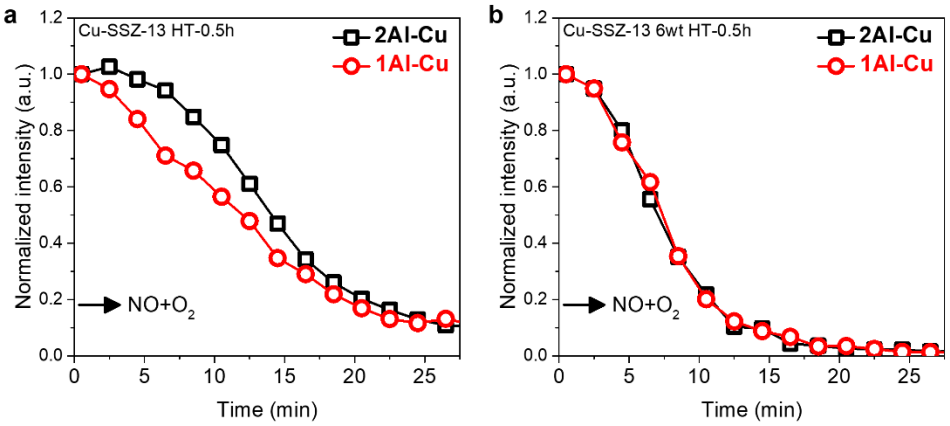

Figure 3-15. Profiles of intensity changes in the 1Al-Cu and 2Al-Cu perturbation peaks during the reaction of $NO+O_2$ with pre-adsorbed NH_3 at 200 ºC over (a) the Cu-SSZ-13 HT-0.5h, (b) the Cu-SSZ-13 6wt HT-0.5h. Each peak was normalized by their initial intensity.

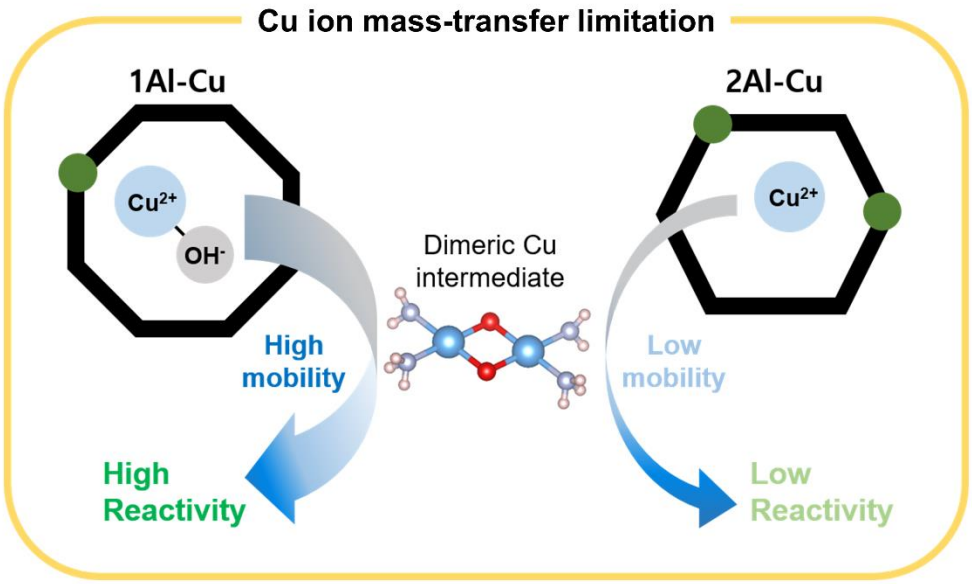

Figure 3-16. Schematic of the SCR reactivity determined by the mobility of Cu ion species.

Chapter 4. Rational Cu-SSZ-13 catalyst design for NH_3-SCR via Cu species control by addition of Co ions

4.1. Introduction

Cu-SSZ-13 catalyst, which is Cu ion exchanged zeolite with a chabazite structure, brought a huge breakthrough in the NH_3-SCR industry due to their superior NOx removal ability and hydrothermal stability [11]. The Cu-SSZ-13 catalysts maintained their performance even after the hydrothermal aging at 850 °C where the previous catalysts were seriously deactivated [47, 50, 51]. It was suggested that small pore structure of chabazite gave rise to their superior hydrothermal stability because the steric effect of their small pore hindered the formation of $Al(OH)_3$ and $CuAlO_x$ like species that were deactivation-causing materials [12]. In spite of their excellent performances, there have been many efforts to improve the catalysts due to the strengthened regulation on NOx emission and implementation of real-driving emission [23-26]. In order to design better catalysts, many researchers have tried to investigate the nature of Cu^{2+} ion that is an active site of NH_3-SCR, and consequently to understand its mechanism [15, 34].

Kwak et al. reported that two types of Cu species exist in the Cu-SSZ-13, which are classified by their cationic locations in the SSZ-13 framework

[36]. The subsequent studies revealed that these species are Cu species located at 6-membered and 8-membered ring depending on their interaction strength with the framework [34]. A Cu ion located at 6-membered ring interacts with two Al atoms of the SSZ-13 existing as a 2Z-Cu^{2+} (2Al-Cu). In contrast, a Cu ion at 8-membered ring interacts with only one Al atom as a form of Z-[Cu^{2+}-OH^{-}] (1Al-Cu) where the presence of hydroxyl group compensates the charge balance. Difference in the location makes the two Cu species have different properties, and as a result demonstrate the different responses on various reactions and circumstances. Verma et al. suggested that the NO oxidation reaction occurred on Z-[Cu^{2+}-OH^{-}] species selectively [55]. They found that the Cu_xO_y species was active site of NO oxidation, which originated from Z-[Cu^{2+}-OH^{-}] species. As the Cu species exists as the 2Z-Cu^{2+} species preferentially in the low loading Cu-SSZ-13, the Cu-SSZ-13 catalysts below a certain Cu loading did not have any NO oxidation activity. NH_3 oxidation over Cu-SSZ-13 also was proposed to be catalyzed on the dimeric Cu species formed from the Z-[Cu^{2+}-OH^{-}] species [42]. Recently, these species have received great attention in the methane partial oxidation reaction to methanol. Grundner et al. suggested tri-nuclear Cu clusters in mordenite as an active site of conversion of methane to methanol [73]. Oord et al. found that the production of methanol enhanced as the IR peak of Cu-OH increased

proposing that Cu-OH is an active site of methane to methanol reaction over Cu-SSZ-13 catalyst.

As mentioned above, many different kinds of reactions in the Cu-SSZ-13 were obviously dependent on the species of Cu ion, and such species-dependent reactivity also has been investigated in the case of NH_3-SCR reaction. Gao et al. found the unique homogenous catalyst-like mechanism in the Cu-SSZ-13, which was governed by the ion transfer of mobile Cu ions [20]. They suggested that 1Al-Cu species could be more active than 2Al-Cu species due to their higher mobility. Zhang et al. illustrated that immobility of 2Al-Cu species hindered SCR redox cycle, so this species could deteriorate the overall SCR reactivity of the catalyst [62]. Our previous study found the 1Al-Cu species have higher SCR reactivity under specific kinetic regime, and revealed that higher mobility of 1Al-Cu species give rise to superior SCR reactivity than the 2Al-Cu species via kinetic studies. We proposed that the mobility of Cu ions would be a key property to improve the SCR performance of Cu-SSZ-13 catalyst. In the present study, we introduced the strategy to improve the reactivity of Cu-SSZ-13 catalyst under standard SCR condition by tuning the species of Cu ion. The species of Cu ion were controlled by the addition of Co ions to block the specific ion exchange site, which makes the Cu ions located at the another specific position.

4.2. Experimental

4.2.1. Catalysts preparation

NH_4^+-SSZ-13 was prepared using NH_4^+ ion exchange with H-SSZ-13 (Si/Al_2 = 23, Heesung catalysis). Co-SSZ-13 was synthesized by using ion exchange method with $Co(NO_3)_2 \cdot 6H_2O$ (Sigma Aldrich) precursor solution (0.03 M) at 65 °C, and calcined at 550 °C for 2h. Cu was impregnated by using incipient wetness impregnation method with $Cu(NO_3)_2 \cdot 3H_2O$ (Sigma Aldrich) on the Co-SSZ-13 and NH_4^+-SSZ-13 with Cu loadings 0.5, 0.75 and 1.0 wt. %, and also calcined at 550 °C for 4h. The catalysts were denoted as Cu(x)Co and Cu(x) (x = loadings of Cu). CoO (Sigma Aldrich) was used as the reference.

4.2.2. Catalysts characterization

Contents of the Cu, Co and Al in the catalysts were measured using an inductively coupled plasma atomic emission spectroscopy (ICP-AES, OPTIMA 8300, Perkin-Elmer) (Table 4-1). TEM images and EDS mapping were obtained using a CS-STEM (JEM-ARM200F, JEOL Ltd, Japan). Diffuse reflectance infrared fourier transform spectroscopy (DRIFT) analysis was performed on a Nicolet 6700 FT-IR spectrometer (Thermo Fisher Scientific) with an Praying Mantis cell and chamber. Gas adsorbed spectra were obtained 1h gas adsorption after 20% O_2/N_2 pretreatment at 400 °C. H_2-temeperature programmed reduction (H_2-TPR) was conducted to understand the redox properties of the catalysts on a BELCAT-II (BEL-Japan). H_2 consumption was measured with a thermal conductivity detector under 5% H_2/Ar condition ramping from ambient temperature to 800 °C without the pretreatment.

Solid-state ^{29}Si-NMR and ^{27}Al-NMR were conducted at 130.32 MHz on a Brucker Avance III HD (Brucker) under ambient condition (299 K). All data were measured under magic angle spinning (MAS) at a spinning rate of 10 kHz. The pulse length was 2 μs, and the delay time was 0.1 s. Electron paramagnetic resonance (EPR) spectra were obtained on an EMXmicro-9.5/2.7 spectrometer (Brucker). For complete hydration, the sample were hydrated under saturated vapor pressure overnight at an ambient condition.

Powder samples (~10 mg) were loaded in 5 mm OD quartz tube (Wilmad). Microwave power was 0.73 mW, and the frequency was 9.41 GHz. The field was swept by 3000 G in 60 s, and modulated at 100 kHz with 1 G amplitude. Time constant was 1.28 ms. All spectra were obtained at 150 K to freeze mobile Cu ions. All measurements were conducted three times per each samples. Amount of Cu ion species was obtained by integrate the spectra twice, and errors of the data were below 5%. X-ray absorption spectroscopy around Co K-edge (E_0 = 7709 eV)were conducted in 7D beamline of the Pohang Light Source (PLS) using Si[111] monochromator. The obtained spectra were normalized using Athena software package.

4.2.3. SCR reaction test and kinetic study

NH_3-SCR experiments were performed in a down-flow 1/4'' ID tubular quartz reactor with samples sieved into 300-500 μm particles. Reactions were performed under 500 ppm NO, 500 ppm NH_3, 10% O_2, 5% H_2O and balance N_2 with gas hourly space velocity (GHSV) of 240,000 mL/h·g_{cat}. NOx concentration was recorded using NOx chemiluminescence analyzer (42i High level, Thermo Scientific). NO oxidation experiments were conducted in same reaction system under 500 ppm NO, 10% O_2 balance N_2 with GHSV = 120,000 mL/ h·g_{cat}. Concentration of NO was measured by using FT-IR (Nicolet 6700, Thermo fisher Scuentific) with 2 m gas cell (International Crystal Laboratory). Reactivity of each reactions was displayed by the NOx conversion and NO conversion calculated using the following equations

$$NOx\ \ conversion\ \ (\%) = \frac{[NOx]_{in} - [NOx]_{out}}{[NOx]_{in}} \times 100$$

$$NO\ \ conversion\ \ (\%) = \frac{[NO]_{in} - [NO]_{out}}{[NO]_{in}} \times 100$$

Rate of the reactions is calculated using

$$r = \frac{F}{W}(-ln(1 - X))$$

where F is the molar NOx feed rate (mol/s), W the catalyst weight (g) and X the NOx conversion. NH_3-SCR reactivity of the catalyst is represented by turnover rate (TOR) defined as the NOx consumption rate per g catalyst. The apparent activation energy of the catalyst is obtained from Arrhenius equation by plotting 1000/T (K^{-1}) vs ln(TOF).

4.3. Results and Discussion

4.3.1. Characterization of Co species

Cobalt cations are well known to be located selectively on the 2Al sites in the SSZ-13, so they were widely used to titrate the amount of 2Al sites in the SSZ-13 [16, 34]. Based on the previous studies, Cobalt ion exchanged SSZ-13 (Co-SSZ-13, Co/Al=0.15) was prepared by using conventional ion exchange method to block the 2Al sites in advance. Through blocking the 2Al sites, we tried to induce Cu ions to be located on the 1Al sites as a form of Z-[Cu^{2+}-OH^{-}] rather than the 2Al sites. We have to make sure that the Co-SSZ-13 was successfully synthesized as we intended, i.e. only Co^{2+} ions are present. Figure 4-1 shows the NO adsorption DRIFT spectra on the Co-SSZ-13 at 200 °C. Single peak at 1815 cm^{-1} was only major adsorption peak, which is assigned to the vibration of dinitrosyl group adsorbed on isolated Co^{2+} ions [74-76]. There was no other NO adsorption peak assigned to the other cobalt species such as CoO and Co_2O_3, which is observed at 1795 and 1940 cm^{-1} [74, 76]. It guarantees that the majority of cobalt exists as isolated Co^{2+} ion, not the CoO or Co_3O_4 species [74]. The DRIFT spectra of Co-SSZ-13 and H-SSZ-13 were displayed in Figure 4-2. The IR absorption peak at 3650 cm^{-1} which is assigned to the M^{2+}-OH species was not observed in the spectra. It indicates that there is no Co^{2+}-OH species in Co-SSZ-13. Then, the active Cu ions were

impregnated on the Co ion exchanged SSZ-13 by using incipient wetness impregnation, and their Cu and Co loadings were measured by using ICP-AES (Table 4-1). Figure 4-3 shows the TEM-EDX image of the Cu(1.0)Co catalyst, which makes sure that Co cations are well dispersed on a SSZ-13 particles (Cu cations are also well dispersed).

The XANES and EXAFS spectra were obtained at Co K-edge to investigate the state of cobalt after Cu impregnation (Figure 4-4). All Cu(x)Co catalysts and Co-SSZ-13 showed identical XANES spectra with single peak edge at 7725.4 eV, which corresponds to XANES spectra of Co^{2+} ion [77]. It demonstrates that Co on Cu(x)Co also existed as isolated Co^{2+} cation, after the impregnation of Cu. Their adsorption edges were slightly lower than that of CoO reference, which was consistent to the edge position of adsorption peak of Co^{2+} ion from the previous report [78]. In the EXAFS spectra, Co-O scattering peaks of Cu(x)Co and Co-SSZ-13 appeared at 1.6 Å shorter than that of CoO (1.7 Å) showing stronger Co-O bond strength of ionic Co^{2+} than CoO. This result is consistent with H_2-TPR results of Co-SSZ-13 and CoO (Figure 4-5). Although the CoO was reduced at 250-400 °C, no reduction peak was observed in the Co-SSZ-13 even up to 800 °C indicating stronger interaction between Co and O in the Co^{2+} ion species than in CoO. There was no Co-Co scattering peak at 2.6 Å in the Cu(x)Co and Co-SSZ-13 catalysts,

supporting the absence of CoO species in the Co-SSZ-13 and Cu(x)Co catalysts.

4.3.2. Characterization of Cu species

To investigate the Cu ion species in the catalysts, we conducted the H_2-TPR analysis over Cu impregnated catalysts. As the ionic Co^{2+} did not reduced in the temperature range 100-800 °C (Figure 4-5), the H_2 consumption profiles in Figure 4-6 represent solely the reduction behaviors of Cu^{2+} ions. There were two reduction peaks at low temperature (200-300 °C) and high temperature (350-500 °C), which indicated the reduction of Z-[Cu^{2+}-OH^-] (1Al-Cu) and 2Z-Cu^{2+} (2Al-Cu) to Cu^+, respectively [36, 56]. We were likely to design the Cu(x)Co catalysts to have more 1Al-Cu species than Cu(x) catalysts by blocking the 2Al sites with Co^{2+} ions. Figure 4-6a displayed that the reduction peak of the Cu(x)Co catalysts increased at the low temperature and decreased at the high temperature compared to Cu(x). The amount of each species was obtained by deconvolution of peaks in the H_2-TPR showing higher 1A-Cu/2Al-Cu ratio in the Cu(x)Co than in the Cu(x) (Table 4-2). It clearly demonstrates that addition of Co^{2+} ions successfully changed distribution of Cu ions from the 2Al-Cu to the 1Al-Cu. There could be the presence of the CuO, which is reduced to Cu^0 metal around 300 °C. However, Figure 4-6b showed that the ratios of total H_2 consumption to the Cu loadings (H_2/Cu) were 0.5 in the all catalysts. This result shows that all Cu^{2+} species were reduced to Cu^+ implying that all Cu species exist as the Cu^{2+} ions. Figure 5 shows EPR

spectra of the Cu(x)Co and Cu(x) catalysts. Only isolated Cu^{2+} species are detected, not the CuO, Cu^{+} in the EPR analyses. As Co^{2+} ions are also EPR-silent, double integrated area of the EPR spectra indicates the amount of isolated Cu^{2+} ions (Figure 4-7a). Calculated EPR areas of the Cu(x)Co and Cu(x) have a linear correlation to Cu loadings, implying that the Cu^{2+} ion is the only species in the Cu(x)Co and Cu(x) (Figure 4-8). To sum up our characterization results, i) all Copper and Cobalt species existed as the divalent ionic form in the SSZ-13, ii) Cu species were successfully controlled from the 2Al-Cu to the 1Al-Cu by addition of Co^{2+} ion.

Table 4-1. Composition properties of Cu(x), Cu(x)Co and Co-SSZ-13 catalysts.

Sample	**Si/Al**	**Cu loading (wt.%)**	**Co loading (wt.%)**
Cu(0.5)	23	0.49	-
Cu(0.5)Co	23	0.50	0.85
Cu(0.75)	23	0.90	-
Cu(0.75)Co	23	0.80	0.77
Cu(1.0)	23	0.98	-
Cu(1.0)Co	23	0.99	0.82
Co-SSZ-13	23	-	0.85

Table 4-2. Amount of 1Al-Cu and 2Al-Cu species from H_2-TPR profiles of the Cu(x) and Cu(x)Co.

Sample	**1Al-Cu (mmol/g)**	**2Al-Cu (mmol/g)**	**Total Cu^{2+} (mmol/g)**	**1Al-Cu /2Al-Cu**
Cu(0.5)	0.016	0.022	0.038	0.75
Cu(0.5)Co	0.027	0.011	0.038	2.39
Cu(0.75)	0.035	0.036	0.071	0.98
Cu(0.75)Co	0.051	0.015	0.065	3.49
Cu(1.0)	0.040	0.039	0.079	1.00
Cu(1.0)Co	0.062	0.016	0.078	3.91

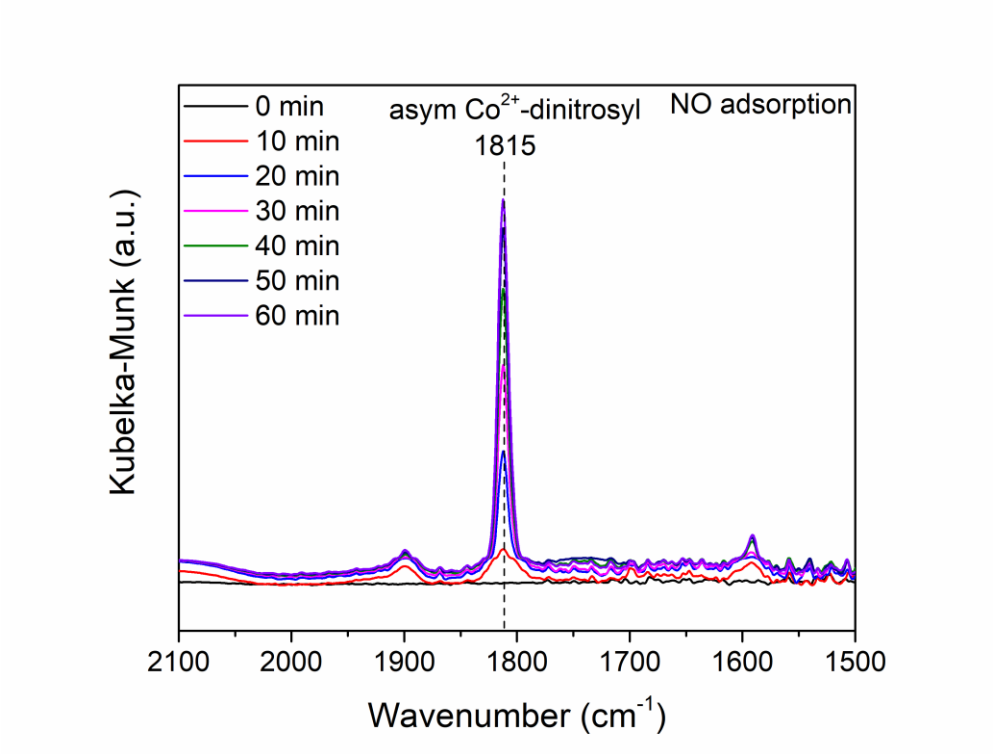

Figure 4-1. DRIFT spectra during NO adsorption (500 ppm NO, N_2 balance) over Co-SSZ-13 catalyst for 60 min at 200 °C.

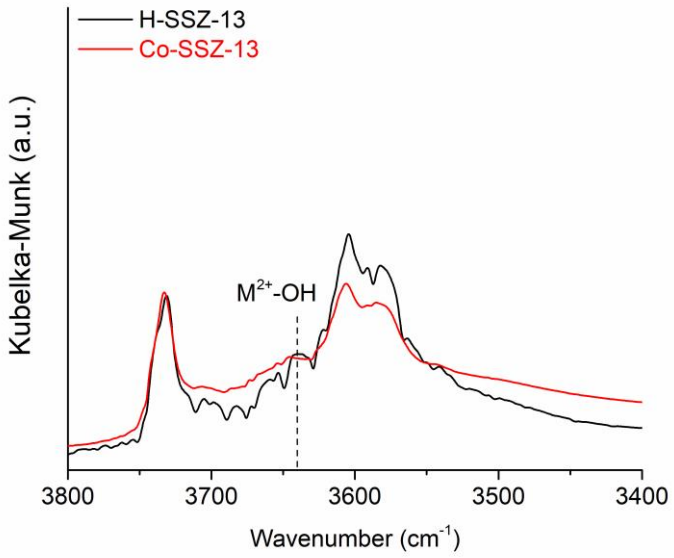

Figure 4-2. DRIFT spectra of H-SSZ-13 and Co-SSZ-13 catalysts at 200 °C.

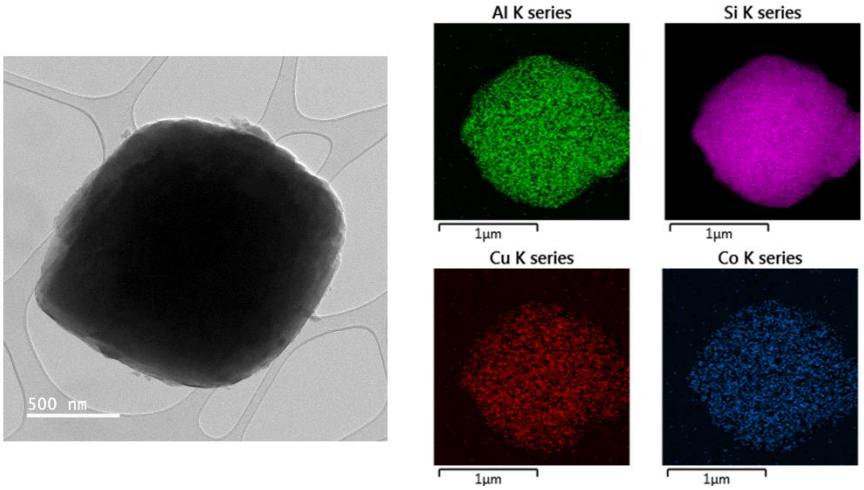

Figure 4-3. STEM image and EDS mapping images of Cu(1.0)Co catalyst.

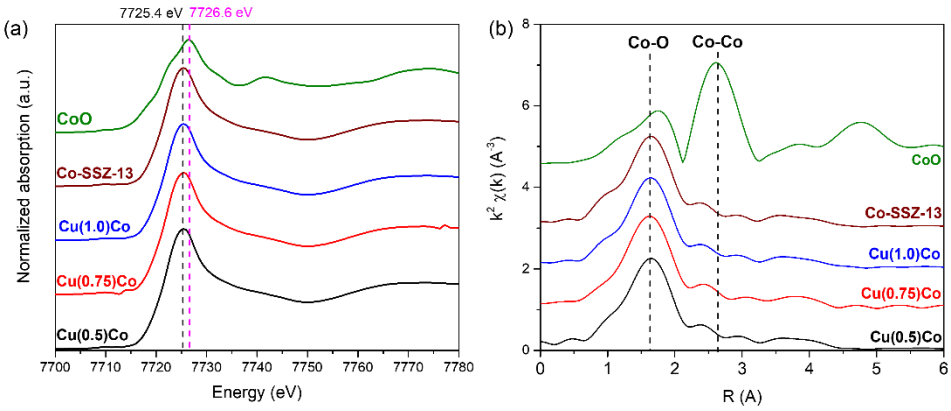

Figure 4-4. (a) Co K edge XANES spectra and (b) EXAFS spectra of Cu(x)Co and Co-SSZ-13 catalysts.

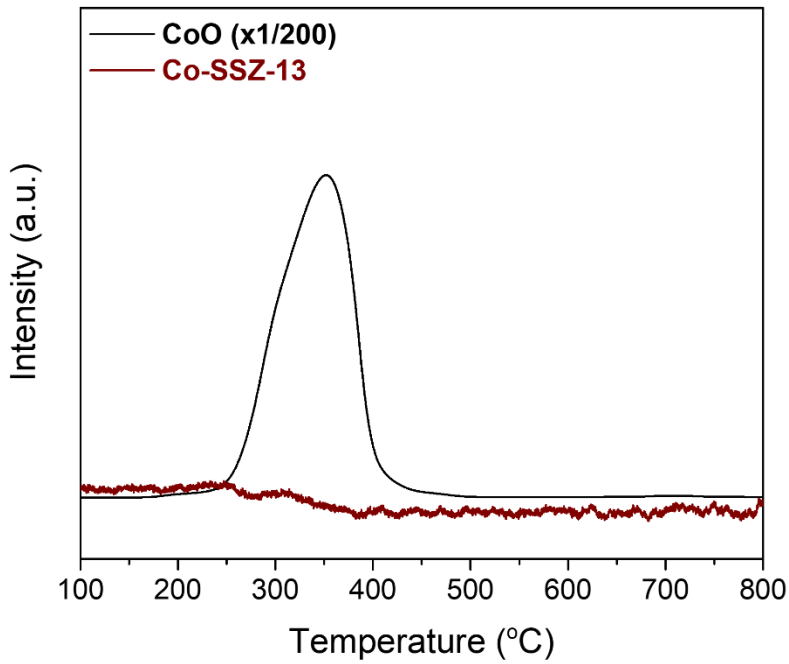

Figure 4-5. H_2-TPR profiles of Co-SSZ-13 and CoO reference.

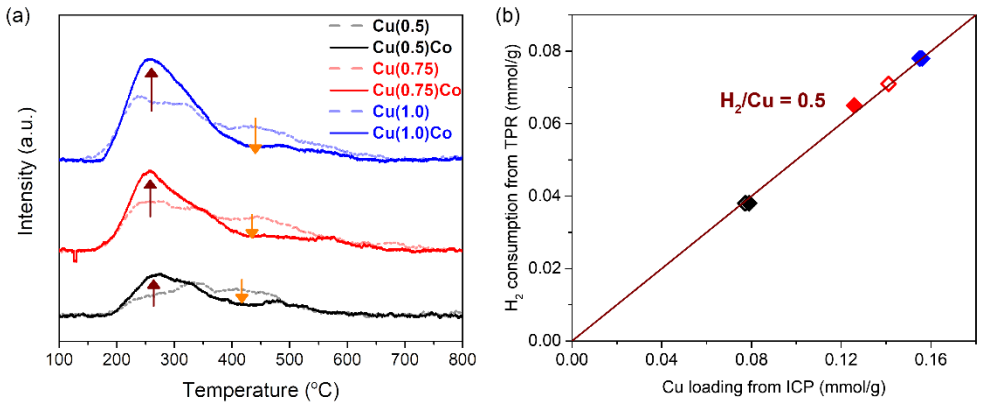

Figure 4-6. (a) H_2-TPR profiles of Cu(x) and Cu(x)Co catalysts and (b) quantitative correlation between H_2 consumption and amount of Cu.

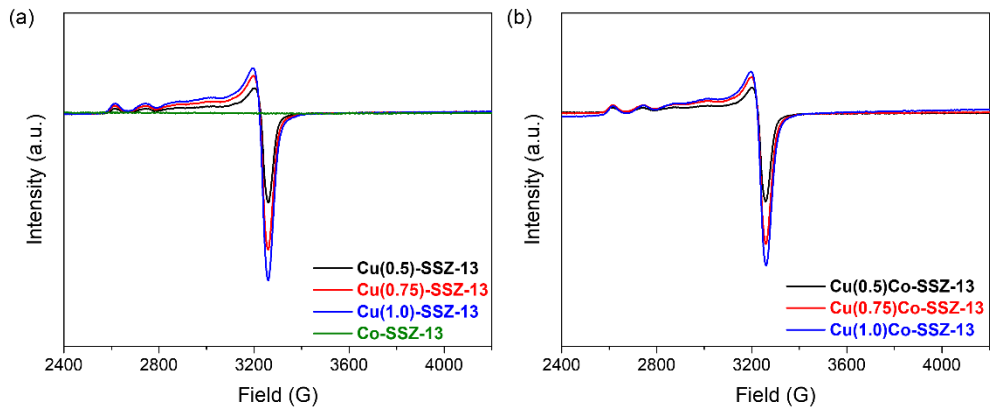

Figure 4-7. EPR spectra of (a) Cu(x), Co-SSZ-13 and (b) Cu(x)Co catalysts at 150 K.

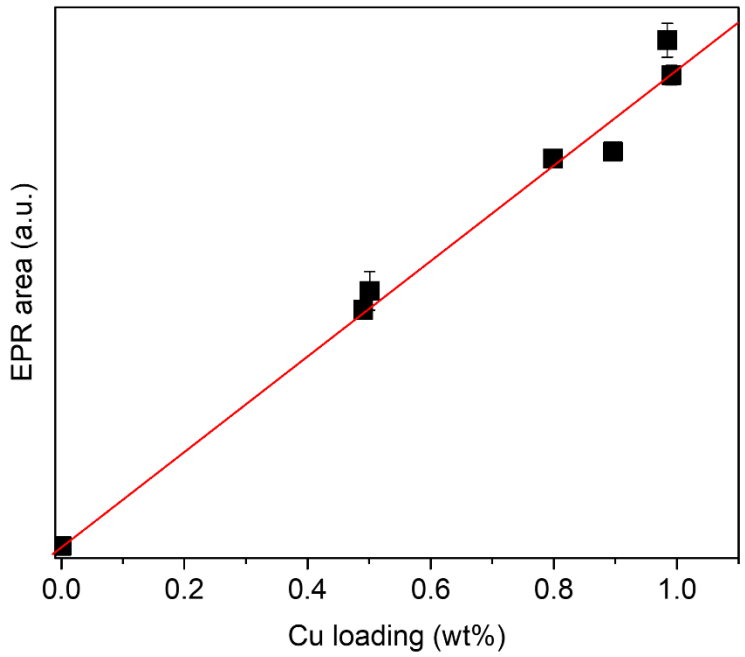

Figure 4-8. Correlation between area of EPR spectra and amount of Cu. EPR area was calculated by double integration the spectra.

4.3.3. Catalytic reactions and kinetic study

We compared the catalytic activities of the designed Cu(x)Co and conventional Cu(x) catalysts for the two kinds of reactions, NO oxidation and NH_3-SCR. Figure 4-9 displayed the NO oxidation reactivity of the Cu(x) and Cu(x)Co catalysts. We demonstrate the NO oxidation rate by NO conversion since there was no N_2O formation in all reactions. In both catalysts, the NO oxidation reactivity increases as the Cu loading increases, which indicates that the Cu ion is the active on NO oxidation reaction. However, NO conversion profiles of the Cu(x) and Cu(x)Co catalysts were totally different. Comparing two series of catalysts, The profiles of Cu(x) catalysts show volcanic curve, but the Cu(x)Co catalysts show parabolic trend. And the Cu(x) catalysts showed higher NO oxidation ability at low temperature (200-250 °C) than Cu(x)Co, instead the reactivity at high temperature (400-450 °C) was much higher in the Cu(x)Co. It indicates that the addition of Co ions dramatically change the NO oxidation ability of the catalyst.

To explain the effect of cobalt, we carefully look into the active sites of NO oxidation. The NO conversion profiles of H-SSZ-13 and Co-SSZ-13 catalysts demonstrate that both Brønsted acid sites and Co^{2+} ions have NO oxidation abilities, however, their operating windows are different (Figure 4-10). The H^+ sites activate the oxidation of NO at the temperature range 200-

300 °C showing volcanic profile, and the NO conversion of Co^{2+} sites increases smoothly as the temperature increases [79, 80]. With the observation about the NO oxidation reaction on the all active sites, we can explain the different NO oxidation behaviors of the Cu(x)Co and Cu(x) catalysts. It can be inferred that the volcanic curves of NO oxidation in the Cu(x) catalysts originate from the Brønsted acid sites unoccupied by metal cation. The H^+ sites from unoccupied framework Al of Cu(x) catalysts would activate the NO oxidation reaction at 200-300 °C. When the Co^{2+} ions were introduced, they anchored to the framework Al sites and substituted the H^+. As a result, the Cu(x)Co catalysts have the lower NO oxidation ability than Cu(x) at low temperature (200-300 °C) due to loss of the active H^+.

To investigate the NO oxidation ability of Cu ion in the Cu(x) and Cu(x)Co catalysts, we compare the NO conversion rate at 450 °C. The NO oxidation on H^+ can be ignored because the H^+ sites are inactive on NO oxidation at 450 °C. The NO oxidation rate of Co-SSZ-13 was subtracted to the NO oxidation rate of Cu(x) and Cu(x)Co to exclude the effect of Co^{2+} ion. At the whole Cu loading, Cu(x)Co catalysts shows higher NO oxidation rate than Cu(x) catalysts. It clearly demonstrates that the addition of Co^{2+} on improve the NO oxidation ability of Cu ion sites (Figure 4-11).

Figure 4-12 shows the standard NH_3-SCR reactivity of the Cu(x)Co,

Cu(x) and Co-SSZ-13 catalysts under the temperature range from 100 to 450 °C. First, the Co-SSZ-13 was almost inert in the NOx removal showing maximum conversion 6.3% at 250 °C. These results allow us to exclude the effect of SCR reaction on the Co^{2+} sites. Then, we compared the SCR reactivity of Cu(x)Co and Cu(x) dividing it into three regimes, low temperature (100-175 °C), medium temperature (175-300 °C) and high temperature regime (300-450 °C). First, at medium temperature range, all Cu(x)Co catalysts showed higher NOx conversion than Cu(x) catalyst. Such improvements were maximized at 250 °C in each catalyst, and the SCR rates at 250 °C were compared in Figure 4-12b. The standard SCR rates of Cu(0.5)Co, Cu(0.75)Co and Cu(1.0)Co catalysts showed 92%, 47% and 22% higher SCR rates than Cu(0.5), Cu(0.75) and Cu(1.0) catalysts, respectively, which evidently illustrated the improvement by Co ion addition. As mentioned above, such improvements are not due to the NOx removal ability of Co^{2+} ions since the SCR rate of Co-SSZ-13 itself was much lower than the increase in the SCR rates of the Cu(x)Co. Then, at high temperature regime, the Cu(0.75)Co and Cu(1.0)Co catalysts also demonstrated higher SCR reactivity than Cu(0.75) and Cu(1.0), respectively, showing maximum improvement of about 8% increase in NOx conversion in the Cu(0.75)Co catalyst. In the case of Cu(0.5)Co, however, there was dramatic decrease in NOx conversion

compared to Cu(0.5), especially at 400 °C. It indicates that the effect of Co^{2+} was totally different at medium temperature and high temperature. Unlike the medium and high temperature, little effect of Co^{2+} was observed at the low temperature regime below 175 °C, showing almost same reactivity in the Cu(x) and Cu(x)Co. Such effect of Co^{2+} ion differently facilitated depending on the reaction temperatures is described in further discussion part.

For the low temperature regime, kinetic analysis was conducted to investigate the effect of Co ion addition. NOx removal rate of the catalyst was calculated from the NOx conversion data below 30% to ignore the diffusion limitation, and apparent activation energy (E_a) was obtained based on Arrhenius equation (Figure 4-13). First of all, regardless of the Co ions addition, the activation energy values of the Cu(x)Co and Cu(x) were almost identical within each Cu loading of 0.5 wt.% (38.4, 38.9 kJ/mol), 0.75 wt.% (43.4, 46.1 kJ/mol) and 1 wt.% (46.3, 47.8 kJ/mol). It clearly demonstrates that the addition of Co ions did not affect the reaction pathway, and SCR reaction of Cu(x) and Cu(x)Co catalysts occurred under the same rate-limiting step. The activation energy values of the catalysts of 38-48 kJ/mol were corresponds to the previous study by Gao et al. reporting that the low loading Cu-SSZ-13 has an activation energy of ~40 kJ/mol.[20] This report also suggested that the activation energy increased as the Cu loading in Cu-SSZ-

13 was getting higher. Same trend was also observed in our results that the activation energy slightly increases from ~38 to 48 kJ/mol as the Cu loading increases from 0.5 to 1 wt.%.

4.3.4. DRIFT analysis

We simulated the SCR reaction by introducing $NO+O_2$ (500 ppm NO, 10% O_2) in the adsorbed NH_3 on Cu-SSZ-13, and investigated the behavior of adsorbed NH_3 using *in-situ* DRIFT analysis. The Cu(1.0) was pretreated under 20% O_2/N_2 condition at 400 °C. After pretreatment, NH_3 was pre-adsorbed under oxidative condition (500 ppm NH_3, 10% O_2) at 170, 200 and 250 °C. The sample spectrum obtained before the NH_3 adsorption was used as a background. In DRIFT spectra, the IR absorption peaks of zeolite framework (T-O-T vibration; Si-O-Si, Si-O-Al) were shown in the range from 1100 cm^{-1} to 800 cm^{-1}. When the Cu ion interacts to zeolite framework, new perturbation peaks appear. Due to their different interaction with framework, the 1Al-Cu and 2Al-Cu species shows different perturbation peaks at 950 cm^{-1} and 900 cm^{-1}, respectively, which can be used to distinguish two Cu ion species [36, 52, 81]. These perturbation peaks fade away after adsorption of NH_3 because interactions between the Cu ions and zeolite framework is weaken by the solvation of Cu ions. Therefore, when we get the spectra after NH_3 adsorption with a background of pristine Cu-SSZ-13, the negative perturbation peaks were displayed at 950 cm^{-1} and 900 cm^{-1} (Figure 4-14).

As the adsorbed NH_3 consumed, the negative perturbation peak decreased by diminishing the solvation effect of NH_3 on Cu ion. We can

compare the SCR reactivity of the 1Al-Cu and 2Al-Cu species through observing the decrease rate of their perturbation peaks during the reaction of $NO+O_2$ with pre-adsorbed NH_3. Normalized intensity profiles of perturbation peak were displayed in Figure 4-15 during the simulated SCR reaction at 170, 200 and 250 °C. Perturbation peaks of these two Cu species decreased with almost same rate during the reaction at 170 °C. However, at 200 °C, the 1Al-Cu perturbation peak (black dot) decreased slightly more rapidly than the 2Al-Cu peak (red dot). It indicates that the 1Al-Cu species were more active in the SCR reaction at 200 °C than the 2Al-Cu species. As the reaction temperature increases to 250 °C, such different reactivity becomes more obvious.

4.3.5. NO oxidation as a probe reaction of 1Al-Cu ion species

We designed the catalysts to have more amount of the 1Al-Cu species by addition of Co cation. Based on the H_2-TPR analysis, we ensure that most of the Cu^{2+} ion species were present as the 1Al-Cu species, which indicates that majority of 2Al sites were blocked by Co^{2+} ions. The theoretical value of the ratio of Cu^{2+} on 2Al sites (2Al-Cu) to framework Al was proposed to be about 0.15 in the SSZ-13 of the Si/Al ratio used in this study [55]. This theoretical value is consistent with the Co loading of the Cu(x)Co catalysts (Co/Al=0.15) demonstrating that the Cu(x)Co catalysts successfully blocked the most of the 2Al sites in the SSZ-13. We investigate how such species control gave rise to an effect on reactivity of Cu-SSZ-13 catalyst.

In previous studies, it is already known that of the 1Al-Cu and 2Al-Cu species, only 1Al-Cu species are selectively active in the NO oxidation reaction. It is well consistent with our results that the NO oxidation rate of catalysts dramatically enhanced after the species control from 2Al-Cu to 1Al-Cu by Co^{2+} ion (Table 4-2). Upon investigation of this species-dependent NO oxidation, Verma et al. found that Cu-SSZ-13 with Cu loading below a certain amount did not show any NO oxidation reactivity. They proposed that Cu_xO_y species catalyzed the NO oxidation and such species existed when Cu/Al ratio is above 0.2 that is the maximum ratio of 2Al-Cu [55]. Based on the results, it

can be inferred that only 1Al-Cu species can activate the oxidation of NO. Ruggeri et al. revealed that the such Cu_xO_y species was dimeric Cu^{2+}-O-Cu^{2+} site formed from two Cu^{2+}-OH^- species located at the 1Al sites by following reaction [58].

$$2(Z\text{-}O\text{-}Cu^{2+}\text{-}OH^-) \rightarrow Z\text{-}O\text{-}[Cu^{2+}\text{-}O\text{-}Cu^{2+}]\text{-}O\text{-}Z + H_2O$$

Because the 2Al-Cu species cannot activate this dehydro-condensation reaction, they are known to be inert in the NO oxidation [55]. This suggest that the NO oxidation can be used as the probe reaction of the 1Al-Cu species, so we can compare the amount of the 1Al-Cu species in the catalysts via NO conversions. Figure 4-16 demonstrates the relationship between NO oxidation rates at 450 °C (Figure 4-11) and the amount of 1Al-Cu that is obtained from H_2-TPR results (Table 4-2). The NO oxidation rate shows a linear dependence on the square of the 1Al-Cu amount. This result clearly shows the participation of two 1Al-Cu species on the NO oxidation reaction deriving dimeric Cu species by the reaction of two 1Al-Cu species.

4.3.6. Different NH_3-SCR reactivity of Cu ion species

Improving effect of Co^{2+} on the NH_3-SCR reactivity was clearly demonstrated at the temperature 250 °C (Figure 4-12b). Since the Co^{2+} cannot activate the NH_3-SCR reaction, the effect of Co^{2+} on NH_3-SCR reactivity would be attributed to its effect on change on Cu ion species. It was confirmed that addition of Co^{2+} changed the distribution of Cu ion species from the 2Al-Cu to the 1Al-Cu by the H_2-TPR (Figure 4-6 and Table 2). Based on the reaction test and characterization data, it can be inferred that the 1Al-Cu has a higher reactivity than the 2Al-Cu species, which gives rise to the superior activity of Cu(x)Co with higher 1Al-Cu ratio. In DRIFT analysis, the NH_3 on the 1Al-Cu species reacted more rapidly than that on the 2Al-Cu at 250 °C, which directly demonstrated the higher reactivity of the 1Al-Cu species (Figure 4-15). In the part 2, we also suggested that the high mobility of 1Al-Cu leads to its higher SCR reactivity. Such discrepant reactivity of two Cu ion species is closely related to the reaction kinetics of SCR reaction on the Cu-SSZ-13 catalyst.

4.3.7. Reaction kinetics and effect of Co^{2+} ion

In the SCR reaction of Cu-SSZ-13, the re-oxidation process of reduced Cu^{+} is suggested as the rate-determining steps of overall reaction with activation energy of 70-80 kJ/mol obtained from both experimental results and DFT calculations. Re-oxidation step is facilitated by the formation of dimeric Cu species ($[Cu^{I}(NH_3)_2]^{+}-O_2-[Cu^{I}(NH_3)_2]^{+}$), which is formed from diffusion of the ($[Cu^{I}(NH_3)_2]^{+}$ complexes inside the SSZ-13 [20-22]. However, in low Cu loadings where the volumetric density of Cu ion is low, the formation of dimeric Cu species becomes much less facile because distance among the Cu ions is too far. Under this situation, the reaction is limited by the mass-transfer of Cu ion species, and consequently apparent activation energy is measured to ~40 kJ/mol that is ~50% of E_a value at high Cu loadings. In this reaction kinetics, the mobility of Cu ion is a key properties of SCR reaction, which is called ion-transfer limiting condition. We have found that the mobility of Cu ion species determines the low-temperature reactivity of Cu-SSZ-13, and the 1Al-Cu species than the 2Al-Cu could be more active due to their higher mobility under this SCR reaction condition.

Combining on the previous studies with the obtained E_a of 38~48 kJ/mol, we can infer that all SCR reaction rates of the Cu(x)Co and Cu(x) catalysts were determined by the diffusion of Cu ion. Figure 4-17

displayed the a linear relationship with a slope of 1.956 between logarithm of Cu/Al ratios and SCR rates with Cu(0.5), Cu(0.75), Cu(1.0) and Cu(1.3) catalysts (data of Cu(1.3) catalyst was not shown). Such relationship demonstrated a second-order dependence of the SCR rates on Cu loading, evidently confirming the diffusion limitation of the Cu ions in the reaction of the catalysts. In this kinetic regime, the higher ratio of 1Al-Cu species in the Cu(x)Co catalyst can enhance the SCR reactivity. As the 1Al-Cu species have a weaker interaction to the SSZ-13 framework than the 2Al-Cu species, they are more mobile in the cage of SSZ-13. It makes the formation of a key intermediate, dimeric Cu species, more facile, which leads to the reactivity enhancement at regime 2 (medium temperature 170-300 °C).

4.3.8. Temperature dependent effect of Co^{2+} ion

Although the Co^{2+} ion improves the SCR reactivity of Cu-SSZ-13 at the medium temperature, its effect was differently facilitated at the other temperature regime (regime 1 and 3). This phenomenon is assumed to originate from the different behavior of Cu ion in the Cu-SSZ-13 with temperature. First, at the regime 1 (100-175 °C), the reactivity was almost same in the Cu(x)Co and Cu(x) catalysts, which have different 1Al-Cu/2Al-Cu ratio. It can be inferred that the discrepant reactivity of 1Al-Cu and 2Al-Cu species do not appear below the temperature of 175 °C. *In-situ* DRIFT results in Figure 4-15 also demonstrated the same SCR reactivity of NH_3 adsorbed on the 1Al-Cu and 2Al-Cu species at 170 °C, which supports our conjecture. As the temperature increased from 170 to 250 °C, the discrepancy between 1Al-Cu and 2Al-Cu was getting clear.

Lomachenko et al. investigated the distribution of Cu ion species in the SSZ-13 using *operando* XANES, and reported that most of the Cu ions are fully solvated at the low temperature (150 °C) by the NH_3 under SCR condition, so have little interaction to SSZ-13 framework [14]. As the different mobility of 1Al-Cu and 2Al-Cu species originate from their different electrostatic interaction to zeolite framework, it can be inferred that there is no difference in the mobility of two Cu ion species at very low temperature where

the interaction between Cu ions and framework does not exist [16]. Considering that the discrepancy was due to the different mobility of two Cu species, this might be the reason why the 1Al-Cu and 2Al-Cu species have same reactivity below 175 °C. When some of NH_3 desorbed from Cu ions as the temperature increases to 200-300 °C, Cu ion can interact to framework by weaken solvation effect, which makes the two Cu species have different mobility and as a result different reactivity.

However, as reaction temperature increases further to above 350 °C, almost of adsorbed NH_3 on the Cu sites desorbed [14, 82]. With the desorption of NH_3, a 'conversion dip' at 350 °C was shown in the NOx conversion profile of the Cu-SSZ-13, giving the curve seagull-like shape (Figure 4-12a). This is a general phenomenon in low loading Cu-SSZ-13 which is attributed to loss of Cu ion mobility by absence of solvation effect. Without the solvation by NH_3 above 350 °C, Cu ions should present as fixed ionic sites that strongly interacts with zeolite framework. This localized Cu species is facilitated as new active species, which leads to high SCR reactivity at high temperature. Due to the change in the active sites, SCR reaction above 350 °C differs from the reaction pathway with that at low temperature. According to Gao et al., the SCR rates at 200 and 380 °C have different dependence on the Cu/Al ratios indicating that they were under different reaction kinetic condition [20].

Despite the second order dependence of reaction rates at 200 °C to Cu/Al ratio, the reaction rates at 380 °C have linear correlation to the Cu/Al ratio. It indicates that the SCR reaction is not determined by the diffusion of mobile Cu ion at high temperature.

At the Cu loading of 0.75 and 1.0 wt%, the CuCo catalysts showed higher NOx conversion even at the high temperatures (350-450 °C). This improvement can also be explained through the change in the Cu ion species. Figure 4-11 demonstrated that the higher NO oxidation ability of CuCo catalysts indicating that more delocalized dimeric Cu species (Cu^{2+}-O-Cu^{2+}) were present in the CuCo catalysts at the high temperature, which is active site of NO oxidation. As Fehami et al. insisted, this immobilized oxygen-bridged dimeric Cu species (Cu^{2+}-O-Cu^{2+}) could also catalyze NH_3-SCR reaction by oxidizing NO, which enhances the re-oxidation process and provides nitrate intermediates. It can be inferred that the higher amount of 1Al-Cu species in the Cu(0.75)Co and Cu(1.0)Co catalysts promoted the formation of localized dimeric Cu species resulting in higher NOx removal ability than Cu(0.75) and Cu(1.0) catalysts, respectively. However, the Cu(0.5)Co catalyst showed different trend with the other two catalysts, which could not be explained by the promoting effect of the 1Al-Cu species. Both Cu(0.5) and Cu(0.5)Co catalysts demonstrated ‘conversion dip’ at 350 °C, which arose from the loss

of mobilized Cu species by desorption of NH_3. At higher temperature above 400 °C, Cu ions gets some extent of mobility to form dimeric species due to thermal energy, which gave rise to the dramatic increase of NOx conversion [15, 82]. In the low loading Cu-SSZ-13 like the Cu(0.5), the Cu ions should migrate to other cage to form the dimeric species since it has low density of Cu, which means long average distance between two Cu ions. Contrast to dramatic activity increase in the Cu(0.5) at 400 °C, the Cu(0.5)Co catalyst showed little increase in NOx conversion indicating that something hindered the formation of dimer at 400 °C, so that the 'conversion dip' could not be recovered until the temperature 450 °C. It is supposed that the presence of Co^{2+} ions deters the formation of dimeric Cu species in the Cu(0.5)Co catalyst by physically blocking the channel of SSZ-13. At the high loading Cu-SSZ-13 catalysts, the two Cu ions are more likely to exist in same cage, which makes the formation of dimeric Cu species irrelevant to the channel blocking effect of Co^{2+} ions. Unfortunately, we could not observe the formation of delocalized oxygen bridged Cu dimer with temperature, therefore, further study should be needed to investigate it.

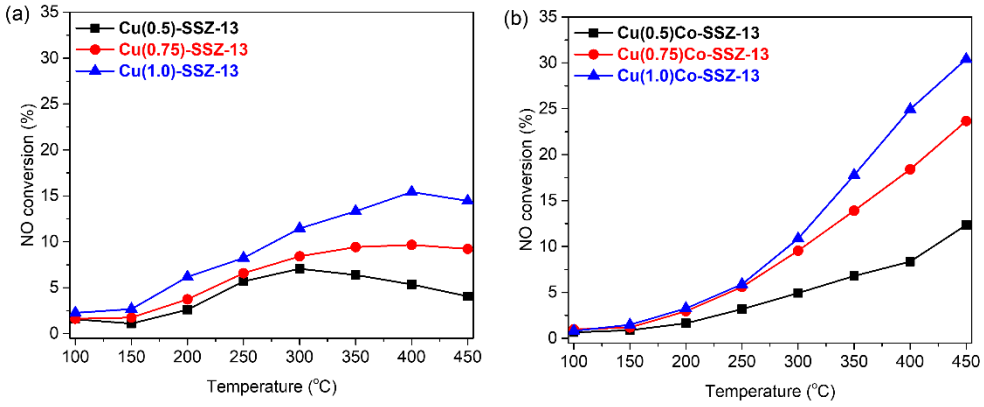

Figure 4-9. NO oxidation reactivity of (a) Cu(x) and (b) Cu(x)Co catalysts under 500 ppm NO and 10% O_2 balance with N_2 GHSV: 120,000 h^{-1}.

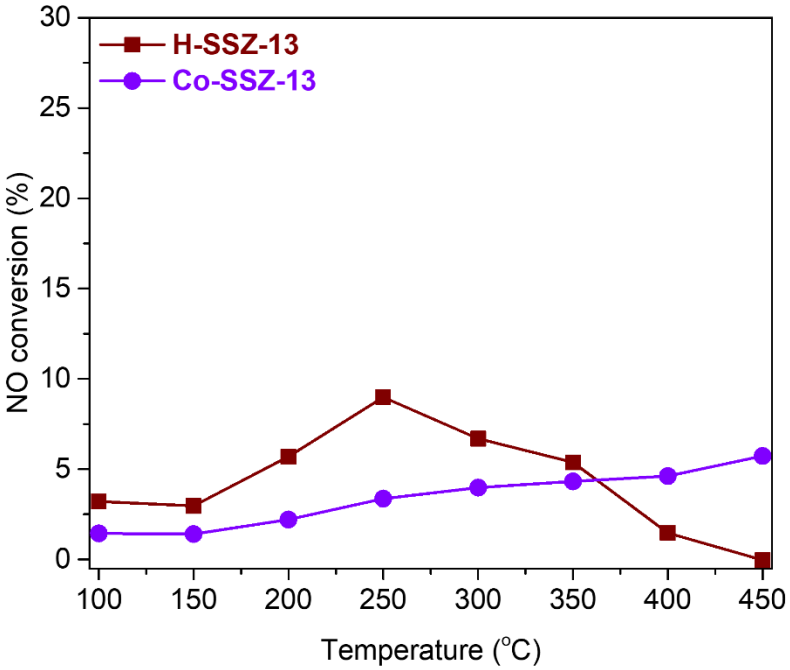

Figure 4-10. NO oxidation reactivity of H-SSZ-13 and Co-SSZ-13 under 500 ppm NO and 10% O_2 balance with N_2 GHSV: 120,000 h^{-1}.

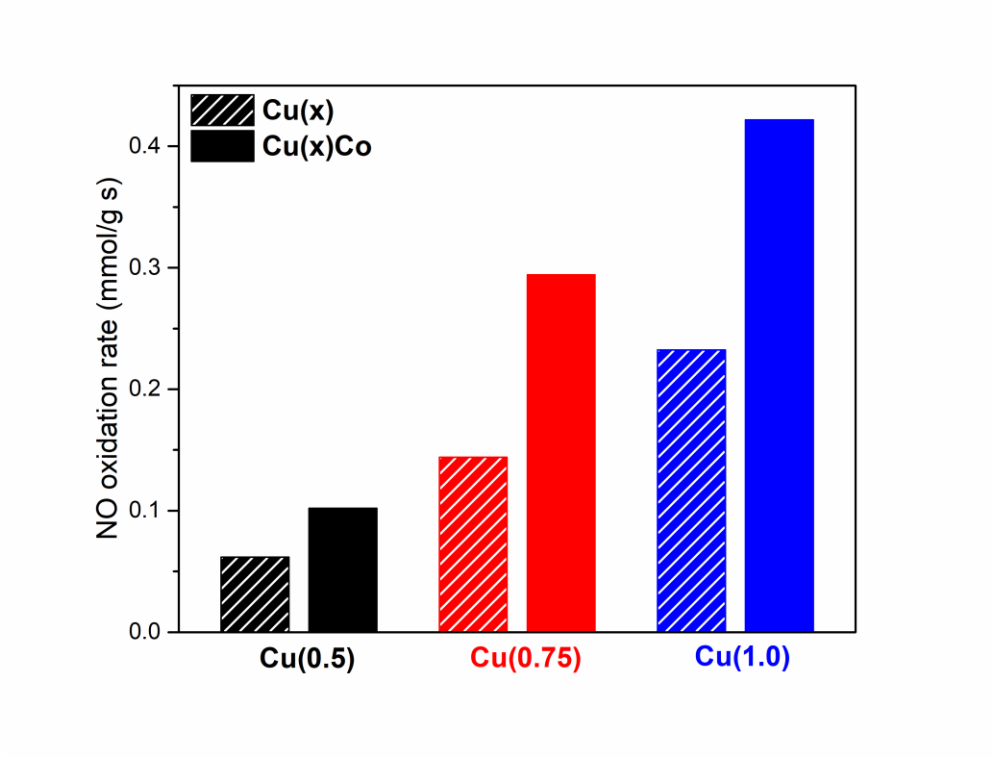

Figure 4-11. Comparison of NO oxidation rate on Cu ion site over Cu(x) and Cu(x)Co catalysts at 450 °C.

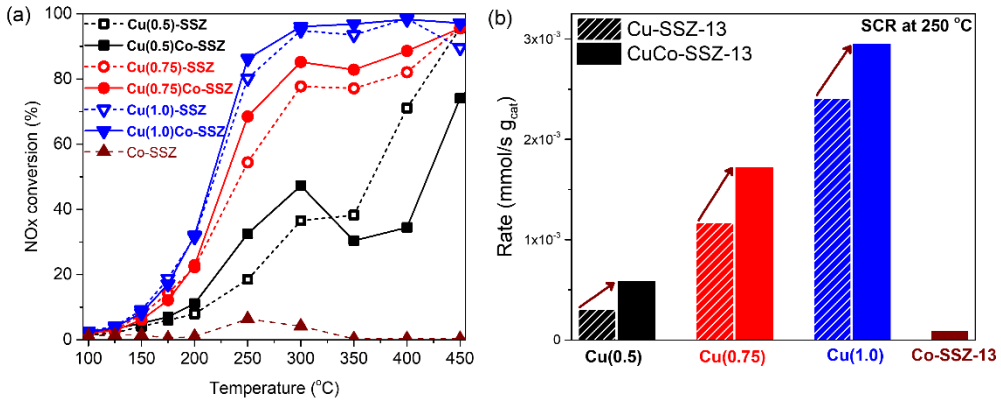

Figure 4-12. (a) NH_3-SCR reactivity and NOx removal rate at 250 °C of Cu(x) and Cu(x)Co catalysts under 500 ppm NO, 500 ppm NH_3 10% O_2, 5% H_2O balanced with N_2, GHSV: 240,000 h^{-1}.

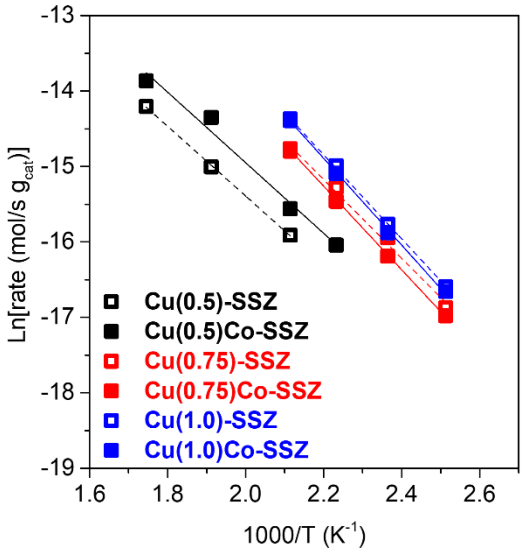

Sample	E_a (kJ/mol)
Cu(0.5)	38.4
Cu(0.5)Co	38.9
Cu(0.75)	43.4
Cu(0.75)Co	46.1
Cu(1.0)	46.3
Cu(1.0)Co	47.8

Figure 4-13. Arrhenius plot of Cu(x) and Cu(x)Co catalysts and their activation energy.

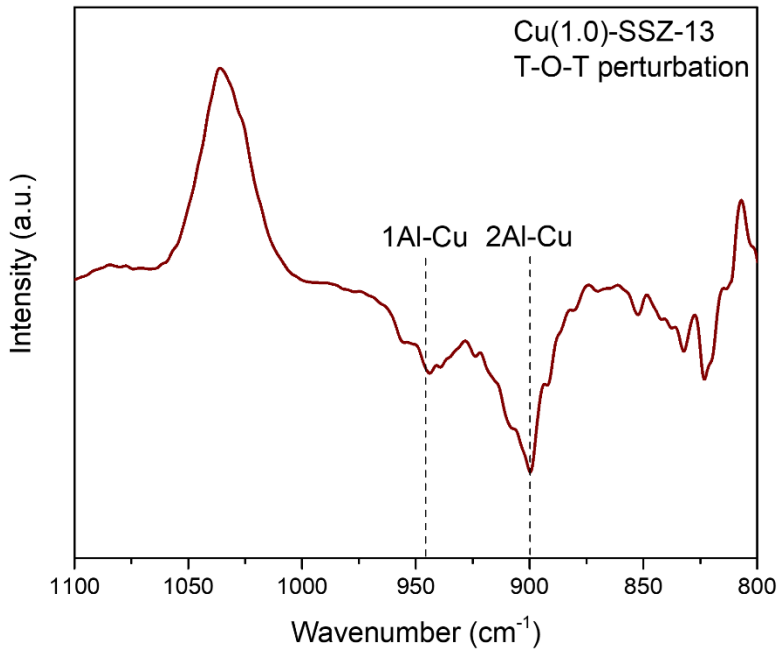

Figure 4-14. DRIFT spectra of T-O-T vibration at Cu(1.0)-SSZ-13 catalyst after NH_3 adsorption at 200 °C.

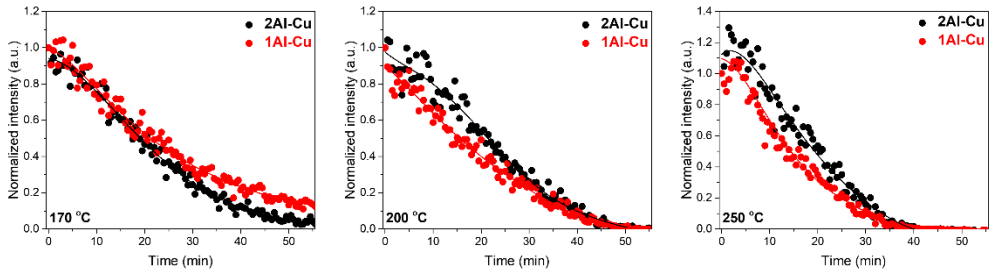

Figure 4-15. Intensity profiles of T-O-T vibration peaks of 1Al-Cu and 2Al-Cu species during the reaction of $NO+O_2$ with pre-adsorbed NH_3 on Cu(1.0) catalyst at 170, 200 and 250 °C.

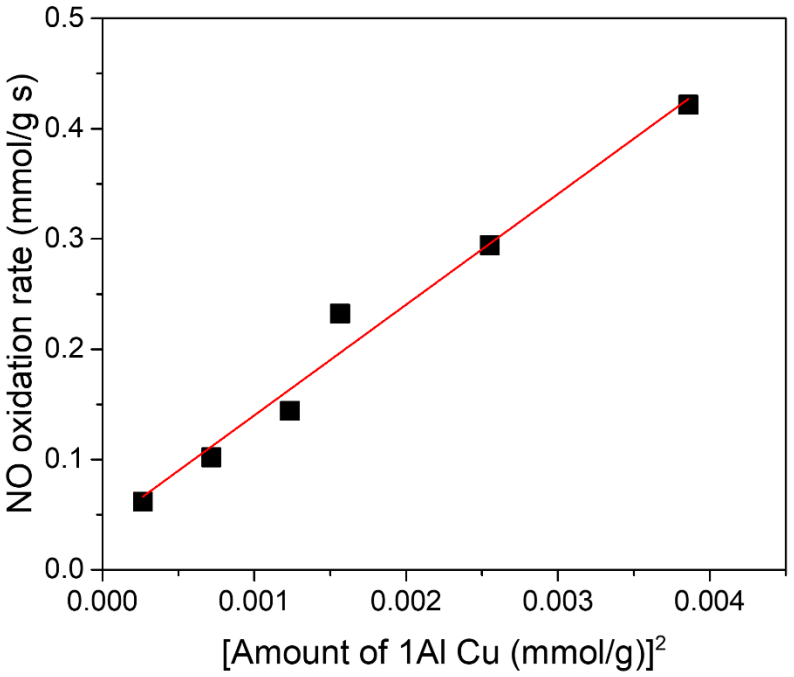

Figure 4-16. Correlation between NO oxidation rate at 450 °C and amount of 1Al-Cu species from H_2-TPR.

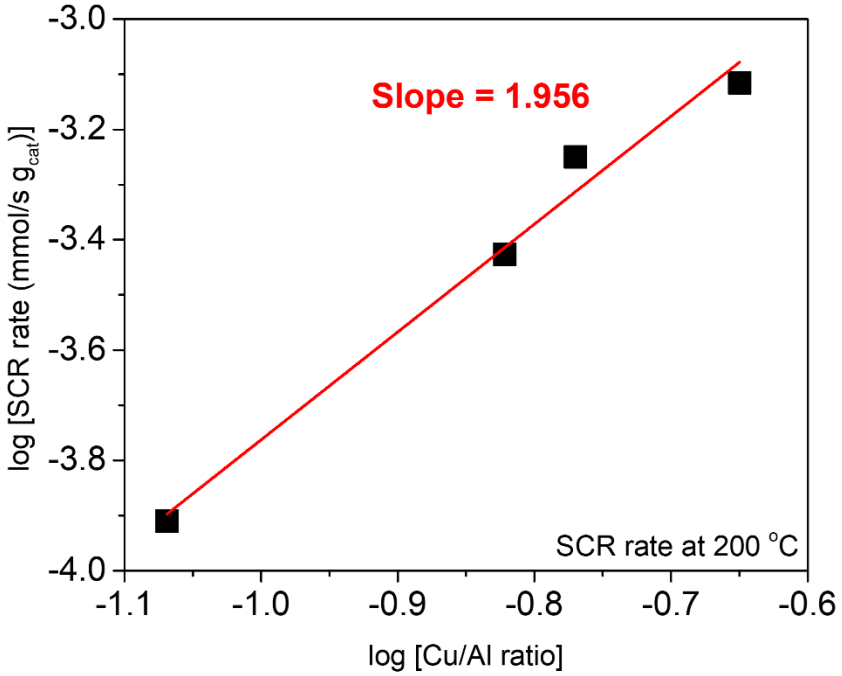

Figure 4-17. Logarithm correlation between SCR rate and Cu/Al ratio of Cu(x) catalysts.

Chapter 5. Summary and Conclusions

In this work, the behavior of Cu ions in the Cu-SSZ-13 was investigated to understand the NH_3-SCR reaction over Cu-SSZ-13 and conclusively develop the improved catalyst. We looked into the properties for Cu ion, especially the mobility of Cu ion in the SSZ-13 cage. Cu-SSZ-13 catalysts were precisely prepared to observe the mobility of Cu ion. Various characterization including in-situ DRIFT and EPR, has revealed that the mobility is closely related to the SCR reactivity of Cu-SSZ-13, which provided the strategy to improve the performance of Cu-SSZ-13.

First of all, the Cu-SSZ-13 and H-SSZ-13 were physically mixed by using different methods to control the extent of contact in the particles. One was the highly contact sample (PM-H-SSZ), whose particles were directly contacted. The other was the loosely contact sample (PM-L-SSZ), whose particles were separated. We compared the catalysts using different characters of two kinds of copper ions, 2Al Cu^{2+} and 1Al $[Cu\text{-}OH]^+$. 2Al Cu^{2+} is more stable, has larger coverage and is located at a thermodynamically more stable site than the 1Al $[Cu\text{-}OH]^+$. The PM-H-SSZ catalyst has a higher ratio of 2Al Cu^{2+} than the PM-L-SSZ, measured by T-O-T vibration in the DRIFT spectra. This indicates that the 1Al $[Cu\text{-}OH]^+$ in Cu-SSZ-13 particles move to the 2Al sites of H-SSZ-13, and change the conformation to 2Al Cu^{2+}. This result is reasonable because copper ion prefer to be located on the 2Al site in the form of 2Al Cu^{2+}. We referred this as ‘inter-particle ion migration.’ The amount of each species was quantified from analyzing hydrogen consumption in the H_2-TPR,

amount of Brønsted acid sites in the NH_3-wet TPD and EPR spectra. All the combined analysis data indicated that the PM-H-SSZ had almost twice as many 2Al Cu^{2+} as the PM-L-SSZ, and commensurate composition of copper species with the reference of $Cu_{0.75}$-SSZ that had almost the same loading of copper. This implies that a considerable amount of copper ions moves, and a large number of the 2Al sites in empty H-SSZ-13 are occupied. Different distributions of copper ions between the physically mixed SSZ-13 also resulted in the variation of the NH_3-SCR activity. With the density of copper ions being lowered in the PM-H-SSZ by the migration of ions, the NH_3-SCR reactivity of the PM-H-SSZ at low temperatures also declined. The presence of water had a significant role to facilitate the inter-particle migration by increasing the mobility of copper ions in a zeolite. This study implies that copper ions in the SSZ-13 can move in a long distance and migrate to different particles passing through particle-particle interface under hydrothermal condition via preference towards the more stable site. The migration of mobile copper ions is an important factor of hydrothermal stability because it determines the formation of copper oxide cluster, which is the primary cause of deactivation.

Then, in order to investigate the relationship between the mobility of Cu ion and SCR activity, the ratio of 1Al-Cu to 2Al-Cu was successfully controlled by using hydrothermal treatment. The Cu-SSZ-13 with higher 1Al-Cu ratio demonstrated superior reactivity, which means that the 1Al-Cu has a higher SCR reactivity than the 2Al-Cu. Interestingly, such different reactivity was valid only under reactions limited by the mass-transfer of Cu ions where the mobility of the Cu ions is significant. *In-*

situ DRIFT analysis clearly showed the different behavior of 1Al-Cu and 2Al-Cu depending on the reaction kinetics. On this account, we propose that a high mobility of the 1Al-Cu ion species determines its superior SCR reactivity by promoting the formation of dimeric Cu intermediates. We believe that this study can provide further information of the active Cu ions to understand the low-temperature NH_3-SCR reaction, which enables us to design rational Cu-SSZ-13 catalysts that are highly active in the low-temperature regime (150-250 °C) by tuning the mobility of the Cu ions in the catalysts.

Based on the fact that the 1Al-Cu species show higher SCR reactivity than the 2Al-Cu species due to their high mobility, the Cu-SSZ-13 catalysts were designed to have more 1Al-Cu species ratio within same Cu loadings by the addition of Co^{2+} ion. As the Co^{2+} ion is known to be selectively located at the 2Al sites, we tried to block the 2Al sites with Co^{2+} ions in advance, and then impregnated the Cu species to induce the Cu ions to be located at 1Al sites. After the introduction of Co^{2+} ions, in the H_2-TPR profiles, low temperature reduction peak (200-300 °C) increased and high temperature peak (350-500 °C) decreased in all Cu loadings (0.5, 0.75 and 1.0 wt%), which indicated that Co^{2+} ions successfully induced the Cu ions to be located at 1Al sites rather than 2Al sites. NO oxidation reactivity at 450 °C were compared and showed linear relationship to the square of the amount of 1Al-Cu species. It clearly demonstrated the participation of two 1Al-Cu ions in the NO oxidation reaction, and made sure that the NO oxidation could be used as the probe molecules of 1Al-Cu species. As we intended, the introduction of Co^{2+} ion improved the NH_3-SCR

reactivity at low temperature, and such improvement was also shown even at the high temperature except the Cu(0.5) and Cu(0.5)Co catalysts. Kinetic studies illustrated that the rate-determining step was not altered by the Co^{2+} ion, and activation energy was ~ 40 kJ/mol, which was the same for all reactions. This result indicates that the reactions were governed by Cu ion diffusion, and under such kinetic regime, the 1Al-Cu species shows higher SCR reactivity due to their higher mobility than the 2Al-Cu species, which was confirmed by *in-situ* DRIFT analysis. Tuning the Cu ion species with Co^{2+} co-cation was a simple, but powerful approach to improve the reactivity of Cu-SSZ-13, and this concept would provide the platform to design rational catalysts in other species-specific catalytic reaction by controlling ion species in the zeolite.

Bibliography

[1] S.C. Anenberg, J. Miller, R. Minjares, L. Du, D.K. Henze, F. Lacey, C.S. Malley, L. Emberson, V. Franco, Z. Klimont, C. Heyes, Nature, 545 (2017) 467-471.
[2] D.L. Davis, J Environmental health perspectives, 110 (2002) A734-A735.
[3] W.H. Organization, in, Copenhagen: WHO Regional Office for Europe, 2003.
[4] M. Iwamoto, H. Furukawa, Y. Mine, F. Uemura, S.-i. Mikuriya, S. Kagawa, J. Chem. Soc., Chem. Commun., (1986) 1272-1273.
[5] R.Q. Long, R.T. Yang, J. Am. Chem. Soc., 121 (1999) 5595-5596.
[6] S. Sato, Y. Yu-u, H. Yahiro, N. Mizuno, M. Iwamoto, Applied catalysis, 70 (1991) L1-L5.
[7] A. Grossale, I. Nova, E. Tronconi, Catal. Today, 136 (2008) 18-27.
[8] P. Balle, B. Geiger, S. Kureti, Applied Catalysis B: Environmental, 85 (2009) 109-119.
[9] J. Sun, H. Fang, P.I. Ravikovitch, D.S. Sholl, The Journal of Physical Chemistry C, (2019).
[10] M. Nielsen, R.Y. Brogaard, H. Falsig, P. Beato, O. Swang, S. Svelle, Acs Catalysis, 5 (2015) 7131-7139.
[11] J.H. Kwak, R.G. Tonkyn, D.H. Kim, J. Szanyi, C.H. Peden, J. Catal., 275 (2010) 187-190.
[12] D.W. Fickel, E. D'Addio, J.A. Lauterbach, R.F. Lobo, Applied Catalysis B: Environmental, 102 (2011) 441-448.
[13] U. Deka, A. Juhin, E.A. Eilertsen, H. Emerich, M.A. Green, S.T. Korhonen, B.M. Weckhuysen, A.M. Beale, The Journal of Physical Chemistry C, 116 (2012) 4809-4818.
[14] K.A. Lomachenko, E. Borfecchia, C. Negri, G. Berlier, C. Lamberti, P. Beato, H. Falsig, S. Bordiga, J. Am. Chem. Soc., 138 (2016) 12025-12028.
[15] H. Lee, I. Song, S.W. Jeon, D.H. Kim, Reaction Chemistry & Engineering, 4 (2019) 1059-1066.
[16] C. Paolucci, A.A. Parekh, I. Khurana, J.R. Di Iorio, H. Li, J.D. Albarracin Caballero, A.J. Shih, T. Anggara, W.N. Delgass, J.T. Miller, F.H. Ribeiro, R. Gounder, W.F. Schneider, J. Am. Chem. Soc., 138 (2016) 6028-6048.
[17] S.A. Bates, A.A. Verma, C. Paolucci, A.A. Parekh, T. Anggara, A. Yezerets, W.F. Schneider, J.T. Miller, W.N. Delgass, F.H. Ribeiro, J. Catal., 312 (2014) 87-97.
[18] A. Marberger, A.W. Petrov, P. Steiger, M. Elsener, O. Kröcher, M. Nachtegaal, D. Ferri, Nature Catalysis, 1 (2018) 221-227.
[19] R. Zhang, J.-S. McEwen, The Journal of Physical Chemistry Letters, 9 (2018) 3035-3042.
[20] F. Gao, D. Mei, Y. Wang, J.n. Szanyi, C.H. Peden, J. Am. Chem. Soc., 139 (2017) 4935-4942.
[21] C. Paolucci, I. Khurana, A.A. Parekh, S. Li, A.J. Shih, H. Li, J.R. Di Iorio, J.D. Albarracin-Caballero, A. Yezerets, J.T. Miller, Science, 357 (2017) 898-903.

[22] C. Negri, T. Selleri, E. Borfecchia, A. Martini, K.A. Lomachenko, T.V.W. Janssens, M. Cutini, S. Bordiga, G. Berlier, J. Am. Chem. Soc., (2020).
[23] F. Gao, Y. Wang, N.M. Washton, M. Kollár, J. Szanyi, C.H.F. Peden, ACS Catalysis, 5 (2015) 6780-6791.
[24] T. Zhang, F. Qiu, J. Li, Applied Catalysis B: Environmental, 195 (2016) 48-58.
[25] B. Peng, K.G. Rappé, Y. Cui, F. Gao, J. Szanyi, M.J. Olszta, E.D. Walter, Y. Wang, J.D. Holladay, R.A. Goffe, Applied Catalysis B: Environmental, 263 (2020).
[26] T. Usui, Z. Liu, S. Ibe, J. Zhu, C. Anand, H. Igarashi, N. Onaya, Y. Sasaki, Y. Shiramata, T. Kusamoto, T. Wakihara, ACS Catalysis, 8 (2018) 9165-9173.
[27] S.T. Korhonen, D.W. Fickel, R.F. Lobo, B.M. Weckhuysen, A.M. Beale, Chem Commun (Camb), 47 (2011) 800-802.
[28] M. Zema, S. Tarantino, G. Montagna, Chem. Mater., 20 (2008) 5876-5887.
[29] F. Gao, D. Mei, Y. Wang, J.n. Szanyi, C.H. Peden, Journal of the American Chemical Society, 139 (2017) 4935-4942.
[30] A.M. Beale, I. Lezcano-Gonzalez, W.A. Slawinksi, D.S. Wragg, Chem Commun (Camb), 52 (2016) 6170-6173.
[31] M. Müller, G. Harvey, R. Prins, Microporous Mesoporous Mater., 34 (2000) 135-147.
[32] J. Wang, Z. Peng, H. Qiao, L. Han, W. Bao, L. Chang, G. Feng, W. Liu, RSC Adv., 4 (2014) 42403-42411.
[33] Y.J. Kim, J.K. Lee, K.M. Min, S.B. Hong, I.-S. Nam, B.K. Cho, J. Catal., 311 (2014) 447-457.
[34] J. Song, Y. Wang, E.D. Walter, N.M. Washton, D. Mei, L. Kovarik, M.H. Engelhard, S. Prodinger, Y. Wang, C.H.F. Peden, F. Gao, ACS Catalysis, 7 (2017) 8214-8227.
[35] P.G. Blakeman, E.M. Burkholder, H.-Y. Chen, J.E. Collier, J.M. Fedeyko, H. Jobson, R.R. Rajaram, Catal Today, 231 (2014) 56-63.
[36] J.H. Kwak, H. Zhu, J.H. Lee, C.H. Peden, J. Szanyi, Chem. Commun., 48 (2012) 4758-4760.
[37] F. Giordanino, P.N. Vennestrom, L.F. Lundegaard, F.N. Stappen, S. Mossin, P. Beato, S. Bordiga, C. Lamberti, Dalton Trans, 42 (2013) 12741-12761.
[38] E. Borfecchia, K.A. Lomachenko, F. Giordanino, H. Falsig, P. Beato, A.V. Soldatov, S. Bordiga, C. Lamberti, Chem Sci, 6 (2015) 548-563.
[39] J. Luo, F. Gao, K. Kamasamudram, N. Currier, C.H. Peden, A. Yezerets, J. Catal., 348 (2017) 291-299.
[40] J.R. Di Iorio, S.A. Bates, A.A. Verma, W.N. Delgass, F.H. Ribeiro, J.T. Miller, R. Gounder, in: Top. Catal., 2015, pp. 424-434.
[41] S.A. Bates, W.N. Delgass, F.H. Ribeiro, J.T. Miller, R. Gounder, J. Catal., 312 (2014) 26-36.
[42] F. Gao, E.D. Walter, M. Kollar, Y. Wang, J. Szanyi, C.H.F. Peden, J. Catal., 319 (2014) 1-14.
[43] F. Gao, E.D. Walter, E.M. Karp, J. Luo, R.G. Tonkyn, J.H. Kwak, J. Szanyi, C.H.F. Peden, J. Catal., 300 (2013) 20-29.
[44] T.H. Vuong, J. Radnik, J. Rabeah, U. Bentrup, M. Schneider, H. Atia, U.

Armbruster, W. Grünert, A. Brückner, ACS Catalysis, 7 (2017) 1693-1705.
[45] F. Göltl, R.E. Bulo, J. Hafner, P. Sautet, The Journal of Physical Chemistry Letters, 4 (2013) 2244-2249.
[46] G.M. Psofogiannakis, J.F. McCleerey, E. Jaramillo, A.C.T. van Duin, The Journal of Physical Chemistry C, 119 (2015) 6678-6686.
[47] S.J. Schmieg, S.H. Oh, C.H. Kim, D.B. Brown, J.H. Lee, C.H.F. Peden, D.H. Kim, Catal. Today, 184 (2012) 252-261.
[48] D. Wang, Y. Jangjou, Y. Liu, M.K. Sharma, J. Luo, J. Li, K. Kamasamudram, W.S. Epling, Applied Catalysis B: Environmental, 165 (2015) 438-445.
[49] P. Wu, T. Komatsu, T. Yashima, J. Phys. Chem., 99 (1995) 10923-10931.
[50] J.H. Kwak, D. Tran, S.D. Burton, J. Szanyi, J.H. Lee, C.H.F. Peden, J. Catal., 287 (2012) 203-209.
[51] L. Ma, Y. Cheng, G. Cavataio, R.W. McCabe, L. Fu, J. Li, Chem. Eng. J., 225 (2013) 323-330.
[52] J. Luo, D. Wang, A. Kumar, J. Li, K. Kamasamudram, N. Currier, A. Yezerets, Catal. Today, 267 (2016) 3-9.
[53] U. Deka, I. Lezcano-Gonzalez, B.M. Weckhuysen, A.M. Beale, ACS Catalysis, 3 (2013) 413-427.
[54] Y. Shan, J. Du, Y. Yu, W. Shan, X. Shi, H. He, Applied Catalysis B: Environmental, 266 (2020).
[55] A.A. Verma, S.A. Bates, T. Anggara, C. Paolucci, A.A. Parekh, K. Kamasamudram, A. Yezerets, J.T. Miller, W.N. Delgass, W.F. Schneider, F.H. Ribeiro, J. Catal., 312 (2014) 179-190.
[56] F. Gao, N.M. Washton, Y. Wang, M. Kollár, J. Szanyi, C.H.F. Peden, J. Catal., 331 (2015) 25-38.
[57] R. Villamaina, U. Iacobone, I. Nova, M.P. Ruggeri, J. Collier, D. Thompsett, E. Tronconi, ChemCatChem, 12 (2020) 3795-3795.
[58] M.P. Ruggeri, I. Nova, E. Tronconi, J.A. Pihl, T.J. Toops, W.P. Partridge, Applied Catalysis B: Environmental, 166-167 (2015) 181-192.
[59] R. Villamaina, S. Liu, I. Nova, E. Tronconi, M.P. Ruggeri, J. Collier, A. York, D. Thompsett, ACS Catalysis, 9 (2019) 8916-8927.
[60] Y. Jangjou, Q. Do, Y. Gu, L.-G. Lim, H. Sun, D. Wang, A. Kumar, J. Li, L.C. Grabow, W.S. Epling, ACS Catalysis, 8 (2018) 1325-1337.
[61] A. Godiksen, O.L. Isaksen, S.B. Rasmussen, P.N.R. Vennestrøm, S. Mossin, ChemCatChem, 10 (2018) 366-370.
[62] Y. Zhang, Y. Peng, J. Li, K. Groden, J.-S. McEwen, E.D. Walter, Y. Chen, Y. Wang, F. Gao, ACS Catalysis, 10 (2020) 9410-9419.
[63] J. Kim, S.J. Cho, D.H. Kim, ACS Catalysis, 7 (2017) 6070-6081.
[64] J.S. McEwen, T. Anggara, W.F. Schneider, V.F. Kispersky, J.T. Miller, W.N. Delgass, F.H. Ribeiro, Catal. Today, 184 (2012) 129-144.
[65] A. Godiksen, F.N. Stappen, P.N.R. Vennestrøm, F. Giordanino, S.B. Rasmussen, L.F. Lundegaard, S. Mossin, The Journal of Physical Chemistry C, 118 (2014) 23126-23138.
[66] Y. Zhang, Y. Peng, K. Li, S. Liu, J. Chen, J. Li, F. Gao, C.H.F. Peden, ACS

Catalysis, 9 (2019) 6137-6145.
[67] D. Wang, L. Zhang, K. Kamasamudram, W.S. Epling, ACS Catalysis, 3 (2013) 871-881.
[68] W. Su, H. Chang, Y. Peng, C. Zhang, J. Li, Environ. Sci. Technol., 49 (2015) 467-473.
[69] L. Chen, T.V.W. Janssens, P.N.R. Vennestrøm, J. Jansson, M. Skoglundh, H. Grönbeck, ACS Catalysis, 10 (2020) 5646-5656.
[70] G.M. Psofogiannakis, J.F. McCleerey, E. Jaramillo, A.C. Van Duin, The Journal of Physical Chemistry C, 119 (2015) 6678-6686.
[71] F. Göltl, A.M. Love, I. Hermans, The Journal of Physical Chemistry C, 121 (2017) 6160-6169.
[72] L. Chen, H. Falsig, T.V.W. Janssens, J. Jansson, M. Skoglundh, H. Grönbeck, Catalysis Science & Technology, 8 (2018) 2131-2136.
[73] S. Grundner, M.A. Markovits, G. Li, M. Tromp, E.A. Pidko, E.J. Hensen, A. Jentys, M. Sanchez-Sanchez, J.A. Lercher, Nat Commun, 6 (2015) 7546.
[74] X. Zhang, Q. Shen, C. He, C. Ma, J. Cheng, Z. Liu, Z. Hao, Catalysis Science & Technology, 2 (2012).
[75] L.B. Gutierrez, E.E. Miró, M.A. Ulla, Applied Catalysis A: General, 321 (2007) 7-16.
[76] K. Góra-Marek, B. Gil, M. Śliwa, J. Datka, Applied Catalysis A: General, 330 (2007) 33-42.
[77] M.I. Shilina, G.Y. Vasilevskii, T.N. Rostovshchikova, V.Y. Murzin, Dalton Trans, 44 (2015) 13282-13293.
[78] K. Nakamura, A. Okuda, K. Ohta, H. Matsubara, K. Okumura, K. Yamamoto, R. Itagaki, S. Suganuma, E. Tsuji, N. Katada, ChemCatChem, 10 (2018) 3806-3812.
[79] J.A. Loiland, R.F. Lobo, J. Catal., 325 (2015) 68-78.
[80] J. Miller, E. Glusker, R. Peddi, T. Zheng, J. Regalbuto, Catal. Lett., 51 (1998) 15-22.
[81] J.H. Kwak, T. Varga, C.H. Peden, F. Gao, J.C. Hanson, J. Szanyi, J. Catal., 314 (2014) 83-93.
[82] A.R. Fahami, T. Günter, D.E. Doronkin, M. Casapu, D. Zengel, T.H. Vuong, M. Simon, F. Breher, A.V. Kucherov, A. Brückner, J.-D. Grunwaldt, Reaction Chemistry & Engineering, (2019).

국 문 초 록

질소산화물은 인체의 건강과 환경에 치명적인 영향을 주는 오염물질로 이를 제거하는 기술에 대한 관심이 더욱 높아지고 있다. 이러한 기술 중, 선택적 촉매 환원 반응(NH_3-SCR)은 암모니아를 환원제로 하여 NOx를 인체에 무해한 N_2로 전환시키는 기술로 NOx 제거에 가장 효율적인 기술로 알려져 있다. Cu 이온을 교환한 SSZ-13 촉매는 우수한 활성과 수열안정성을 가지는 NH_3-SCR 촉매로 이미 성공적으로 상용화된 촉매이다. 그러나 최근에 더욱 강화된 규제로 더 우수한 촉매의 필요성이 대두되고 있다. Cu-SSZ-13 촉매의 성능을 향상시키기 위해서는 반응의 활성점인 Cu 이온의 거동을 이해하는 것이 중요하다.

Cu-SSZ-13 촉매에는 Cu 이온의 위치에 따라 1Al-Cu와 2Al-Cu, 두 종류의 Cu 이온이 존재한다. 1Al-Cu는 한 개의 Al과 결합하여 Z-(Cu^{2+}-OH^-) 형태로 존재하는종이며 2A-Cu는 인접한 두 개의 Al과결합하여 2Z-Cu^{2+} 형태로 존재하는 종이다. 이 두 종의 Cu 이온은 서로 다른 성질을 가지고 있는데 그 중 하나가 두 종의 이동성이 다르다는 것이다. 본 연구에서는 이 두 종의 이동성을 관찰하고 이와 SCR 활성과의 상관관계를 밝히고자 한다. 제올라이트 구조 안에서 Cu 이온의 이동성을 확인하기 위해 Cu-SSZ-13을 H-SSZ-13과 두 가지 방법을 이용해 물리적으로 혼합하였다. 첫번째 방법은 두 물질을 막자 사발로 갈면서 섞는 것이고 두번째 방법은 각자 큰 알갱이로 만든 후에 그 알갱이들을 섞는 것이다. 첫번째 방법으로 섞은 촉매는 두 물질이 가깝게 접촉하고 있는 반면 (PM-C) 두번째 방법으로 섞은 촉매는 두 물질이 접촉이 거의 없이 분리되어 있는 형태이다 (PM-L). 분리되어 있기 때문에 Cu 이온이 이동할 수 없는 PM-L 촉매와 비교했을 때, PM-C 촉매에서 1Al-Cu가 2Al-Cu 종으로

변화하는 현상이 관찰되었다. 이러한 Cu 이온 종 변화로부터 PM-C 촉매에서 이온의 이동이 일어 났다는 것을 유추할 수 있다. 이런 형상은 물이 없는 조건에서는 일어나지 않았고 이를 통해 물이 Cu 이온 이동에 중요한 역할을 한다는 것을 의미한다. 이 연구는 Cu 이온이 수열 조건에서 입자에서 다른 입자로 굉장히 먼 거리를 이동할 수 있다는 것을 보여준다.

SCR 반응의 반응 중간체가 Cu 이온의 확산에 의해 형성되기 때문에 Cu 이온의 이동성은 SCR반응을 결정하는 굉장히 중요한 성질로 알려져 있다. 1Al-Cu와 2Al-Cu는 다른 이동성을 가지고 있기 때문에 두 종의 Cu 이온의 SCR 활성이 다를 것으로 유추할 수 있으나 이에 대해 명확히 밝혀진 바가 없다. 이를 확인하기 위해 수열 처리를 통해 1Al-Cu와 2Al-Cu의 비율을 조절한 Cu-SSZ-13 촉매를 제조하였다. 반응 결과와 DRIFT 분석결과를 통해 1Al-Cu가 2Al-Cu 종보다 더 높은 SCR 활성을 가지는 것을 확인 할 수 있었다. 이러한 두 종의 차이는 특정한 속도 결정 단계에 의해 반응이 결정되는 조건에서만 나타났다. 반응속도론 연구를 통해 Cu 이온의 이동성이 두 종의 이러한 반응성 차이를 가져온다는 것을 확인할 수 있었고, 이는 곧 1Al-Cu의 높은 이동성이 우수한 반응성을 결정짓는다는 것을 의미한다.

Cu-SSZ-13의 성능을 향상시키기 위해서 더 높은 활성을 가지는 1Al-Cu 종을 가지도록 촉매를 설계하였다. Co^{2+} 이온을 담지하여 2Al-Cu가 형성되는 2Al site를 선택적으로 막아 Cu 이온이 1Al site에 위치하도록 유도하였다. H2-TPR 결과를 통해 Co^{2+} 도입 후에 의도했던 대로 1Al-Cu/2Al-Cu 비율이 크게 증가한 것을 확인하였다. 이러한 Co^{2+}의 반응 활성에서의 효과는 온도에 따라 다르게 나타난다. 중 저온에서는 Co^{2+}를 도입한 촉매가 기존의 촉매보다 확연히 더 높은 활성을 보였다. 반응속

도론 연구를 통해 이러한 높은 활성은 1Al-Cu의 높은 이동성으로 인한 중간체 형성이 촉진되었기 때문임을 밝혀냈다. 반면 저온에서는 이러한 차이가 희미해 졌고 이는 Co^{2+} 도입에 의한 Cu의 이동성 증진 효과가 저온에서는 나타나지 않았음을 의미한다. 이 연구는 더 우수한 Cu-SSZ-13 촉매를 개발하기 위해 이온의 이동성을 조절하는 새로운 방향성을 제시한다.

주요어: 질소산화물; 선택적 촉매 환원; Cu-SSZ-13; 구리 이온; 이온의 이동성; 반응 속도론

학번: 2015-21081